# Structural and Morphological Investigations of Poly(3-alkylthiophene) Thin Films Prepared by Low and Room Temperature Casting and Spin Coating Techniques

**DISSERTATION**

zur Erlangung des Grades eines Doktors

der Naturwissenschaften

vorgelegt von

M.Phil.

**Shabi Thankaraj Salammal**

geb. in Kirathoor (Indien)

eingereicht beim Fachbereich Physik

der Universität Siegen

**Siegen, 2012**

| | |
|---|---|
| Gutachter: | **Prof. Dr. Ullrich Pietsch** |
| Tag der mündlichen Prüfung: | **05.06.2012** |
| Prüfer: | **Prof. Dr. Martin Brinkmann** |
| | **Prof. Dr. Otfried Gühne** |

## Abstract

The regioregular poly(3-alkylthiophenes) (RR-P3ATs) have emerged as a benchmark in semiconducting polymers due to their availability, self-organization, solution processability, and promising electrical and optical properties arising from an enhanced crystalline microstructure. The mobility of P3AT organic field effect transistor (OFET) increases when the polymers are self-organized in a thermodynamically most stable "edge-on" orientation. Especially, crystallizing the P3AT polymeric thin films with only edge-on orientation is an important task because of their semicrystalline nature and anisotropic electrical conductivity.

The X-ray and transmission electron microscopy analyses have been performed for various P3AT thin films in this thesis shows that the decrease of cast temperature (below room temperature (RT)) is an elegant way to fabricate highly crystalline, mostly edge-on oriented, homogeneous, and very thin films. In particular, thin films of P3ATs such as poly(3-pentylthiophene) (P3PT), poly(3-hexylthiophene) (P3HT), poly(3-heptylthiophene) (P3HeptT), and poly(3-octylthiophene) (P3OT) were prepared by casting 250 µl solution (concentration of 2 mg/ml) at various temperatures like 23°C, 8°C, -12°C, and -30°C. Temperature of -12°C was found to be the optimum casting temperature for the concentration of 2 mg/ml. The randomly oriented crystallites are started to orient along out-of-plane stacking direction while reducing the cast temperature from 23°C to -30°C i.e. forming more edge-on oriented crystallites. In addition to that, the in-plane stacking and crystallinity of P3AT crystallites are increased as the cast temperature decreases, which are most important for the charge transport. The enhancement of edge-on oriented crystallites while decreasing the cast temperature can be explained by the reduced evaporation rate of the solvent ($CHCl_3$).

The orientation and sizes of the P3AT crystallites were further enhanced by reducing the concentration of the solution. The out-of-plane stacking of P3AT crystallites increases with the alkyl side chain length due to the increased solubility. On the contrary, the in-plane ordering and crystallinity of P3AT thin films get worse as the alkyl side chain length increases, due to the stimulation of torsion in the thiophene backbone caused by the augment in steric hindrance between the grafted alkyl side chains. Subsequently, it hinders the OFET performance as well as the luminescent intensity. The field effect mobility of -30°C cast P3OT is twofold lesser than the P3PT even though the P3OT film is composed of bigger and more edge-on oriented crystallites because of its poor interchain stacking. The mobility of

P3AT OFET cast at -30°C is higher than the ones cast at RT due to the growth of highly interchain stacked edge-on oriented crystallites. It concludes that the highly interchain stacked edge-on oriented P3AT crystallites are necessary for the fast charge transport where the growth along the chain axis ($l_c$) is restricted due to thiophene backbone folding and entanglement as observed through the high resolution transmission electron microscope.

The overall findings in this thesis show that the proper selection of cast temperature and concentration are mandatory for the fabrication of very thin and uniform films with enhanced crystallinity and orientation. The degree of preferential orientation and size of the nanodomains can be further increased by depositing the films on n-octadecyltrichlorosilane treated $SiO_2$ substrates as well as by annealing the films at a proper annealing temperature for an hour.

## Zusammenfassung

Regioregulare poly(3-alkylthiophene)s (RR-P3ATs) gelten als Maßstab für Halbleiterpolymere aufgrund ihrer Verfügbarkeit, Selbstorganisation und Lösungsverarbeitbarkeit und wegen ihrer vielversprechenden elektrischen und optischen Eigenschaften, die von einer hochkristallinen Mikrostruktur stammen. Die elektrische Mobilität in P3AT organischen Feldeffekttransistoren (OFETs) und deren Leistungsfähigkeit in Solarzellen steigt für den Fall, dass sich die Moleküle durch Selbstorganisation in der thermodynamisch stabilen „edge-on“ Orientierung ausrichten.

Die Kristallisation von P3AT Polymeren in dünnen Schichten ist eine großartige Herausforderung aufgrund der semi-kristallinen Natur und der anisotropen elektrischen und optischen Eigenschaften. Infolge thermodynamischer Randbedingungen ist es schwierig, dünne Schichten aus P3AT Polymeren zu kristallisieren, die nur „edge-on” Kristallite enthalten.

Transmission electron microscopic (TEM) - und Röntgenanalysen, die in dieser Arbeit dargestellt werden, zeigen, dass hochkristalline und sehr dünne Filme hergestellt werden können, indem sie bei Temperaturen unterhalb der Raumtemperatur (RT) präpariert werden. Die Abscheidetemperatur von dünnen Filmen aus P3AT-Lösungen wurde optimiert, indem verschiedene Temperaturen wie z. B. 23°C, 8°C, -12°C und -30°C bei einer Konzentration von 2mg/ml ausprobiert wurden. Die genannten Analysen wurden an mehreren P3ATs durchgeführt wie z. B. bei poly(3-pentylthiophen) (P3PT), poly(3-hexylthiophen) (P3HT), poly(3-heptylthiophen) (P3HeptT), und poly(3-octylthiophen) (P3OT). Dabei stellt sich heraus, dass die Wachstumstemperatur unterschiedlich zu wählen ist, da mit ihr diverse Parameter der Filme eingestellt werden können, wie beispielsweise die Kristallitgröße, Orientierung, Gleichförmigkeit der Oberfläche oder die Dicke. Wir waren in der Lage, 38-48 nm dünne Filme mit einer guten Oberflächenbeschaffenheit herzustellen, indem wir eine Wachstumstemperatur von -30°C bei einer Konzentration von 1mg/14ml verwendet haben, welches nach Gburek *et al* in 2010 die optimale Dicke für die OFET Fabrikation liefert. Die diversen löslichen P3AT Polymere gegossen bei verschiedenen Temperaturen zeigen, dass nur „edge-on“ orientiert Kristallite präpariert werden können, wenn die Gießtemperatur reduziert wird. Eine Temperatur von -12°C wurde in diesem Fall als ein optimaler Wert für eine Konzentration von 2mg/ml gefunden. Zudem kann man schlussfolgern, dass eine Optimierung der Konzentration und Gießtemperatur zwingend erforderlich ist, wenn größere Kristallite erzeugt werden sollen, indem mehrfache Keimbildung reduziert wird. Die

Stapelung von P3AT Kristalliten in einer Ebene kann verbessert werden, indem die Filme bei einer tieferen Temperatur gegossen wurden, aber sie verschlechtert sich, falls die Länge der Alkylseitenkette vergrößert wird. Die zahlenmäßige Zunahme von Kohlenwasserstoffen in der aufgepfropften Alkylseitenkette behindert die Stapelung in der Ebene der P3AT Kristallite aufgrund der Vergrößerung der räumlichen Hindernisse zwischen den Alkylseitenketten bezogen auf ihre Flexibilität. Die schlechte Stapelung in der Ebene der P3AT Kristallite nach Zunahme der Anzahl der Kohlenwasserstoffe in der Alkylseitenkette reduziert die Leistungsfähigkeit der OFETs sowie die Intensität ihrer Luminiszenz. Die Mobilität der bei -30°C gegossenen OFETs erhöht sich um eine Größenordnung verglichen mit denen die bei RT gegossen wurden, wegen der Zunahme der Kristallit-Stapelung zwischen den Ketten. Die Mobilität des bei -30°C gegossenen P3PT erhöht sich um den Faktor zwei verglichen mit dem bei -30°C gegossenen P3OT, obwohl P3OT größere und in höchstem Maße „edge-on" orientierte Kristallite an der Schnittstelle zwischen Substrat und Film aufweist. Neben der Mobilität verringert sich auch die Intensität der Luminiszenz des P3AT sobald sich die Seitenkettenlänge erhöht. Daraus ist zu folgern, dass die Zwischenkettenstapelung der Kristallite für den schnellen Ladungstransport notwendig ist, wobei das Wachsen entlang der Kettenachse ($\boldsymbol{l_c}$) aufgrund des Zusammenfaltens des Thiophen–Rückgrades beschränkt ist.

Die hochauflösende Transmissionselektronenmikroskopische Analyse, die für die dünnen Filme aus P3AT durchgeführt wurde, ergab, dass die Entstehung des nanofaserigen Wachstums mit der Beschränkung des Wachstums entlang der c-Achse infolge des Zusammenklappens des Thiophen-Rückgrades zusammenhängt. Nachfolgend haben sie die Freiheit, entlang der Stapelung der Alkylseitenkette (h00) und der π-π Stapelrichtung zu wachsen (0k0). Der Grad der Vorzugsorientierung und die Größe der Kristallite kann weiter erhöht werden, indem die Filme auf mit n-octadecyltrichlorosilane (OTS) behandelte $SiO_2$ Substrate aufgebracht werden oder aber indem die Filme für eine Stunde getempert werden.

## Table of Contents

## Introduction

Organic semiconductors are playing a vital role in the growing electronic industries for the fabrication of light weight, flexible, and low-cost electronic components. The flexible devices can be prepared on the metal foil substrates which can be used to prepare the devices at higher temperatures. The main disadvantages of flexible metal foils are their heaviness and opacity. The transparent plastic substrates like polyethylene terephthalate (PET), polyethylene naphthalate (PEN), etc. are widely used to prepare flexible organic devices.[1] Especially PEN is widely in use because of its solvent resistance, malleability, transparency, etc. They cannot be used for high temperature processing because of their poor thermal resistivity (shrinkage). This is one of the reasons why amorphous silicon which contains higher charge carrier mobility (0.5$cm^2$/Vs) is being replaced with solution processable semiconducting conjugated polymers.[2]

Nowadays, some of the derivatives of polythiophenes (PTs) are used for the fabrication of flexible devices at room temperature (RT) via solution processing techniques.[1, 2] The solubility limit of PT in common organic solvents is making the synthesis become more complicated.[3] The researchers made them soluble in common organic solvents such as chloroform, xylene, tolune, etc. by grafting an alkyl ($C_nH_{2n+1}$) side chain on the 3$^{rd}$ position of the thiophene ring.[4-6] Subsequently, the grafted insulating alkyl side chains can hinder the charge transport along the alkyl side chain stacking direction and it increases with increasing the number of hydrocarbons in the grafted alkyl side chain.[2, 7] This is a reason why the poly(3-alkylthiophene)s (P3AT)s are needed of edge-on oriented crystallites which can provide 2D charge transport in an organic field effect transistor (OFET).[7-9] The mobility of P3AT OFETs lies in the range of $10^{-1}$ – $10^{-4}$ $cm^2$/Vs and it varies with respect to the film properties such as the amount of edge-on oriented crystallites, crystallinity, crystallite size, etc.[1, 2]

Large area P3AT thin films can be prepared by various cheap solution processing methodologies such as spin coating, casting, printing, doctor blading, etc.[10] The mainly used spin coating and casting techniques produces thermodynamically instable crystallites which are not suitable for the 2D charge transport in an OFET (face-on oriented crystallites).[7, 9] Lot of methodologies were proposed by various researchers for the fabrication of only edge-on oriented crystallites; i) using higher boiling point solvents, ii) post growth annealing, iii) silanization of substrate, iv) solvent annealing, etc.[8, 11-14] To the

best of my knowledge, still there is no unique technique available to prepare completely edge-on oriented P3AT crystallites. Brinkmann *et al* have epitaxially crystallized the poly(3-hexylthiophene) (P3HT) in an edge-on oriented fashion but the bright field images collected for the same film envisages the coexistence of both the amorphous and crystalline phases. This technique needs multiple processing steps and high processing temperature (180°C) which are not friendlier for the fabrication of cheap devices on the low thermal resist plastic substrates.[15] In this thesis, a simple method has been proposed, which can be used to prepare highly edge-on oriented and crystalline P3AT thin films by reducing the cast temperature below RT.

## Scope and Outline of the Thesis

It has been documented that the fast growth processes hampers the formation of thermodynamically most stable edge-on oriented P3AT crystallites on the substrate because of the rapid evaporation of solvent.[16-18] Detailed X-ray and electron diffraction analysis carried out in this thesis under various geometries will show that the highly edge-on oriented crystallites can be prepared by reducing the cast temperature which can help to prolong the growth time of the nanocrystallites by reducing the evaporation rate of the solvent. It also helps us to control the other important parameters such as orientation of the crystallites, crystallite size, film thickness, surface coverage, uniformity, and surface roughness by choosing the proper concentration and cast temperature. In addition, the influence of alkyl side chain length on the structural disordering as well as their impact on the electrical and optical performances of P3AT films will be addressed. It will be explained much more elaborately in the corresponding chapters. The outline of the chapters are given below

**Chapter I:** Explains the brief history of: i) conjugated polymers and their uses, ii) novelty of solution processable P3ATs, and iii) widely used cheap solution processing techniques

**Chapter II:** Theoretical background of formation of nucleation and the influence of crystallization temperature on the formation of nucleation

**Chapter III:** Working principle of X-ray diffractometer and transmission electron microscope (TEM) under various modes and their vital role in the structural and morphological analysis of polymeric thin films

**Chapter IV:** In this chapter, influence of cast temperature and concentration on the formation of highly edge-on oriented P3HT crystallites will be discussed

**Chapter V:** Clarifies the influence of alkyl side chain length on the in-plane stacking of P3AT crystallites and its vital role on their electrical and optical properties

**Chapter VI:** Addresses the anisotropic growth of P3AT polymers upon annealing due to the polymer chain entanglement, thiophene backbone folding, and reduction in slide diffusion of PT backbones. In addition, influence of alkyl side chain length on the formation and orientation of the P3AT crystallites were thoroughly analyzed

**Chapter VII:** Conclusions and outlook

# Chapter I

## 1 Innovation and Importance of Conjugated Polymers

Till the year 1977, organic polymers like polyvinyl chloride (PVC), polyethylene, polypropylene (PP), etc. were widely synthesized due to their durability, malleability, and manufacturing cost for the production of tons of insulating, packaging, transporting materials, etc. The discovery of Shirakawa *et al* have made a tremendous change in the polymer field and brought a new application in the electronic industries due to their electrical conductivity.[19, 20] It has brought about a ***Nobel Prize*** in chemistry in the year of 2000 "for the innovation and development of **conducting polymers"**.[21] Hopefully, the conjugated conducting polymers can bring a delightful future in the renewable energy sources as well as for the fabrication of cheap, light weight, and flexible electronic devices.[1] The main advantage of conducting polymers is their solution processability. Compared to the inorganic semiconductors, conjugated conducting polymers are expensive because of the requirement of multiple synthesizing steps. For example, the poor solubility of many polymers requires the introduction of solubilizing agents or substituent for pattering them through cheap solution processing techniques.[5, 6]

### 1.1 Polymers

Polymers are long chain organic molecules that consist of large number of repeating units called monomers. The organic polymers are made up of carbon which is rather common in the inorganic world too (graphite, cyanides, carbonates, diamond, etc.). The carbons can make more compounds than the other atoms do. We know that the polymers like PVC, polyethylene, etc. cannot conduct electricity. The polyethylene is a best example for non-conducting plastics and its molecular structure is shown in Figure 1.1a. The electrons in polyethylene are not free to conduct electricity because the four $sp^3$ hybridized orbitals can make four sigma (σ) bonds with three hydrogen and one carbon atoms. The electrons involved in the σ bonds are fixed and immobile. The hybridization of ethane is shown in Figure 1.1c. Here the three $sp^3$ hybridized orbitals are overlapped with the 1s orbital of hydrogens and the rest $sp^3$ hybridized orbital can make a covalent bond with the other $sp^3$ hybridized carbon. The deficiency of single hydrogen in each carbon in the polyethylene can completely changes its hybridization as well as the chemical structure of the polymer. This polymer is called polyacetylene and its molecular structure is shown in Figure 1.1b.

Polyacetylene was the first semiconducting polymer synthesized by Natta *et al.*[22] The bonding of polyacetylene is completely different from polyethylene. It makes $sp^2$ hybridization instead of $sp^3$ hybridization. For example, $sp^2$ hybridized ethylene is schematically shown in Figure 1.1d. The three $sp^2$ hybridized orbitals can make σ bond with the adjacent carbon and two hydrogen atoms. A second carbon-carbon bond will be formed through the overlap of those two remaining $p_z$ orbitals called π-bond (Figure 1.1d). The π-bonds are weaker than the sigma bonds. The most notable properties of these polymers are electrical conductivity which results from the delocalization of electrons along the conjugated polymer backbones.[19]

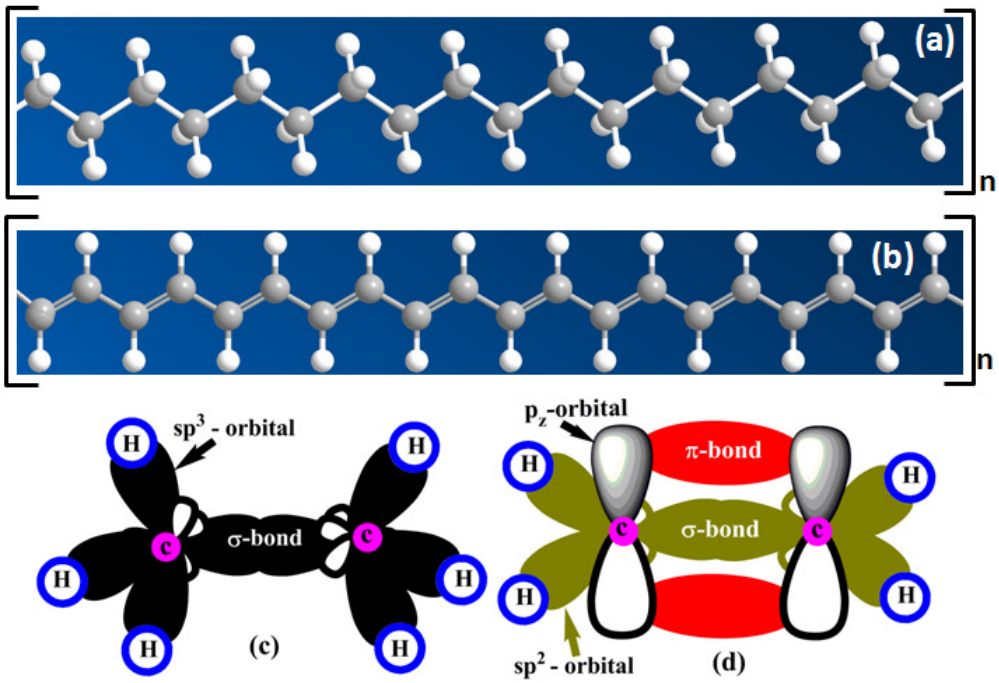


Figure 1.1: The molecular structure of polyethylene (a), polyacetylene (b); the orbital structure of $sp^2$ and $sp^3$ hybridized ethane (c) and ethylene (d), respectively

## 1.2 Conjugated Polymers

The polymer molecule which contains alternating single and multiple bonds (e.g. double) are called conjugated polymers (Figure 1.2). The π-electrons used in the double bonds are spread out over the long chain-like molecules. For example, $C_2$ carbon in Figure 1.2 can make either π-bond with $C_1$ or $C_3$ carbon and the electrons involved in the π-bonds are free inside the whole polymer chain (contour length) and they are named as conjugated electrons. However, this isn't quite enough to conduct electricity yet. The electrons are still packed tightly and some of them have to be removed or added from the conjugated backbone to make

them electrically conductive. Specifically, this involves a process known as “doping”, which is the addition of chemicals having electron-removing property like bromine, iodine, etc.

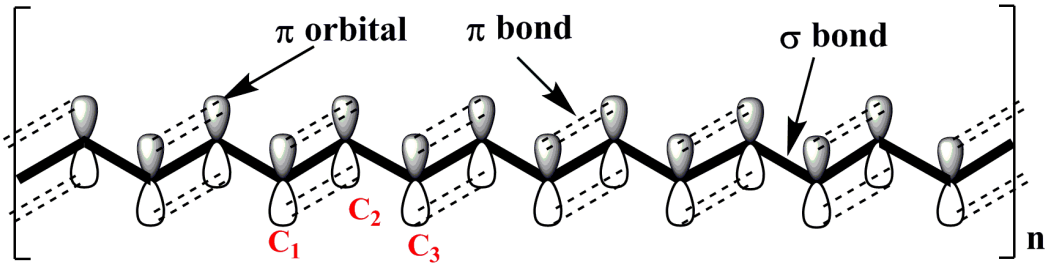


Figure 1.2: Shows the conjugated backbone of polyacetylene and its bonding

### 1.2.1 Doping

The well-known inorganic semiconductors like Si, Ge, GaAs, etc., we can also prepare n- and p-type organic semiconductors by choosing the appropriate dopants. Both the n-type (Na, K, Li, Ca)[23] and p-type ($I_2$, $AsF_5$, Br, Cl) [3, 19, 20, 24-26] dopants have been utilized to induce an insulator-to-conductor transition in conjugated polymers. Polyacetylene is a semiconductor on its own, but the conductivity is increased near to that of metals when the polymer is doped with the corresponding elements.[19, 27] Shirakawa *et al* reported that the conductivity of iodine doped polyacetylene is seven orders of magnitude higher than the Br doped one.[21] During oxidation, the iodine molecule will attract an electron from the polyacetylene chain and becomes $I_3^-$ (a negatively charged ion), the polyacetylene molecule, now positively charged, is termed as radical cation or polaron.[27] Doping can increase the conductivity of conjugated polymers by billions of times, up to the level matching that of metallic materials.[19, 20, 27] The p-type and n-type polymers can be synthesized by oxidation and reduction processes, respectively. In practice, most of the organic semiconductors are doped oxidatively to give p-type materials. If an electric field is applied then the electrons constituting the π-bonds can move rapidly along the conjugated chain. The lonely electron of the double bond from which an electron has been removed, can move easily. As a consequence, the double bond successively moves along the molecules.[27]

Followed by the innovation of Shirakawa *et al*, a lot of conjugated polymers have been synthesized and analyzed due to their inherent properties.[19] Some of the well-known conjugated polymers like polyacetylene, poly(3,3’’’-didodecyl quarter thiophene) (PQT), PTs, polyaniline, poly(3-alkylthiophene)s (P3ATs), polypyrrole (PPy), poly(p-phenylene vinylene) (PPV), poly(2,5-bis(3-alkylthiophen-2-yl) thieno[3,2-b]thiophene) (PBTTT), and phenyl-$C_{61}$

butyric acid methyl ester (PCBM) etc. are shown in Figure 1.3. Among all the polymers, PT family was found to be satisfactorily environmentally stable than the other polymers like PPV, PPy etc.[2, 28-31]

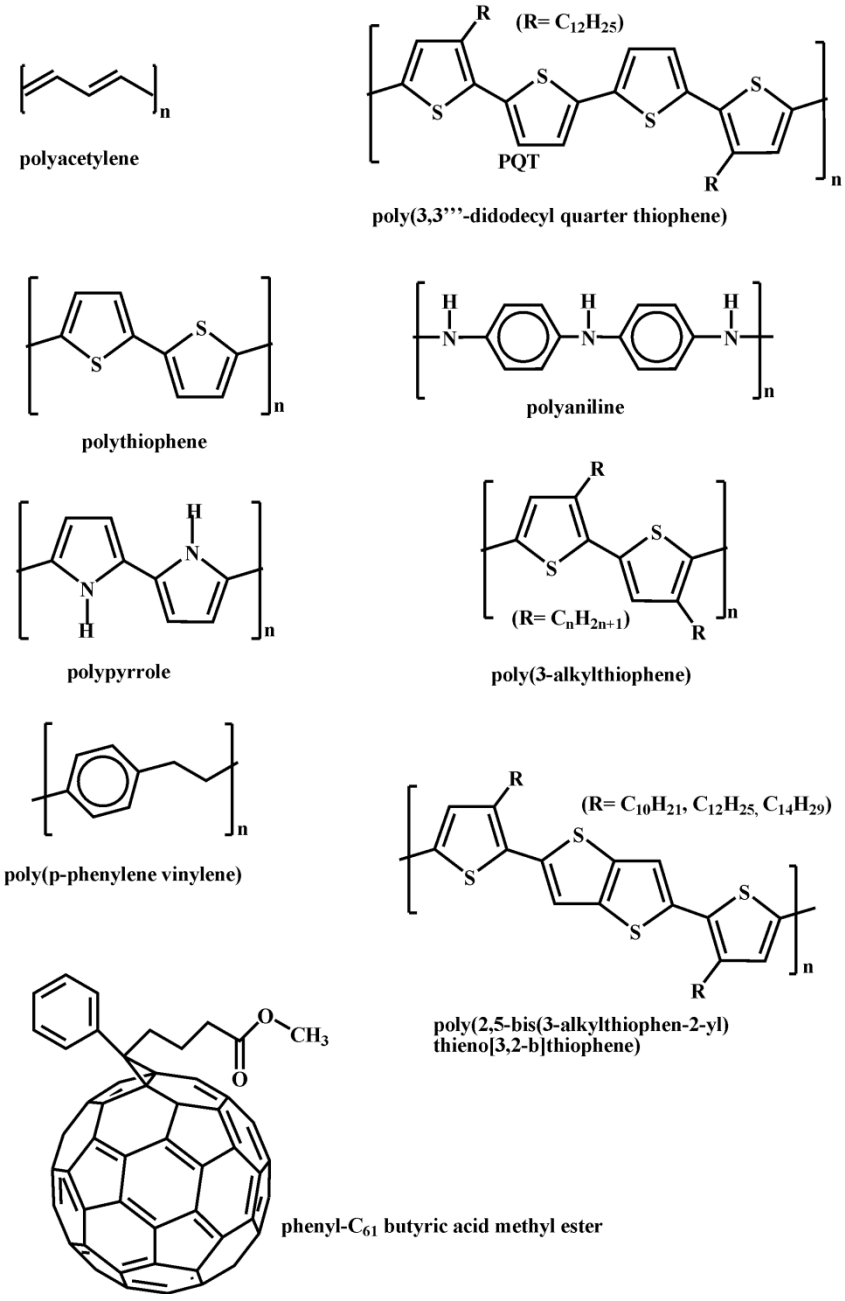


Figure 1.3: Chemical structure of some of the well studied conducting polymers

## 1.3 Polythiophenes

The conjugated PT is one of the important classes of polymers because a lot of derivatives of PTs are widely in use. Its chemical structure is shown in Figure 1.3. The conjugated PTs are highly conductive and satisfactorily environmental stable as compared to the other polymers like PPy, polyaniline, etc.[28] The 2-5 coupled polythiophene was first

synthesized in the year of 1980.[32, 33] The PTs can be synthesized via electrochemical deposition and chemical routes.[25, 32, 34] PT is not soluble in common organic solvents such as chloroform ($CHCl_3$), toluene, xylene, trichlorobenzene (TCB), etc. because of its backbone rigidity, crystallinity, and increased molecule-molecule interactions. The insolubility of PTs in common organic solvents suppresses the solution processability and uniform doping with extrinsic charge carriers. The extrinsic charge carriers have been introduced into the organic semiconductors via *ex situ* or *in situ* doping process by exposing it to the dopant vapor or to the liquid phase and during the electrochemical deposition process, respectively.[25, 32, 34] Mainly iodine vapor treatment was used to dope the PT films, subsequently the conductivity of PT is increased from $10^{-10}$ $(\Omega cm)^{-1}$ to $10^{-1}(\Omega cm)^{-1}$. [32, 33] In general, it is difficult to control the doping level precisely and to achieve uniform doping by exposing the neutral solid conjugated polymers to the corresponding dopant vapor. Frommer *et al* reported that the PTs can be doped by arsenic pentafluoride ($AsF_5$) through solution casting process by dissolving it in arsenic trifluoride ($AsF_3$).[3] Arsenic is toxic and it can cause cancer. So, it is quite risky to work with such a non-user friendly solvents. However, in spite of their scientific interest, the practical applications of these results are limited. The conductivity of conjugated poly(p-phenylene sulfide) (PPS) doped through solution casting process is higher than the one doped through conventional methods because of homogeneous distribution of dopants throughout the polymer films.[3]

Not only the uniform doping, it also suppresses the processability of conducting polymers on the substrate via cheap solution processing methodologies such as printing, spin coating, casting, etc., which can help us to prepare them in a useful form. The uniaxially oriented crystallites are mandatory for the fabrication of high efficient PT based devices and it can be obtained via solution processing by applying various growth methodologies. The insolubility issue of PT was first solved in the year 1986 by grafting an alkyl side chain on the 3$^{rd}$ position of the thiophene ring, they are named as P3ATs. When such a good solubility was established in PTs by substituting an alkyl side chain, it has started to attract the researchers and industries for the fabrication of doped semicrystalline P3AT thin films with enhanced crystallinity and orientation.[8, 18, 35, 36]

A lot of conjugated polymers were synthesized using the thiophene aromatic ring, such as P3ATs, PBTTT, PQT, etc. Among them, PQT and PBTTT has overtaken poly(3-hexylthiophene) (P3HT) for the fabrication of OFETs because of their enhanced crystallinity and π-π orbital overlapping.[30, 37-39] The PBTTT polymer can produce long range order as

compared to the P3HT because of the possibility of interdigitation of alkyl chains due to the presence of less dense alkyl side chains with larger spacing distance (Figure 1.3).[2] In photovoltaic (PV) applications still P3ATs are playing a vital role with the combination of PCBM and poly((9,9-dioctylfluorene)-2,7-diyl-alt-[4,7-bis(3-hexylthien-5-yl)-2,1,3-benzothiadiazole]-2´,2´´-diyl) (F8TBT) due to their uniform mixing.[31, 40, 41]

## 1.4 Poly(3-alkylthiophene)s

P3AT was first synthesized in the year 1986 for widening the solution processability of thiophene based polymers.[4-6] The PTs grafted with more than 4 hydrocarbons in the alkyl chain is readily soluble in common organic solvents such as $CHCl_3$, xylene, toluene, etc. at RT and the solubility increases with the alkyl side chain length (i.e. increase in number of hydrocarbons in the alkyl side chain).[5, 6] Together with the solubility, the melting point of P3AT decreases as the alkyl side chain length increases (enthalpy of fusion).[24] It has also some disadvantages like; i) steric interaction between the grafted alkyl side chain decreases the π-π orbital overlap between the adjacent molecules, ii) increase of alkyl side chain flexibility with the alkyl side chain length, iii) induced torsion in the thiophene backbones caused by the alkyl side chains, etc.[4, 42-44] Kawai *et al* and Corish *et al* reported that the π-π stacking distance is not affected by the alkyl side chain length when it contains less than 10 hydrocarbon units and it increases further with the alkyl side chain length through experimentally and computer based simulations, respectively.[45, 46] The solubility of P3ATs is a precondition to prepare thin films through cheap solution processing techniques, but the self-organization and orientation of these polymers are mainly depending on their regioregularity (RR).[9]

### 1.4.1 Regioregularity

The RR of P3ATs can be varied due to the asymmetric coupling of 3-substituted thiophenes linked between the $2^{nd}$ and $5^{th}$ positions. It produces three diads like; i) 2,5', or head–tail (HT), coupling ii) 2,2', or head–head (HH), coupling, and iii) 5,5', or tail–tail (TT), coupling. These three diads can be combined into four distinct triads as shown in Figure 1.4.[47-49] The triads can be distinguished by nuclear magnetic resonance spectroscopy (NMR), and the degree of RR can be estimated by integration.[48] The HT–HT coupling of P3AT is known to be extremely favorable for the formation of highly regular structure with excellent alignment of the polymer chains.[49, 50] The HT-HT coupled P3ATs with greater than 99% RR were synthesized by Loewe *et al* using Grignard metathesis.[51, 52] The

conjugation length of HH–TT coupled P3AT is very less due to the steric reasons, which cause an out-of-plane twisting of adjacent thiophene rings. As a result, this material possessed a very low level of conductivity because of its poor crystallinity which severely limited its ability to form aggregates with extended electronic states.[50] Sirringhaus *et al* reported that the self-organized P3HT shows two main orientations with respect to the substrate normal called edge-on and face-on. Thin films of 81% RR-P3HT produces mainly face-on oriented crystallites. The amount of edge-on oriented crystallites is increased as the RR of P3HT increases.[9] Consequently, it enhances the performance of OFETs and solar cell efficiency.[9, 49, 53]

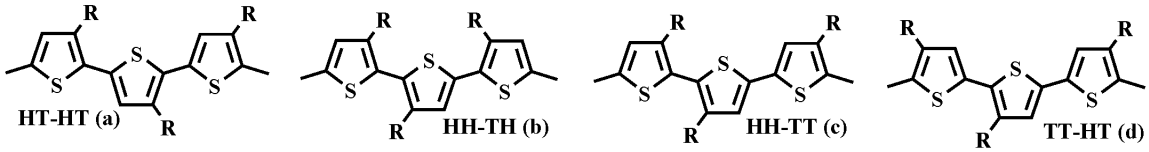


Figure 1.4: The four possible triads results from the coupling of 3-substituted thiophenes

### 1.4.2 Edge- Face-, and Flat-on Orientations

The P3AT crystallites undergoes two main orientations called edge- and face-on when the phase transformation occurs from the amorphous to the crystalline state.[9, 54] The formation of edge- and face-on oriented crystallites can be distinguished through the direction of π-π stacking which lies along parallel and perpendicular to the substrate plane as shown in Figure 1.5. In a very rare case flat-on oriented P3AT crystallites will form. Lu *et al* reported that the as-grown edge-on oriented poly(3-butylthiophene) (P3BT) crystallites are altering their orientation to flat-on after the solvent (carbon disulfide ($CS_2$)) annealing.[55] Brinkmann *et al* have also documented the formation of flat-on oriented crystallites during epitaxialization of P3HT on the 1,3,5-trichlorobenzene (1,3,5-TCB).[56] Among the three possible orientations, edge-on is found to be preferential and thermodynamically most stable orientation of P3AT nanocrystallites.[7, 9]

The unit cell of P3AT is monoclinic which is independent of the orientation of the crystallites. The $\boldsymbol{d_{(100)}}$ (alkyl side chain stacking direction) and $\boldsymbol{d_{(020)}}$ (π-π stacking) lattice spacing of P3AT crystallites varies with respect to the number-average molecular weight (Mn) of the polymers.[54, 57] The unit cell of P3AT crystallites was first suggested by Tashiro *et al*.[58] They have reported that the P3HT crystallites are resulting orthorhombic unit cell with the lattice parameters a = 16.63 Å, b = 7.75 Å, and c = 7.77Å. Recently, Kayunkid *et al* have constructed the unit cell of P3HT crystallites via electron diffraction

analysis using the epitaxially crystallized films. They have concluded that the P3HT crystallites consist of monoclinic unit cell with the space group $P2_1/c$, the lattice parameters are a = 16.7 Å, b = 7.8 Å, and c = 7.75 Å; α = β = 90° and γ = 86.5°.[59] It is in agreement with the lattice parameters reported by Joshi *et al*.[13] The $d_{(100)}$ lattice spacing of P3AT increases gradually with the number of hydrocarbons in the grafted alkyl side chain.[43, 45, 46]

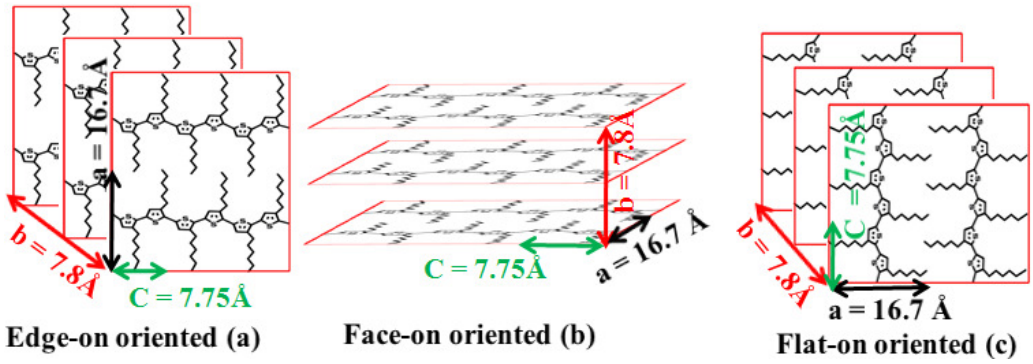


Figure 1.5: Structure of (a) edge-, (b) face-, and (c) flat-on oriented crystallites

### 1.4.3 Intrachain (conjugation) and Interchain (hopping) Transport in an OFET

The thiophene based polymers are playing a vital role in the fabrication of OFETs because of their enhanced performance, satisfactorily environmental stability, ease of processability, etc.[1, 8, 9, 30, 60] The charge transport in P3AT crystallites are completely anisotropic.[7, 61] The electrical conductivity analysis performed by Satoh *et al* for the stretched PT shows the highest conductivity along the stretching direction as compared to the perpendicular direction because of the alignment of conjugated backbones along the direction of stretching.[25] The OFETs fabricated out of edge-on oriented crystallites can provide 2D charge transport by means of conjugation and hopping. Here hopping means the electronic transport which occurs between the molecules inside the crystals but it does not mean the hopping and tunneling which occurs between the disordered regions. For example, two OFET designs are schematically shown in Figure 1.6 which of them are made up of purely edge- and face-on oriented crystallites. The edge-on oriented crystallites can conduct electricity along two directions through the conjugated backbones and interchain stacking via conjugation (intrachain transport) and hopping (interchain transport), respectively (Figure 1.6a). Hopping of the charge carriers along the alkyl side chain stacking direction is restricted due to its insulating properties (Figure 1.6b).[7] Therefore, enhancement in edge-on oriented crystallites and their sizes can helps to produce high efficient OFETs than the face-on oriented crystallites.

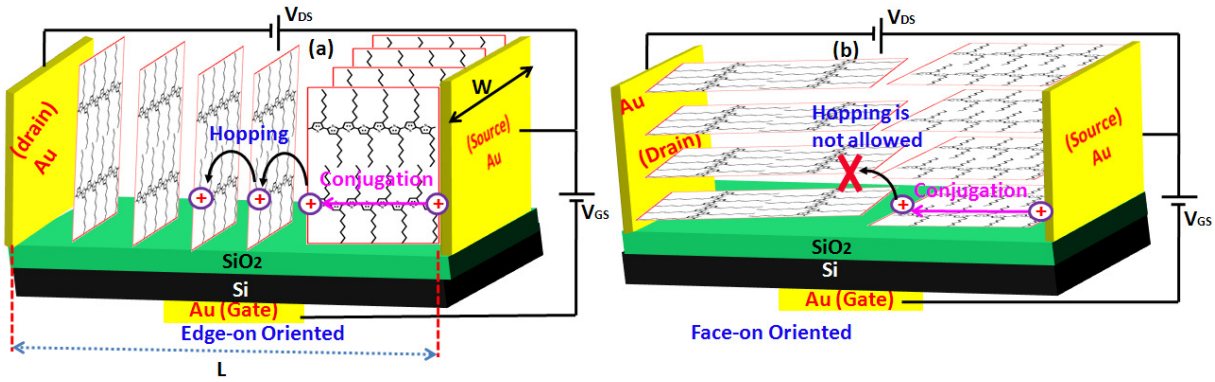


Figure 1.6: Charge transport in the OFETs fabricated out of edge-on (a) and face-on (b) oriented crystallites

The well ordered backbones of P3AT crystallites can theoretically conduct the electrons through π-π conjugated backbones up to its contour length. The detailed investigations of different molecular weight (MW) RR-P3HT carried out by various researchers shows that the increase in mobility of holes with increasing the contour length and their interconnection between the crystalline domains.[57, 62-64] In HMW P3ATs, the long conjugated polymer backbones can interconnect the nanocrystallites and it can prevent the charge carriers being trapped in the disordered regions as well as in the grain boundaries. The P3HT polymer backbones undergo folding as increasing the MW.[64, 65] The semicrystalline nature of polymeric thin film contains nanocrystallites which are embedded in an amorphous matrix.[15, 56] Mainly the flow of charge carriers in a thin film can be hampered due to the following i) crystallinity, ii) poor in-plane stacking, iii) grain boundaries, etc.[1, 49] It can be solved through the crystallization (film fabrication) processes. There is a lot of literature available where the researchers have been taken effort to increase the crystallinity and in-plane stacking of P3AT films.[8, 66-68]

## 1.5 P3AT Thin Film Processing Methodologies via Solution

The solubility of P3ATs in common organic solvents makes them solution processable through cheap and large area film preparation techniques. A major concern for solution processing methods is the effect of the solvent on underlying organic features (substrates), requiring chemically compatible materials. The solution processability of P3AT polymers brought many ways to improve the ordering of them in a way to fabricate low-cost displays, solar cells, etc. Some of the well-known techniques like printing, casting, spin coating, doctor blading, etc. which are widely used in the industries for the mass production is discussed below.[10]

### 1.5.1 Spin Coating

The spin coating is a widely used technique for the fabrication of uniform thin films on the substrate using centrifugal force. This technique is widely used to prepare organic and inorganic thin films. Thin films with controlled thickness and minimized surface roughness can be obtained by careful optimization of the parameters such as MW, solvent, concentration, angular frequency of the rotating substrate, spinning time, and temperature. Lower angular frequency and higher the concentration of the solution can increase the thickness of the films.[17, 69] The spin coating technique has higher reproducibility and ability to form homogenous films over a large area of around 30 cm in diameter.[10, 69] During spinning, most of the solutions will be thrown away due to the centrifugal force (Figure 1.7). The evaporation of the remaining solvent present on the substrate can produce uniform thin films on the substrate. The schematic illustration of spin coating is shown in Figure 1.7.

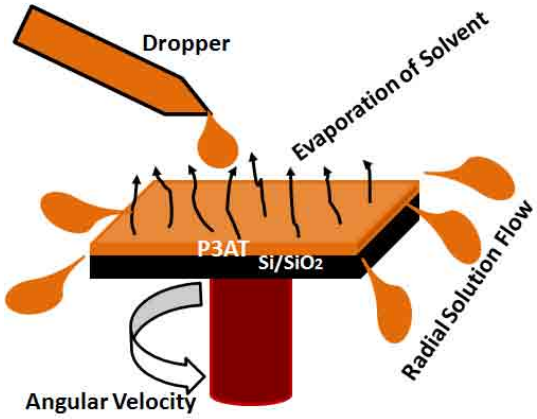


Figure 1.7: Schematic diagram of spin coating

The thickness ($t_{sp}$) of a spin coated film can be calculated using the derivation of Emslie *et al*.[70] Thickness of the films can be calculated by considering the angular velocity (ω), concentration, and viscosity of the solution being used. The corresponding expression is given below in equation 1.1.

$$t_{sp} = k_1 \omega^{\alpha} \qquad 1.1$$

The constants k and α depends on various parameters such as physical properties of polymers, solvents, and substrates, also it depends on various interactions such as polymer-solvent and solution-substrate. Some of the parameters like solvent evaporation and solute diffusivity were neglected in the earlier equation 1.1. It has been further improved and explained more elaborately in the reference.[69]

A lot of efforts have been taken by the researchers to optimize the fabrication of P3AT thin films through the spin coating technique. Especially, efforts have been taken to enhance the edge-on oriented crystallites via increasing the concentration of the solution as well as by varying the angular velocity. The P3HT thin film spin coated with various spinning velocity shows that the highly edge-on oriented crystallites can be prepared by reducing the spinning velocity due to the reduction in solvent evaporation rate.[17] Around 100 nm thin P3HT:PCBM bulk heterojunction film spin coated from various concentrations of the solution envisages the formation of non-crystalline and less interchain stacked crystallites while increasing the concentration due to the fast evaporation of solvent.[71] Kline *et al* have reported that the substrate silanization and reduction in MW are the elegant ways to increase the edge-on oriented crystallites at the substrate-film interface.[8]

The literature clarifies that the spin coated P3HT films are producing non-thermodynamically stable crystallites due to the fast evaporation of solvent.[71, 72] They are mainly producing face-on oriented crystallites which are not suitable for the OFET fabrication.[16] The spin coating technique is assisted with the following methodologies in order to enhance the edge-on oriented crystallites; i) treating the substrate surface with self assembled monolayers (SAM), ii) pattering using the higher boiling point solvents, iii) concentrations, iv) post growth annealing, etc.[8, 13, 72, 73]

### 1.5.2 Annealing

Post growth annealing treatment has been widely used for the recrystallization of polymeric thin films because of the formation of non-thermodynamically stable crystallites due to the complex interplay of solvent evaporation and molecular aggregation. Annealing can increase the mobility of polymer chains which can help them to self-organize in a most thermodynamically stable state.[11] It can also reduce the internal stress and defects present in the crystallites. The *in situ* annealing analysis performed by Joshi *et al* clarifies the increase of edge-on oriented P3HT crystallites with the annealing temperature, but it has less influence along the π-π stacking (020) than the alkyl side chain stacking (h00) directions.[13] X-ray rocking scan analysis performed for the (200) peak of PBTTT shows the increase of crystallite size and orientation with the annealing temperature.[74] Subsequently, post growth annealing enhances the OFET performances as well as the efficiency of solar cells due to the recrystallization of polymers.[8, 11, 18, 53, 71] The post growth annealing can improve the edge-on oriented crystallites but it suppresses the processing of devices on the plastic substrates. It has certain drawbacks such as, i) it cannot be applied to the thermally

deformable polymers ii) we cannot exceed the melting point of the polymers, and iii) it cannot be applied to the polymers which undergo degradation during annealing. Thermal annealing is a critical route to enhance the efficiency of P3HT/PCBM bulk heterojunction solar cells but the higher temperature used in this study like 150°C is not favorable to pattern the devices on flexible plastics.[1, 71] Due to these drawbacks, solvent annealing has started to play a vital role where one can work at around room temperature.[55]

#### 1.5.2.1 Solvent Annealing

Solvent annealing is found to be an elegant way to improve the orientation of the crystallites, nucleation density, rate of formation of nucleations, etc.[14] Mainly solvent annealing is applied to the as-grown polymeric thin films for the further enhancement in their structural ordering. During solvent annealing, solvents will be vaporized to bring the vapor into contact with the film. Here the solvent and polymer thin films will be placed on two different well controlled heating stages.[68] The chemical potential of the vapor molecules will be controlled to provide an interaction with an organic semiconductor film in order to alter the molecular arrangement. The chemical potential of vapor can be adjusted by controlling the temperature of the solvent. Mostly, good solvents like $CS_2$ has been used to perform the solvent annealing of P3AT films.[55, 68] The *in situ* solvent annealing analysis performed by Crossland *et al* shows that the nucleation density can be controlled by decreasing the solvent vapor pressure after the initial swelling of the films.[68] The detailed structural analysis performed by Lu *et al* shows that the edge-on oriented crystallites changes their orientation to flat-on after the solvent annealing.[55] The flat-on oriented crystallites are not favorable for the fabrication of OFETs because the insulating alkyl side chains will lie parallel to the substrate plane (Figure 1.5c).

### 1.5.3 Self Assembled Monolayer Treatment

The substrate-film interfacial ordering is found to be most important for the 2D charge transport and it can be obtained by increasing the substrate sub-surface energy via treating with hydrophobic medium.[75] Mainly, silanization of $SiO_2$ dielectric was carried out by various compounds like, n-octadecyltrichlorosilane (OTS), hexamethyldisilazane (HMDS), γ-aminopropyltriethoxysilane (γ-APS), etc.[8, 13, 73] The morphology and orientation of P3HT crystallites as well as the field effect mobility of the OFET varies with respect to the SAM.[73] The enhancement in mobility of OFETs prepared on the SAM treated substrate is attributed to the orientation, increase in number of edge-on oriented crystallites at the film-

substrate interface, and reduction in interfacial area of contact between the crystallites due to the augment in grain sizes.[8, 74] It has been further proved by Kline *et al* using X-ray rocking scan analysis which is used to probe the orientation of the crystallites. They have reported that the OTS treatment can help to increase the edge-on oriented crystallites at the substrate-film interface than the HMDS.[8]

### 1.5.4 Processing Solvents

It is obvious that the nature of solvent can also impact the morphology of dried films. The formation of face-on oriented P3AT crystallites is attributed to the fast evaporation rate of the solvent during spin coating.[18] It has been solved by the researchers via processing the films using higher boiling point solvents.[12, 57, 76] Chang *et al* reported that the highly edge-on oriented crystallites can be prepared by spin coating using 1,2,4-trichlorobenzene (1,2,4-TCB) solvent as compared to $CHCl_3$.[12] In opposite, Yang *et al* reported that the P3HT thin film spin coated at 40°C by dissolving it in the $CH_2Cl_2$ solvent produces more face-on oriented crystallites than the one spin coated at RT. This observation proposes that the P3HT in $CH_2Cl_2$ starts to crystallize from a pre-seeded crystal on the "cold" substrate held at RT before the rapid solvent evaporation during spin coating.[16] Thin films cast from the higher boiling point solvents like toluene does not improve the mobility of OFETs as compared to the one cast using $CHCl_3$ because of their spherulitic grain boundary and the formation of small nanofibrils.[76] Also the morphology of the crystallites varies with respect to the solvents. For example, the P3BT thin film cast using $CS_2$ solvent produces the mixtures of both the edge- and flat-on oriented crystallites with whisker and spherulitic kind of morphologies, respectively.[55] Yan *et al* documented the formation of shish-kebab structure while casting the P3HT thin films using blended solvents (triethanolamine (TEA) and 1,2-Dichlorobenzene (DCB)) and the rate of formation of heterogeneous nucleation increases as the amount of poor solvent (TEA) increases.[77]

### 1.5.5 Epitaxial Growth

Directional epitaxial crystallization (DEC) of semicrystalline P3HT on the aromatic organic crystals is an elegant way to improve the crystallinity and orientation of the films because these substrates can direct the chain orientation along certain crystallographic directions of the substrate and it can act as a nucleating surface as well.[54] Brinkmann *et al* have been grown P3HT thin films epitaxially on the 1,3,5-TCB aromatic substrate.[35] The epitaxial crystallization of P3HT on 1,3,5-TCB has been performed in two steps; i) deposition

of 1,3,5-TCB powder on the spin coated or cast P3HT films and ii) dissolving the P3HT thin films by melting the 1,3,5-TCB with the help of a Koeffler bench and dragging it towards the colder part. During dragging, the 1,3,5-TCB undergoes solidification, consequently the concentration of P3HT can increase in the 1,3,5-TCB melt and it can lead to the supersaturation. Subsequently, P3HT can nucleate on the surface of 1,3,5-TCB and can proceed to grow.[35] Followed by Brinkmann *et al*, Jimison *et al* have fabricated OFETs out of epitaxially crystallized P3HT thin films and it shows the anisotropic charge transport along the dragging direction and perpendicular to it.[61] The detailed structural and morphological analysis performed by Brinkmann *et al* for various MW P3HT film epitaxied on the 1,3,5-TCB depicts that this technique is favorable for the low molecular weight (LMW) P3HT.[56] The detailed analysis performed by Brinkmnn *et al*[64] and Kline *et al* [63] on the MW dependent chain packing of P3HT shows the increase of tie-chain interconnection between the grains as the MW increases consequently, it increases the OFET performances. In addition, Brinkmann *et al* have also epitaxialized the P3HT on potassium 4-bromobenzoate (KBrBz) as well, for more details please refer the following articles.[15, 54]

### 1.5.6 Printing

Printing is a widely used technique for the fabrication of large area roll-to-roll (R2R) flexible electronic devices.[1] The smaller channel lengths in the range of 10 μm can be prepared based on the considerations from the motion control of printed drops. In order to increase the resolution achievable with standard printing heads, it is mandatory to control the flow and spreading of ink on the substrate. There are many printing techniques like pad printing, ink jet printing, and screen printing that are available, but ink jet printing is widely used.[1, 10, 78] It is a non-contact patterning method and it is free from the mechanical damages which can be occurred due to the direct contact of tools with the surface of the films. The ink jet printing typically ejects 1- 40 pL of droplet volume depending on the nozzle size and the driving waveform.[79] Droplets will be ejected sequentially to form a liquid pattern that dries down to the film. Thickness of the films ($t_{pr}$) can be calculated using the empirical formula given in equation 1.2.[10]

$$t_{pr} = N_d V_d \frac{c}{\rho_f} \quad 1.2$$

Here: $N_d \rightarrow$ number of droplets delivered per area ($cm^{-2}$)

$V_d \rightarrow$ volume of the droplets ($cm^3$)

$c \rightarrow$ concentration of the solid material in the ink (g $cm^{-3}$)

$\rho_f \rightarrow$ density of the material in the final film (g $cm^{-3}$)

There are still some challenges left like printing a line without any defects and controlling the sizes of the devices due to the spreading of droplets. It mainly depends on the viscosity, surface tension of the solution, droplet placement accuracy, etc.[1, 79] A comparative studies performed by Wong *et al* shows that the ink-jet printed film produces much rougher film at the insulator-P3HT interface as compared to the spin coated and drop cast films; consequently, the mobility of printed OFET is less than the spin coated and drop cast ones due to the trapping of holes at the grain boundaries.[78]

### 1.5.7 Casting

Casting is one of the simplest techniques available to produce large area thin films. The main advantage of this technique is that, it does not need any equipment apart from a very flat working surface. The casting procedure is very simple, just cast the polymer solution on the substrate surface and allow it to dry. It is possible to prepare thick films with good structural quality using this technique. It suffers from the fluctuation in density and layer thickness across the film and often picture framing effects are observed near the edges of the film or precipitation during drying as shown in Figure 1.8.[10] The cause of non-uniformity is due to the contact angle dependent supersaturation of the solution.[80] If the precipitation has to be avoided then there is a requirement that the polymer has to be thoroughly dissolved in the solvent being used.[10] The structural quality as well as the OFET performance of cast P3HT film is better than the one spin coated from the same solution.[9, 16] The lack of surface uniformity of cast thin films was improved by doctor blading technique.

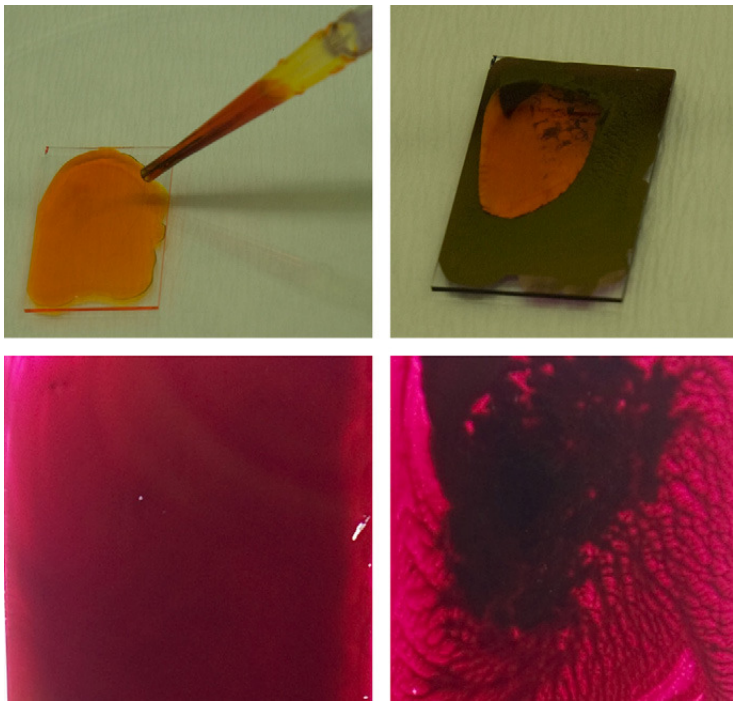

Figure 1.8: Shows the surface nonuniformities of cast polymeric thin films and the casting procedure (adopted from the reference [10])

### 1.5.8 Doctor Blading

Doctor blading is a modified form of casting technique. It helps to produce very thin and uniform films. The setup of widely used doctor blading technique is shown in Figure 1.9. Thickness ($t_{dr}$) of the final dry films can be calculated using the following formula[10]

$$t_{dr} = \frac{1}{2}\left(g\frac{c}{\rho_f}\right) \qquad 1.3$$

Here: g → the distance between the blade and the substrate

Casting is a slow growth process as compared to the spin coating technique because the growth will occur on a longer time scale due to reduced evaporation rate of the solvent. It can produce thermodynamically most stable crystallites as compared to the spin coating technique. Films prepared by doctor blading (casting) and spin coating often show face-on oriented crystallites which are not favorable for the in-plane charge transport in an OFET.[8, 81] The doctor blading technique has also <5% of solution losses during processing, comparatively it is much lesser than the spin coating technique. The doctor blading technique can be easily transferred to the R2R coating environment. It has a plus point over the spin coating technique like the production of highly crystalline, uniform, and large area thin films on the substrate.[81]

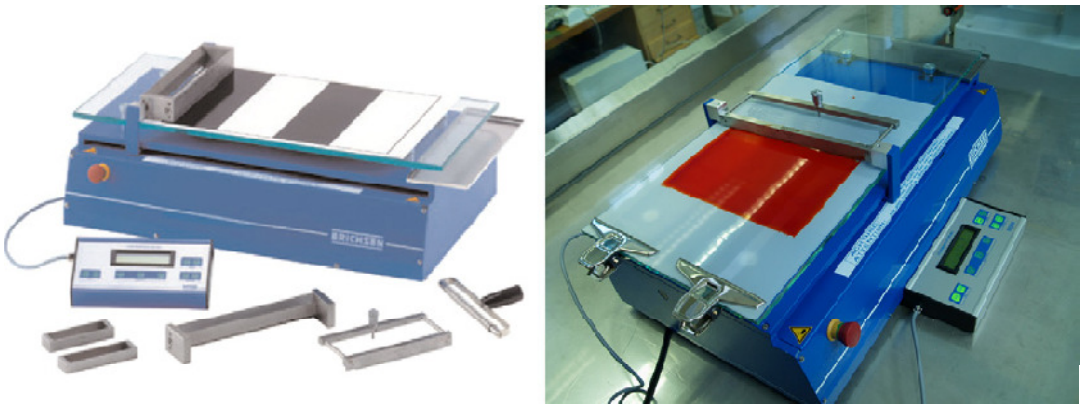

Figure 1.9: Shows the Erichsen Coatmaster 509 MC-I that can be used for doctor blading (left) and a photograph showing doctor blading of MEHPPV(right) (taken from the article [10])

- *Several strategies have been proposed by various researchers in order to improve the crystallinity as well as the orientation of polymeric thin films. The uniaxially edge-on oriented crystallites can be prepared by epitaxial crystallization but it requires high temperature and also multiple patterning steps which are inconvenient for the fabrication of cheap and flexible electronic devices. The substrate silanization has been found to be an elegant way to improve the orientation of the crystallites at the substrate-film interface. They often produce face-on oriented crystallites which are not favorable for the in-plane charge transport. The doctor blading technique is widely used by the industries but it also produces the mixtures of both the edge- and face-on oriented crystallites. The P3HT OFETs fabricated using higher boiling solvents via spin coating technique enhances the device performances due to the formation of more edge-on oriented crystallites, but 1,2,4-TCB is not environmental friendly as compared to the $CHCl_3$. Rather than the formation of edge-on oriented crystallites the interconnection between the crystalline domains and the crystallite sizes are also important for charge transport but they are absent in the film cast using toluene as compared to $CHCl_3$.[76] The spin coating and epitaxial crystallization techniques are mainly favorable for the LMW than the HMW P3ATs.[8, 56, 63] Some of the important parameters of thin films such as surface uniformity, crystallite orientation, crystallite size, and crystallinity can be well controlled by casting the film at below RT where one can control the evaporation rate of the solvent and supersaturation ratio of the solution. The theoretical background of solution processing and formation of nucleations will be explained in the following chapter II.*

# Chapter II

## 2 Importance of Low Temperature Casting

The solution processability of some of the conjugated conducting polymers is a treasure to the industry for the fabrication of cheap devices on flexible substrates. Even though there are some more challenges left like crystallizing and orienting the few nm long polymer molecules for the fabrication of high throughput devices. Especially, in-plane stacking of P3AT crystallites plays a vital role in the optical and electrical properties of the devices.[2] The crystallite size, crystallinity, and orientation of the films can be controlled by growth techniques i.e. controlling the supersaturation ratio, nucleation density, evaporation rate of the solvents, etc.[14, 82, 83]

### 2.1 Supersaturation

Supersaturation is a state where the solution contains an excess amount of solute than the solute that can be dissolved at a certain temperature. The supersaturated solution can be obtained in three ways; i) during the evaporation of solvent, ii) addition of extra solute, and iii) cooling the solution (positive soluble solutes).[83, 84] It is clearly shown in the phase diagram (Figure 2.1).[84] For example, supersaturation can be obtained by dissolving an excess amount of solute by increasing the temperature of the solution in case of positive soluble solute and then carefully returning back to the original state (by cooling). The temperature dependent equilibrium concentration ($C_e$) can be written as [83]

$$C_e = C_o e^{(-\lambda_{ss}/kT_e)} \qquad 2.1$$

Here: $C_o$ → constant

$\lambda_{ss}$ → enthalpy of solution per molecule

k → gas constant per molecule

T → absolute temperature

When the solution is cooled from a temperature $T_a$ to $T_b$ then the saturation ratio (α) can be written as

$$\alpha = \frac{C_a}{C_b} = e^{[\frac{\lambda_{ss}}{n}(\frac{1}{kT_b}-\frac{1}{kT_a})]} \qquad 2.2$$

'n' is the number of ions formed from one molecule of solute

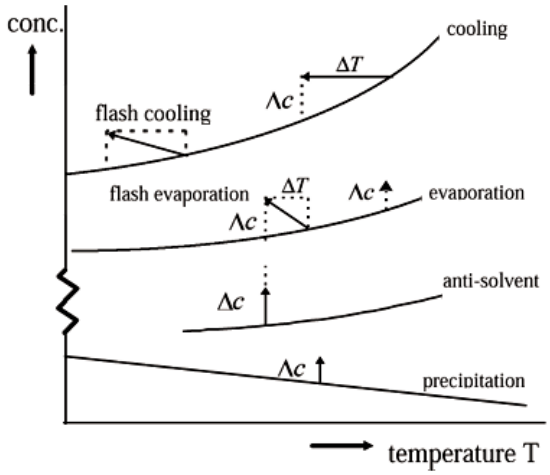


Figure 2.1: Methods for creation of supersaturation in crystallization from solution (adopted from the reference [84])

The driving force for condensation along the path '*ab*' is the free energy difference per atom $'G_\vartheta'$ between the concentration $C_e$ and $C_b$. The free energy of an atom or the molecule decreases with increase of solute concentration

$$G_\vartheta = -nkT_b ln\alpha \qquad 2.3$$

Substituting equation 2.2 in 2.3 yields

$$G_\vartheta = \frac{-\lambda_{ss}\,(T_a - T_b)}{T_a} \qquad 2.4$$

The equation 2.4 states that the saturated solution can be obtained by the addition of extra solute or by cooling. The solution is said to be supersaturated when the solution energy loss outweighs the entropy gain and no more solute particles can be dissolved. Once the supersaturation is set, then it can start to form a new phase called embryo and this process is called nucleation.

## 2.2 Nucleation

The process of nucleation describes the formation of a new phase in the mother phase.[85] It is a key factor for the growth of crystals from the gases and liquid phases. The instability of supersaturated solutions can cause them to crystallize because they are holding more solute than the amount that can be dissolved. The greater the degree of supersaturation, the greater will be the number of nuclei formations. Nucleating and controlling the rate of formation of nucleus are the crucial factors for controlling the final crystallite number, size, perfection, polymorphism, and other characteristics of thin films (or bulk).[82, 83]

Nucleation may occur spontaneously or it may be induced artificially, these two cases are frequently referred as homogeneous and heterogeneous nucleations, respectively. The primary nucleation will be used in both the cases (homogeneous and heterogeneous) where the systems that do not contain any crystalline phases. This classification can be represented as follows

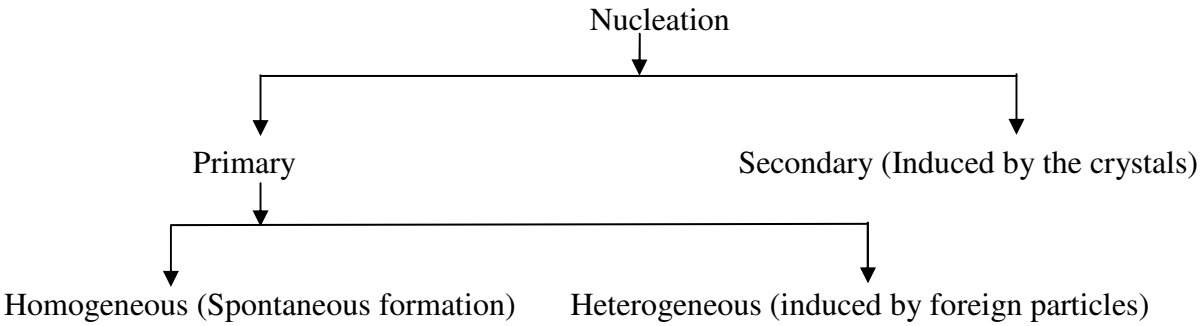


### 2.2.1 Homogenous Nucleation

The free energy of atoms or molecules decreases when the solution becomes supersaturated. As we know that the atoms or molecules are kinetically active when they are inside the mother phase and they will collide with one another. To some extent they collide inelastically where the atoms can stay together for a long time as compared to the case of elastic collisions. If a pair of atoms is stable then it can proceed to grow further by meeting the third atom. The clusters can move inside the mother phase and they can grow or shrink rapidly by adding or releasing the atoms. The stability of crystallites increases as their size increases. After reaching a certain size they are more stable and at this stage they are known as critical nucleus. A critical-sized nucleus is a cluster of a size such that its rate of growth is equal or greater than the rate of decay.[86] Clusters which fluctuate to a size larger than the critical size will probably continue to grow to a macroscopic size, the clusters which are smaller than the critical size most likely shrink.

The formation of solid particles in a liquid phase demands certain amount of energy. The change in free energy is balanced by the energy gain of creating a new volume and the energy cost for the creation of new interfaces. When the overall change in free energy (ΔG) is negative then nucleation is favored. Let us assume that the excess of free energy of an embryo is the addition of its surface and volume free energy. It can be written as follows [82]

$$\Delta G = \Delta G_s + \Delta G_V \qquad 2.5$$

Where $\Delta G_s$ and $\Delta G_V$ are the surface (positive quantity) and volume (negative quantity in a supersaturated solution) free energy of an embryo, respectively. Let us consider that the shape of an embryo is spherical of having radius "r", then the equation 2.5 can be written as

$$\Delta G = 4\pi r^2\sigma + \frac{4}{3}\pi r^3 G_\vartheta \qquad 2.6$$

Where σ is the crystal-solution interfacial tension and $G_\upsilon$ is related to the supersaturation or degree of cooling. The surface and volume free energy change during the formation of a nucleus as a function of its radius is shown in Figure 2.2.

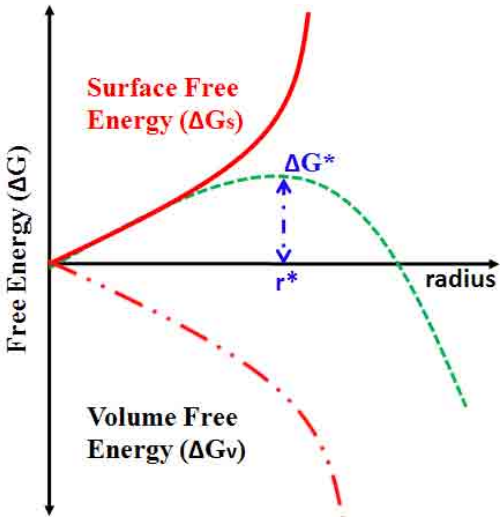


Figure 2.2: Free energy diagram of homogeneous nucleation

The function goes through the maxima at the critical size r = r*, which defines the critical nucleus. If the size is less than the critical nucleus then the nucleus becomes unstable and it can disintegrate. It costs more free energy to add an atom or molecule on the surface of the nucleus, $\frac{d\Delta G}{dr} > 0$; before it reaches the critical size and $\frac{d\Delta G}{dr} = 0$; when it reaches the critical size.

Differentiating the equation 2.6 with respect to 'r' implies

$$r^* = -\frac{2\sigma}{G_\vartheta} \qquad 2.7$$

The free energy formation of a critical nucleus can be obtained by substituting the equation 2.7 in 2.6

$$\Delta G^* = \frac{16\pi\sigma^3}{3(G_\vartheta)^2} \qquad 2.8$$

A greater the degree of cooling favors the phase transformation i.e. initiation of nucleation.[87] We can relate $r^*_c$ and $\Delta G^*$ with respect to the degree of cooling by substituting the equation 2.4 in equation 2.7 and 2.8, respectively

$$r^* = \frac{2\sigma T_a}{\lambda_{ss}(T_a - T_b)} \qquad 2.9$$

$$\Delta G^* = \frac{16\pi\sigma^3 {T_a}^2}{3{\lambda_{ss}}^2(T_a - T_b)^2} \qquad 2.10$$

The equation 2.9 and 2.10 shows that greater the cooling rate, lesser will be the critical nucleus size and it demands less energy to form a critical nucleus, respectively.

### 2.2.2 Heterogeneous Nucleation

The rate of nucleation can be considerably affected by the traces of impurities present in the mother phase. The nucleation catalyst or nucleant may be a solid particle suspended in the liquid or the surface of the container or a solid surface. This process is called heterogeneous nucleation. The formation of a cap shaped nucleus on the non-deformable substrate is schematically shown in Figure 2.3. The contact angle between the nucleus and the substrate is '$\boldsymbol{\Theta}$'.

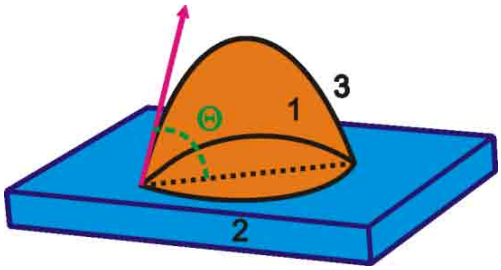


Figure 2.3: Schematic diagram of the formation of cap shaped heterogeneous nucleus

The free energy of formation of an embryo on the solid surface is (taking into account the net interfacial free energy terms and the volume free energy change)

$$\Delta G_{het} = \tfrac{4}{3}\pi r^3 G_\vartheta \left(\frac{2 - 3cos\Theta + cos^3\Theta}{4}\right) + 4\pi r^2 \left(\frac{1 - cos\Theta}{2}\right)\sigma_{13} + \pi r^2 sin^2\Theta(\sigma_{12} - \sigma_{23}) \qquad 2.11$$

Here: $\boldsymbol{\Theta}$ → the contact angle between the cap and substrate

$\sigma_{12}$ → the interfacial tension along the vertical direction between the liquid and substrate

$\sigma_{13}$ → the interfacial tension between the air and liquid

$\sigma_{13}$ → $\sigma_{12} + \sigma_{13}\cos\theta$

r → the radius of curvature of the drop

As we have derived for the homogeneous nucleation case, one can obtain the radius of the critical nucleus $r^*_{het}$ by applying the condition

$\frac{d\Delta G}{dr} = 0$ ; when the nucleus reaches its critical size

$$r_{het}{}^{*} = -\frac{2\sigma_{13}}{G_{\vartheta}} \qquad 2.12$$

The free energy needed for the formation of a heterogeneous critical nucleus can be obtained by substituting the equation 2.12 in 2.11 implies:

$$\Delta G^{*}{}_{het} = \frac{16\pi {\sigma_{13}}^3}{3{G_{\vartheta}}^2}\frac{(1-cos\Theta)^2\,(2+cos\Theta)}{4} \qquad 2.13$$

$$\phi(\Theta) = \frac{(1-cos\Theta)^2\,(2+cos\Theta)}{4} \qquad 2.14$$

The free energy of formation of a nucleus is lowered for all sizes by the multiplicative factor $\phi(\Theta)$ because of the embryo-substrate interaction. The curvature of the critical embryo is not affected and the Gibbs-Thomson equation is still valid for the critical nucleus.

### 2.2.3 Secondary Nucleation

The formation of nucleation in the vicinity of crystals present in the supersaturated system will be referred as secondary nucleation. The rate of formation of secondary nucleus is mainly depends on the degree of cooling, supersaturation ratio, and the type of crystal which is formed when a small nuclei develop but it is independent on the number, size, surface characteristics, and chemical nature of a parent crystal.[88]

- *According to the equation 2.9, the critical size of a nucleus can be varied by changing the growth temperature or by increasing the solute concentration. By taking this equation into account, a low temperature growth technique will be applied to the P3AT polymers because it has two important effects on the growth of the crystallites; i) crystallite size and*

*density of nucleation can be controlled by choosing the appropriate cast temperature and concentration, ii) reduction in cast temperature can help to increase the growth time by reducing the evaporation rate of the solvent. The experimental details are given below*

## 2.3 Experimental Details of Thin Film Preparation

The crystallization of HMW P3AT polymers is a crucial step for the fabrication of flexible electronic devices because it is one of the working host p-type materials for the fabrication of solar cells with the combination of PCBM, F8TBT, etc.[31, 40, 41] The poor crystallinity of HMW P3AT polymers are due to chain entanglement as well as the augment in plasticity of thiophene backbones.[64] In this thesis, I have focused the analysis towards the crystallization of HMW P3AT polymers such as poly(3-pentylthiophene) (P3PT), P3HT, poly(3-heptylthiophene) (P3HeptT), and poly(3-octylthiophene) (P3OT) because of their good electrical performances as compared to the LMW P3ATs.[63] The HMW RR-P3AT polymers were synthesized by our collaborators from the University of Wuppertal.

### 2.3.1 Synthesis of P3AT Polymers

The HMW P3AT polymers such as P3PT, P3HT, P3HeptT, and P3OT with >99% RR were synthesized according to the known reactions from the literature. Ahead of the polymerization, the 3-bromothiophene was alkylated using n-Butyllithium (n-BuLi) and the corresponding alkyl bromide.[89] The next step is dibromination with N-Bromosuccinimide (NBS) in N,N-Dimethylformamide (DMF) at RT.[51] The monomer was then polymerized via the Grignard metathesis scheme (GRIM) as reported by Loewe *et al*.[52]

| Polymers | Molecular Weight (kg/mol) | Melting Point (±2˚C) | Polydispersity Index | Average Number of Monomers per Polymer |
|---|---|---|---|---|
| P3PT | 36.0 | 249.4 | 1.5 | 236 |
| P3HT | 44.9 and 76.4 | 229.3 | 1.2 | 270 and 459 |
| P3HeptT | 42.5 | 205.7 | 1.2 | 235 |
| P3OT | 38.8 | 184.1 | 1.5 | 195 |

Table 2.1: Summarizes the molecular weight, melting point, average number of monomers per polymer unit, and polydispersity index of the undertaken P3AT polymers

The RR and melting point of the as-synthesized polymers were analyzed by NMR and the differential scanning calorimetric (DSC) analyses, respectively. The melting point and polydispersity index (PDI) of the polymers are given in Table 2.1. The MW of P3HT was

varied during the analysis because the well known P3HT was used to optimize the growth conditions, so it has been synthesized twice. The as-synthesized polymers are readily soluble in common organic solvents like $CHCl_3$, toluene, xylene, etc. Prior to the film preparation step, P3AT solutions were freshly prepared.

### 2.3.2 Solution Preparation

Mainly two different concentrations like 2mg/ml (high) and 1mg/14ml (low) that were used to prepare thin films having different thicknesses at around 400 nm and 40 nm, respectively. The thicknesses of the films were measured using atomic force microscopy (AFM) and X-ray reflectivity techniques. It will be discussed more elaborately in chapter III. The corresponding amount of $CHCl_3$ was added to the weighed P3AT polymers and then stirred for 4 - 5 hrs in a small closed vial at 50°C. The as-prepared solutions were subjected to ultraviolet-visible spectroscopy (UV-Vis) analysis for the confirmation of complete dissolution of P3AT polymers where one can distinguish the absorption peaks corresponds to the amorphous and the aggregate phases.[65, 90] The freshly prepared solutions were cooled to the desired growth temperature and then the films were spin coated and cast on the cleaned $Si/SiO_2$ substrate under various conditions.

### 2.3.3 Substrate Cleaning

Heavily doped n-type Si (100) oriented substrates were subjected to thermal oxidation process in order to produce nearly 300 nm thick $SiO_2$ dielectric layer on the surface of the wafers. Thermally oxidized $Si/SiO_2$ wafers were purchased from the Silchem Company. The wafers were cut into small pieces having sizes 2.5x2.5 $cm^2$. The substrates were cleaned by sonication process, at first with diluted hellmanex®II (Hellma GmbH) at 60°C and then rinsed with 2-propanol, acetone, and distilled water. The cleaned substrates were dried at 150°C and blown with dried $N_2$ gas. Some of the cleaned substrates were coated with SAM by immersing into the OTS (purchased from Merck) solution (1 ml of OTS was dissolved in 10 ml of $CHCl_3$). Prior to the film preparation step, the OTS deposited substrates were successively rinsed with hexane and 2-propanol and then dried with blowing dry $N_2$.

### 2.3.4 Thin Film Preparation

Thin films were prepared using two well known techniques such as drop casting and spin coating in order to correlate their structural properties with electrical and optical properties.

### 2.3.4.1 Casting

Thin films were cast under $N_2$ ambient conditions in order to avoid two things, i) oxidation of P3ATs and ii) to avoid the condensation of humidity on the substrate while casting below RT. After mounting the cleaned substrate inside the growth chamber, the chamber was purged with $N_2$ gas. Prior to dropping, the whole chamber was placed inside the refrigerator. The temperature of the chamber was readout using a resistance thermometer (PT100). After the desired temperature was reached, around 250 µl solution was dropped on the substrate and then allowed to dry at 1 bar $N_2$ pressure. The setup which has been used to cast the P3AT thin films at various temperatures is shown in Figure 2.4. Prior to the dropping, the solution was thermalised for 10 minutes at the respective cast temperature. Thin films were prepared at different temperatures like 23°C, 8°C, -12°C, and -30°C in order to understand the growth temperature dependent enhancement in crystallinity and orientation of the films. Thin films were also cast at -30°C and RT by varying the concentration of a well studied P3HT solution in order to optimize the concentration. It varies with respect to the polymer, 1 mg/14 ml was found to be the optimum concentration. Further reduction in concentration of P3OT does not yield uniform thin films while casting at -30°C due to its high solubility.

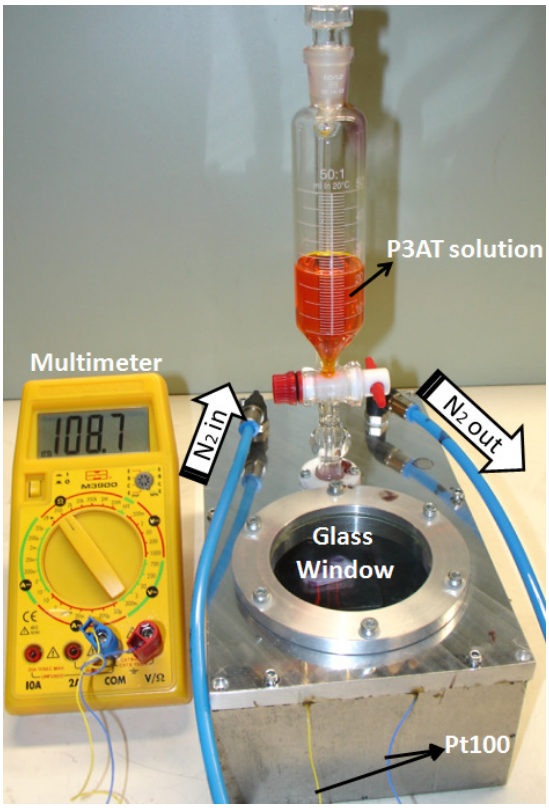


Figure 2.4: The chamber that has been used to drop cast P3AT thin films at various temperatures

### 2.3.4.2 Spin Coating

Nearly 17 nm thin films were spin coated using the concentration of 2mg/ml. The angular velocity and spinning time of the spin coater were fixed at 2000 rpm and 30 seconds, respectively. Thin films were spin coated under ambient conditions using the SÜSS$_+$MicroTec spin coater (Figure 2.5). During spinning, the substrate has been mounted on the substrate holder against the centrifugal force using a sucking unit assisted with the spin coater.

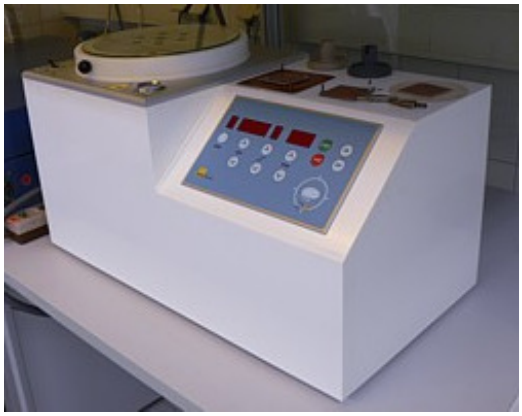

Figure 2.5: SÜSS$_+$MicroTec spin coating unit

### 2.3.4.3 Annealing Analysis

A set of drop cast and spin coated P3AT films were annealed at an undercooling of 45°C (see Table 2.1). The annealing time and temperature of the polymers were optimized by performing the *in situ* grazing incidence X-ray diffraction (GIXD) analysis during annealing. The experimental details of the annealing procedure will be explained in chapter III. In addition, different temperature cast P3HT thin films were annealed at 100°C, 150°C, and 200°C in a glass oven under $N_2$ ambient conditions.

- *The enhancement in crystallinity and orientation of the as-cast and annealed films were studied using X-ray and transmission electron microscope (TEM). The mobility of charge carriers and luminescence intensity of the low-temperature cast P3AT films are increased due to the enhancement in interchain stacking of the crystallites. The theoretical background and the experimental details of these techniques will be explained in chapter III.*

# Chapter III

## 3 Characterization Techniques and Experimental Details

X-ray and electron diffraction techniques are widely used for the structural investigations of P3AT thin films.[8, 15] The TEM has been usually used to bridge the structural and morphological properties of polymeric thin films with their optical and electrical characteristics.[67, 76, 91] So, it is mandatory to understand the growth technique dependent variation in structure and morphology of P3AT thin films for the fabrication of high throughput devices with their ultimate morphologies.[8, 67]

### 3.1 X-ray Analysis

X-ray is an electromagnetic wave which is mainly used to probe the structural properties of matter. X-ray beam can interact with the matter elastically or inelastically as shown in Figure 3.1.[92, 93] That's why X-rays are widely used in different fields like structural analysis of crystalline materials, medicine, imaging, elemental composition analysis, etc. X-ray is an electromagnetic radiation and it is convenient to describe them in terms of energy. X-rays are classified into two categories with respect to their energies and the distinction is not well defined; i) hard X-rays are in the range of ≈5 to 120keV (2.48 to 0.1Å) and ii) soft X-rays are in the range of ≈20eV to 5keV (620-2.48Å).

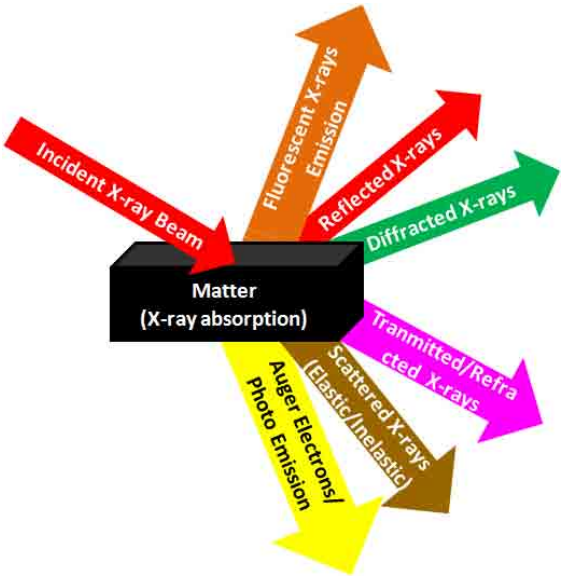


Figure 3.1: Illustrates the interaction of X-rays with matter

In this thesis, the structure of P3AT thin films was analyzed using hard X-rays produced at the home lab by copper and molybdenum X-ray tube sources (8.05 and

17.46keV) and the synchrotron radiation sources (15.5 and 8keV). Mainly two techniques were used such as X-ray reflectivity (XRR) and X-ray diffraction in order to estimate the thickness, roughness, electron density, crystalline perfection, orientation of the crystallites, crystallite sizes, etc.[92-94]

### 3.1.1 X-ray Reflectivity

X-ray reflectivity is a nondestructive technique used to probe the thickness, roughness, and electron density of thin films.[92] XRR technique is widely used for the analysis of multilayers to find out their interfacial roughness, periodicity, average electron density, etc. by simulating the measured profiles.[94-96] For the accurate determination of electron density of matter, the X-ray diffractometer demands of much better angular resolution and monochromatic radiation. The geometry of X-ray reflectivity technique is shown in Figure 3.2. In this method the diffractometer is operated in a symmetric configuration ($\alpha_i = \alpha_f$).

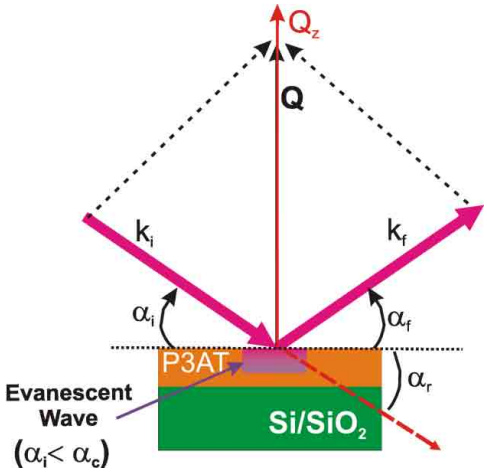


Figure 3.2: A schematic diagram of X-ray reflectivity technique and the penetration of X-rays as an evanescent wave when $\alpha_i < \alpha_c$

X-ray is an electromagnetic wave, so we have to consider the refraction phenomena between two different mediums. As per definition, the refractive index of vacuum is one. For X-rays, refractive index is in the order of $1 - 10^{-5}$. The refractive index of materials in the X-ray range can be expressed as [92]

$$n = 1 - \delta + i\beta \qquad 3.1$$

Here, $\delta$ is in the order of $10^{-5}$ in solid materials and around $10^{-8}$ in air. The imaginary part '$\beta$' is much smaller than the $\delta$ at this range. Snell's law relates the incidence angle '$\alpha_i$' to the refracted angle '$\alpha_r$' through the equation 3.2 [92]

$$cos\alpha_i = ncos\alpha_r \qquad 3.2$$

The total external reflection of X-rays can occur when $\alpha_i \leq$ critical angle ($\alpha_c$) of the matter due to the fact that the index of refraction is less than unity.[92] When the angle of incidence is greater than the critical angle then the X-rays can start to penetrate deeper into the medium. The total external reflection will occur when $\alpha_r = 0$, by expanding equation 3.2 yields

$$\alpha_c = \sqrt{2\delta} \tag{3.3}$$

The δ depends on the scattering properties of materials such as density of electrons (ρ), classical electron radius ($r_0 = 2.82 \times 10^{-5}$ Å), and wave vector ($k = \frac{2\pi}{\lambda}$). It can be expressed as follows

$$\delta = \frac{2\pi\rho r_0}{k^2} \tag{3.4}$$

It would be possible to calculate the electron density of materials using the relation 3.5 when the critical angle of that material is known from the XRR profile. It can be obtained by substituting the equation 3.4 in 3.3.[92]

$$\alpha_c = \frac{\sqrt{4\pi\rho r_0}}{k} \tag{3.5}$$

The X-ray reflectivity profile contains mainly three important messages such as; i) critical angle (used to calculate the average electron density of the films), ii) Kiessig fringes (used to extract the thickness of the films), and iii) roughness (which corresponds to the slope of the curve). The reflected intensity decays faster as the roughness increases.[92, 95, 97] It can be quantified by simulating the reflectivity profile using software such as Parratt32.[98]

The Kiessig fringes are formed due to the inference of X-rays reflected from the top and bottom interfaces of the layer. The thickness of the films can be estimated using the following relation 3.6.[92]

$$t = \frac{2\pi}{\Delta Q_z} \tag{3.6}$$

Here: $Q_z$ is the momentum transfer vector

$$Q_z = \frac{2\pi sin2\theta}{\lambda} \tag{3.7}$$

and

$$2\theta = \alpha_i + \alpha_f \tag{3.8}$$

$\Delta Q_z$ can be obtained from the difference between two consecutive maxima (crests) of fringes which can be obtained from the XRR profile which plots intensity versus $Q_z$. The θ (or $\alpha_i$) is the angle between the incoming beam and surface of the film (Figure 3.2).

When the angle of incidence is smaller than the critical angle then the X-ray undergoes total external reflection (the reflection is almost 100%). Under such a condition, X-rays can penetrate into the material as an evanescent wave (Figure 3.2) and its amplitude decays rapidly in the material. The evanescent wave can penetrate only a few nanometers into the medium and it moves parallel and close to the surface.[92] So, it is generally used for the analysis of surface of materials. It can be used to analyze the depth dependent packing of materials under GIXD geometry by varying the $\alpha_i$.[99, 100]

### 3.1.2 X-ray Diffraction

X-ray diffraction in a crystal occurs due to the combination of two different phenomena; i) scattering of X-rays by individual atoms, and ii) interference of the X-rays scattered by these atoms.[93] The elastically scattered (Thompson scattering) X-rays are used for the structural analysis of matter. The scattering amplitude of an atom is proportional to the atomic number (Z) of an atom times the amplitude of waves scattered by an electron. It would be valid only when all the electrons from a single atom scatters in the same direction as well as in phase.[99] So, the scattering amplitude of an atom can be derived using the classical model. The scattered intensity of an atom is proportional to the number density of electrons (ρ(r)) and the phase difference between the scattered wave from a volume element around the origin and one around 'r' is '–k´.r.' The resulting phase difference is thus [92]

$$\Delta\phi(r) = (k - k').r = Q.r \qquad 3.9$$

As illustrated in Figure 3.3a, when the scattering is elastic, with |k| = |k´|, the volume element (dr) at (r) will contribute an amount $-r_0\rho(r)dr$ to the scattered field with the phase factor ($e^{iQ.r}$). The total scattering length of an atom is [92]

$$-r_0 f^0(Q) = -r_0 \int \rho(r) e^{iQ.r} dr \qquad 3.10$$

Here: $f^0(Q) \rightarrow$ the atomic form factor

When Q tends to 0, then all the different volume elements will scatter in phase so that $f^0(Q=0) = Z$. As Q increases the volume elements will start to scatter out of phase; consequently, $f^0(Q \rightarrow \infty) = 0$.

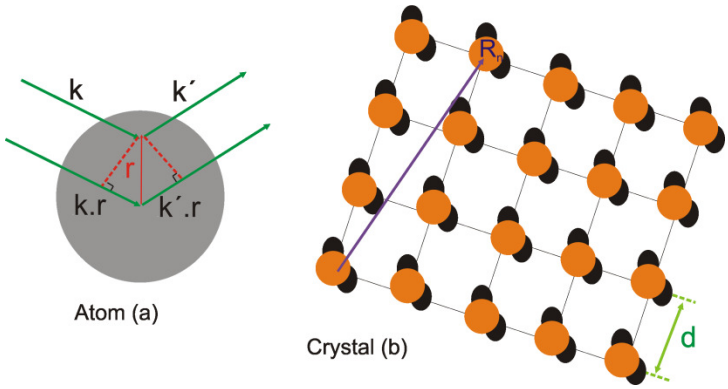


Figure 3.3: The elastic scattering of X-rays from (a) an atom and (b) a crystal which contains the lattice spacing'd'

The molecules are composed of atoms. The scattering length of a molecule can be written by labeling the different atoms in the molecule index 'j'

$$F^{mol}(Q) = \sum_{r_j} f_j(Q) e^{iQ.r_j} \qquad 3.11$$

Where $f_j(Q)$ is the atomic form factor of $j^{th}$ atom in the molecules, and one should remember to include the multiplicative factor of $-r_0$, if the intensity is required in absolute units.

In crystals, the atoms or molecules are arranged in a periodic fashion. So, the diffracted X-ray will consist of sharp interference maxima with the same symmetry as in the distribution of atoms in the crystals. As shown in Figure 3.3b, in crystals, the molecules or the atoms form a set of planes with the interplanar distance (d), the diffraction condition of such a set of planes can be explained by the formula proposed by W.L.Bragg in 1913 [101]

$$2dsin\theta = n'\lambda \qquad 3.12$$

Here: $n'$ is an integer and θ is the Bragg angle (some places it will be denoted by $\theta_b$)

The total scattering amplitude of a crystal is the product of two terms and it can be written as

$$F^{crystal}(Q) = \overbrace{\sum_{r_j} f_j(Q) e^{iQ.r_j}}^{\text{Unit cell structure factor}} \overbrace{\sum_{R_n} e^{iQ.R_n}}^{\text{Lattice sum}} \qquad 3.13$$

$R_n$ is the lattice vector that define the lattice, and $r_j$ is the position of the atoms with respect to any one particular lattice site, then the position of any atom in a crystal is given by $R_n+r_j$.

The equation 3.13 clarifies that the total scattering intensity of a crystal depends on its electron density and thickness. X-ray diffraction technique has been widely used to probe the structural quality of materials, lattice spacing, crystal structures, phase transitions, etc.[13, 59, 92, 93] In order to understand the structural properties of P3AT films, well known X-ray diffraction analysis was carried out under various geometries and it will be discussed elaborately in the following subchapter.

During X-ray diffraction analysis, the direction of momentum transfer vector 'Q' will be determined by the incident and the scattered X-ray beam vectors. Mainly two geometries such as X-ray specular (θ/2θ) and GIXD are widely used for the structural analysis of the crystallites which are sensitive to various crystalline planes (aligned perpendicular to the momentum transfer vector).

### 3.1.2.1 X-ray Specular Scan

Normally, X-ray specular scan is used to probe the crystalline planes which are aligned parallel to the substrate plane, in other words perpendicular to the momentum transfer vector ($Q_z$) as shown in Figure 3.4. The sample will be placed on the centre of the goniometer and then the X-ray beam will be directed on the surface of the sample with an angle $\alpha_i$ and the detector monitors the scattered beam. During the scan, both the incoming beam and the detector will move with the same angle ($\alpha_i = \alpha_f$); consequently, the Q vector stays parallel to the substrate normal vector $Q_z$ as shown in Figure 3.4. This scan is also called as θ/2θ scan. This technique is mainly used for the structural analysis of single crystals, epitaxial films, and polycrystalline samples.

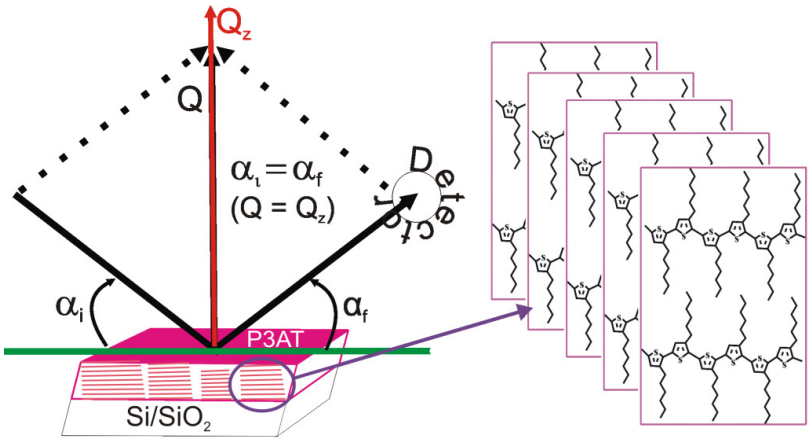


Figure 3.4: Illustrates the scanning geometry of X-ray specular scan and the corresponding probing planes which are aligned perpendicular to the momentum transfer vector $Q_z$

The scanning geometry of X-ray specular scan is schematically shown in Figure 3.4. The specular scan has been used for the detailed understanding of P3AT crystalline planes

which are aligned parallel to the substrate plane as shown in the right side of Figure 3.4. The scattering intensity will be plotted with respect to the movement of the detector (2θ) which is dependent on the wavelength of X-ray being used. Various X-ray sources were used for the structural analysis of P3AT thin films therefore, all the plot profiles are presented in Q space. The scattering angles can be converted into the momentum transfer vector ***(it will be denoted as $Q_z$ for the specular and reflectivity scans)*** using the relation 3.7

### 3.1.2.2 Grazing Incidence X-ray Diffraction

GIXD is widely used to understand the depth dependent structural analysis of thin films by varying the incidence angle of the incoming X-ray beam.[13] When the angle of incidence is less than the critical angle of the film ($\alpha_i < \alpha_c$) then the X-ray can penetrate a few nanometers as an evanescent wave. In such a case, thin film is mainly visible to the X-ray than the substrate. The intensity of evanescent wave is higher at the surface of the film and it scatters much from the surface. It is possible to increase the surface sensitivity further by reducing the incidence angle. The depth dependent structural properties, surface-induced disorder, phase transitions, and surface chemical reactions can be studied by varying the $\alpha_i$.[96, 102, 103] It would be possible to enhance the scattering intensity of the films by choosing the $\alpha_i$ in between the critical angle of the film ($\alpha_{cp}$) and the critical angle of the substrate ($\alpha_{cs}$). As the $\alpha_i$ increases, the penetration depth of X-ray increases, it can penetrate around 0.1 mm to 10 mm with respect to the energy of the incoming beam, density of the materials, and absorption in the medium. It can be mathematically expressed as follows [92]

$$\Lambda(q) = \frac{1}{Q_c Im(q')} \tag{3.14}$$

The complex q´ can be derived from the equation 3.15

$$q^2 = q'^2 + 1 - 2ib_\mu \tag{3.15}$$

$b_\mu$ is related to the absorption coefficient $\mu$ through

$$b_\mu = \left(\frac{4\pi}{\lambda Q_c}\right)^2 \frac{\mu\lambda}{4\pi} = \frac{4\pi}{{Q_c}^2}\mu \tag{3.16}$$

The momentum transfer vector $Q_c$ at the critical angle is

$$Q_c = 4\sqrt{\pi\rho r_0\left(1 + \frac{f'}{Z}\right)} \tag{3.17}$$

Here $q' \equiv \frac{Q'}{Q_c} \cong \left(\frac{4\pi}{\lambda Q_c}\right)\alpha'$ ; $q \equiv \frac{Q}{Q_c} \cong \left(\frac{4\pi}{\lambda Q_c}\right)\alpha$ ; f′ is the dispersion correction and it can be obtained from standard sources like international tables for crystallography.

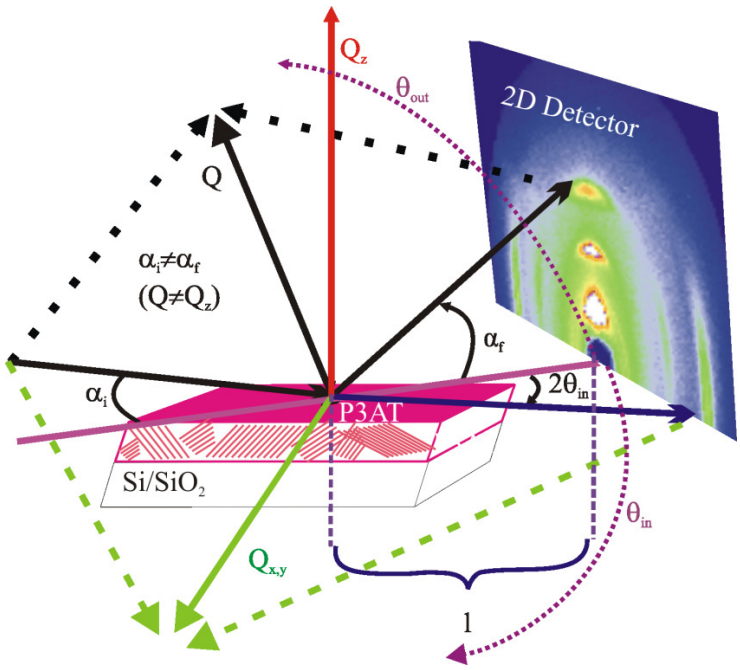


Figure 3.5: Illustrates the scanning geometry of GIXD and the corresponding probing in- and out-of plane directions and their momentum transfer vectors $Q_{x,y}$ and Q

Nowadays, GIXD is widely used for the analysis of organic and inorganic thin films but it has the following drawbacks; i) it works well for smooth surfaces (X-rays can get lost due to total external reflection when the long-range and short-range variation in the surface normal is nearer to the critical angle of the films) and ii) part of the incoming X-ray beam can get lost due to an increased foot print because of less incidence angle and beam size. The corresponding GIXD geometry is shown in Figure 3.5. Here $\alpha_i$ is fixed and the detector will move along its own axis consequently, the momentum transfer vector will also move gradually and it will probe the planes which are aligned perpendicular to Q. It is an asymmetric scan because the angle of incidence and the angle of exist will not be the same. Therefore, mainly thin films with randomly distributed crystallites and asymmetric planes are used to analyze using this technique.[103] The structural investigations of P3AT thin films were mainly encountered under GIXD geometry combined with a 2D detector.[13, 16]

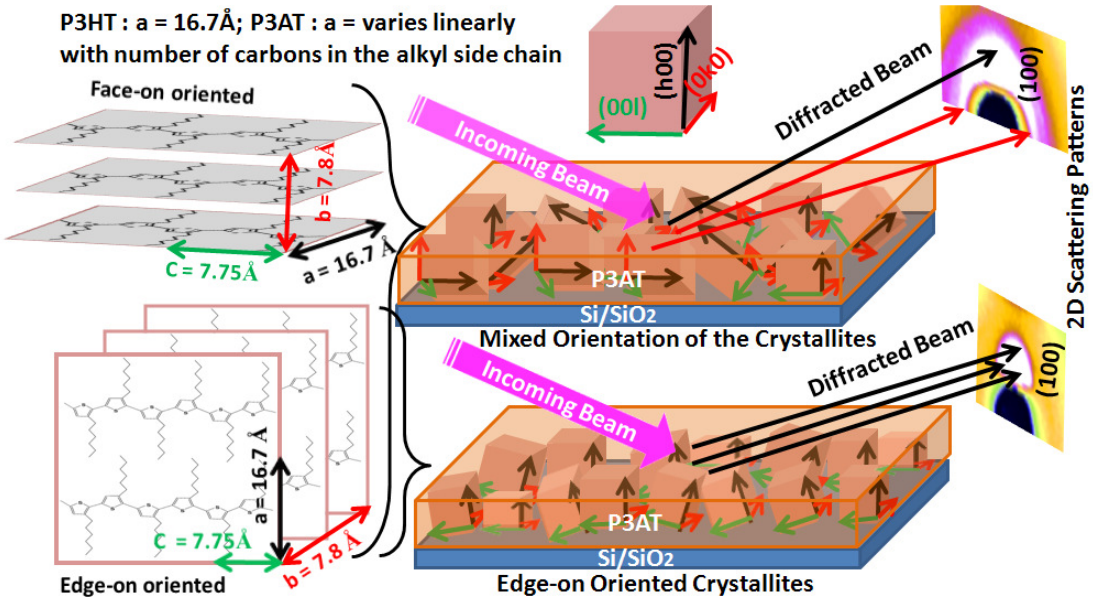


Figure 3.6: Illustrates the separation of face-and edge-on oriented crystallites from the diffraction patterns of P3AT thin films

It would be possible to recognize the face- and edge-on oriented crystallites from the 2D X-ray diffraction pattern because of their difference in scattering directions as shown in Figure 3.6. The face- and edge-on oriented crystallites present in the films can be separated by the black arrows which are aligned parallel and perpendicular to the substrate plane, respectively. When the film contains face-on oriented crystallites then the alkyl side chains will lie parallel to the substrate plane. Eventually it will diffract along the in-plane direction as shown in Figure 3.6. The red colored arrows represent the diffracted signal which comes from the face-on oriented crystallites and the black color represents the edge-on oriented crystallites. If the film is composed of only edge-on oriented crystallites then the (h00) planes will diffract only along the out-of-plane direction (Figure 3.6). The GIXD scan enables simultaneous measurements of both the grazing incidence out-of-plane (GOD) and in-plane (GID) diffraction patterns. It would be possible to extract both the GID and GOD profile from the 2D diffraction pattern by taking a line profile along in- and out-of-plane directions, respectively.[8, 16]

### 3.1.2.3 Grazing Incidence Out-of-plane Diffraction

GOD technique is widely used to understand the crystallites which are stacked along the out-of-plane direction. Here the incoming beam will be fixed and the detector will move along the $\theta_{out}$ circle as schematically shown in the Figure 3.5. During GOD scan, the Q vector will never be parallel to the surface normal except at only one angle when the angle of exit is

equal to the angle of incidence. It always probes the crystallites which are randomly distributed. This technique is mainly used for the analysis of powder like samples and thin films because of its surface sensitivity as stated earlier. During the scan, the scattered intensity will be plotted with respect to the detector movement. This can be converted into momentum transfer vector using the relation 3.18.[13] All the GOD graphs presented in this thesis were plotted intensity versus Q.

$$Q = \frac{2\pi\ (sin\alpha_i + sin\alpha_f)}{\lambda} \qquad 3.18$$

### 3.1.2.4 Grazing Incidence In-plane Diffraction

The in-plane diffraction occurs from the planes which are aligned perpendicular to the substrate plane. The in-plane stacking of the films can be analyzed under transmission geometry but the substrate must be transparent or the film must be peeled out from the substrate but it is very difficult to peel out and handle the ultra thin films. The in-plane stacking of the crystallites can be studied using GID scan. It mainly avoids the scattering from the substrate and it does not necessitate of transparent substrates. It would be possible to calculate the in-plane lattice spacing and crystallite size due to the fact that the momentum transfer vector of the in-plane scan ($Q_{x,y}$) will lie in the same x,y plane like the incoming beam as shown in Figure 3.5.

Similar to the GOD, GID profile can be obtained by moving the detector along $\theta_{in}$ circle (close to the surface plane) after fixing the incidence angle. GID scan probes the lattice spacing of the vertically inclined lattices. Similar to GOD scan, GID is also a surface sensitive diffraction technique and it can be performed by varying the $\alpha_i$. The scattered intensity of the films will be very weak because of the thickness of the films. Mainly, GID analysis was performed for the ultrathin films using synchrotron radiations.[96] Rather than probing the out-of-plane stacking of P3AT edge-on oriented crystallites, their in-plane stacking analysis is also mandatory in order to correlate with their electrical and optical performances.[7, 49] The in-plane momentum transfer vector at fixed $\alpha_i$ (if $\alpha_i$ is very small) can be expressed as [13]

$$Q_{x,y} \approx \frac{2\pi}{\lambda}\sqrt{1 + cos^2\alpha_f - 2cos\alpha_f\ cos2\theta_{in}} \approx \frac{4\pi sin\theta_{in}}{\lambda} \qquad 3.19$$

- *The orientation of the crystallites can be quantified only by combining X-ray diffraction phenomenon with the other motors like 'ψ' and 'ω' in order to probe the azimuthal distribution and lateral orientation of the crystallites, respectively.*

### 3.1.3 Azimuthal ψ Scan

High degrees of ordering in semicrystalline polymers are mandatory for the enhanced performances of electronic devices like solar cells, thin film transistors, etc.[7, 8, 53, 65, 74] Azimuthal scan is used to understand the relationship between the film processing and orientation of the crystallites. For azimuthal ψ scan, a Bragg peak will be chosen which has a strong scattering intensity, less signal-to-noise ratio, and far from the direct beam in order to avoid the background air scattering.[104] It is a viable technique to understand the distribution of crystallites in the film and to compare it with their electrical and optical performances. This technique has been mainly used for the detailed understanding of crystallite distribution of the solution processed organic thin films.[16, 76]

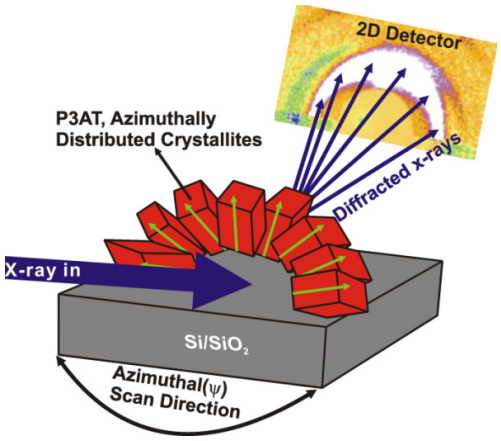


Figure 3.7: Schematic illustration of azimuthal distribution of the crystallites and their corresponding diffraction pattern

The corresponding azimuthal scanning geometry is shown in Figure 3.7. It can be combined either with GIXD or specular scan.[104] Azimuthal distribution of the crystallites can be extracted using the specular scan by rotating the sample azimuthally after fixing the incidence beam and the detector at the Bragg angle of the corresponding peak which we are interested in. It would be also possible to extract the azimuthal ψ profile from the 2D scattering pattern using the appropriate software after performing the background subtraction. The azimuthal profile extracted from the 2D pattern of spin coated P3HT films by Yang *et al* helps to understand the misorientation of edge- and face-on oriented crystallites with respect to the preparation conditions.[16] This technique is simple, efficient, and applicable to any thin films containing microstructures. Such measurements can be used to improve the orientation of the crystallites by optimizing the growth conditions.

### 3.1.4 X-ray Rocking Scan

X-ray rocking curves are widely used to analyze the crystallite orientation, lateral crystallite sizes, defects (stress) present in the crystals, etc.[96, 105] Rocking scans can be performed either by rocking the sample or by rocking the incoming beam and the detector together after fixing the incoming beam and the detector at the Bragg angle of corresponding peak as shown in Figure 3.8. The width of a rocking curve is a direct measure of the range of orientation and to a lesser extent, the amount of strain present in the area of investigated crystals.[8, 74] The FWHM of a rocking curve can be used to extract the lateral crystallite size ($L_{lat}$).[105] Peaks from the individual blocks often can be resolved in a rocking curve.[99] The integrated intensity of a rocking curve is greater compared to the specular scan because many more individual crystallites will have an opportunity to diffract.

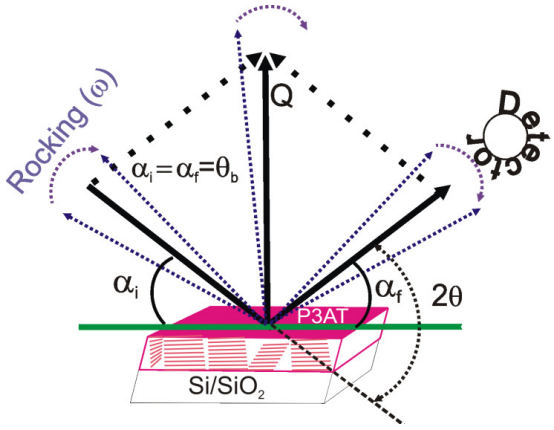


Figure 3.8: Geometry of X-ray rocking scan

Together with the specular and GIXD scan, X-ray rocking scan has started to play a vital role for the detailed understanding of orientation of semicrystalline polymer crystallites due to the evolution of different polymer crystallization processes.[8, 11, 74] Especially, X-ray rocking curves are used for the visualization of enhancement in film-substrate interfacial ordering of P3HT and PBTTT-C12 polymers while spin coating them on the SAM treated substrate and to correlate with their OFET performances.[8, 74] In this research work, X-ray rocking scan was used to understand the enhancement in orientation of P3AT thin films while reducing the cast temperature and concentration.

### 3.1.5 Synchrotron Radiation Source

Synchrotron radiation is the name given to the radiation which occurs when charged particles like electrons or positrons moving at relativistic velocities are deflected along a curved trajectory by a magnetic field. It can emit a very broad spectrum, ranging from the far

infrared till hard X-rays.[92, 99] Synchrotron radiation sources can produce $10^{12}$ times brighter X-rays than the lab based sources.[92] The high flux produced by the synchrotron sources are indispensable tools to study the surface of the matter, monolayers, and ultrathin films even though the scattering of the monolayers are weak. Such powerful sources have been used for the wide range of structural investigations and brought advances in numerous fields of science and technology. The structural investigation of spin coated P3AT polymers were performed using synchrotron sources due to their poor crystallinity.[8, 13, 53]

## 3.2 Experimental Set-up of X-ray Scattering Techniques

X-ray diffraction analysis was performed at different synchrotron and lab sources in order to probe the structural quality of P3AT thin films. The measurements were performed at the home lab using the high resolution Seifert XRD 3003 PTS HR and STOE Theta/Theta diffractometer combined with a point detector. In the home lab, X-ray radiations were produced using Cu and Mo X-ray tubes. The synchrotron radiations were used from different German synchrotron sources like DELTA (BL9) and PETRA III (P08). GIXD technique is widely used to understand the structural properties of P3AT films. A 2D image plate detector (MarCCD) has been used at BL9 for recording the 2D scattering pattern of the films. A 2D detector was used to probe the in-plane and out-of-plane scattering patterns as well as their azimuthal distribution of the crystallites simultaneously without scanning the detector. The sample to detector distance (l) and $\alpha_i$ were not kept constant because of the variation in X-ray wavelength with respect to the source. The $\alpha_i$ was fixed slightly above the critical angle of the P3AT films but slightly below the critical angle of the substrate ($\alpha_{cp} < \alpha_i < \alpha_{cs}$) in order to maximize the scattering signal of the films. The line scans were recorded over a large range of diffraction angle (2θ) with a step size of 0.02°. The 2D detector was placed apart from the film in order to cover some of the important Bragg peaks such as (h00) and (020) as shown in Figure 3.5. The exposure time of the image plate detector was varied in between 2 to 30 minutes depending on the diffracted intensity of the films.

Thicknesses of the films were determined by performing X-ray reflectivity scan. The azimuthal distribution and lateral orientation of the crystallites were probed by performing the azimuthal ψ scan and rocking scans, respectively. Azimuthal distribution of the crystallites were extracted from the 2D diffraction patterns as well as using a point detector by rotating ($\psi = \pm 45°$) the film azimuthally at a fixed Bragg condition ($\alpha_i = \alpha_f = \theta_b$) of the (100) peak as shown in Figure 3.7. The azimuthal profile 'ψ' has been extracted from the 2D detector using the appropriate fit2d software after performing the proper background subtraction.

Background subtraction was performed by recording the background scattering patterns using the $Si/SiO_2$ substrate. X-ray rocking scan analysis was carried out for the (100) Bragg peak of P3AT thin films by rocking the sample ±0.1°, it has been performed after fixing the detector and the incoming beam under Bragg condition ($\alpha_i = \alpha_f = \theta_b$).

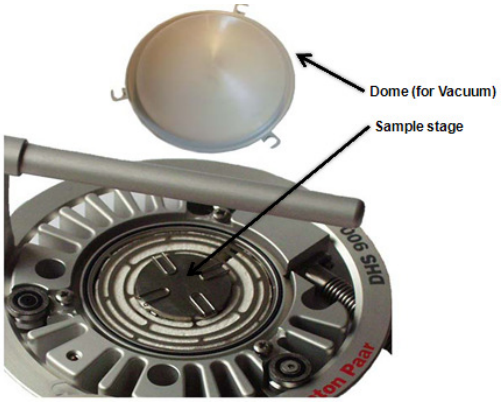


Figure 3.9: Shows the Anton Paar DHS 900 heating stage used to perform *in situ* annealing analysis under vacuum

*In situ* annealing analysis was carried out under primary vacuum (1Torr) using an Anton Paar DHS 900 (heating stage) (Figure 3.9). While increasing the temperature at a rate of 10°C per minute, the (100) diffraction peak shifted to smaller scattering angles due to the lattice expansion. Once the desired temperature (200°C) was reached, the peak intensity was recorded every ten seconds in order to quantify the annealing time. It shows that, half an hour of annealing is enough for the recrystallization of P3AT polymers because further increase of annealing time does not enhance the structural ordering much. When the film is annealed for more than 12 hours, decrease in scattering intensity and change in color of the film from brown to brownish black was observed. The *in situ* annealing analysis was carried out using the well studied RT and -30°C cast P3HT thin films. It does not vary much with respect to the growth temperature. The corresponding intensity versus annealing time profile is shown in Figure 3.10a.

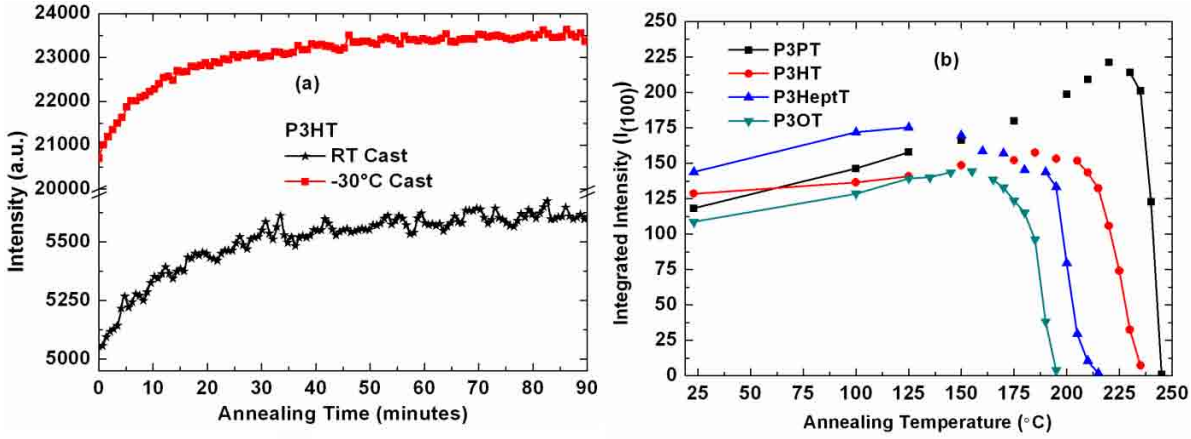


Figure 3.10: The enhancement in scattering intensity of the (100) Bragg peak of P3HT films during annealing (a); the integrated intensity of the (100) Bragg peak of -30°C cast P3AT thin films *in situ* monitored during annealing (b)

In addition, the proper annealing temperatures of P3AT polymers were determined by performing *in situ* GOD scan during annealing. The measurements were performed at home lab using the -30°C cast films because of their enhanced scattering intensity. The annealing temperature dependent enhancement in ordering of the crystallites were monitored by probing the (100) Bragg peak. The (100) Bragg peak was recorded 15 minutes after reaching the desired annealing temperature with the heating rate of 5°C/minute. The integrated intensity of (100) Bragg peak versus annealing temperature is shown in Figure 3.10b. The melting temperature of P3AT polymers decreases while increasing the alkyl side chain length because of the reduction in enthalpy of fusion.[106] The integrated intensity of the (100) Bragg peak has started to decrease ≈25°C below from their corresponding melting point i.e. increase of structural disordering further increase of annealing temperature. The melting point of P3AT polymers obtained through *in situ* GOD scan is in agreement with the values obtained through DSC analysis (Table 2.1).

## 3.3 Investigation of Matter using Electrons

Together with X-ray, subatomic particles like electrons and neutrons are also usually used for the structural investigations of matter. Mainly TEM is widely used for the structural and morphological investigations of P3AT thin films which is using the electrons as a probing subatomic particle. The electrons will be scattered more strongly than the X-rays because they interact with both the nucleus and electrons of the scattering atoms through Coulomb forces. When the electron interacts with matter, they undergo two types of scattering called elastic and inelastic scatterings. During elastic scattering, the kinetic energy and velocity of the

electrons does not change but the trajectory of electrons may change. Elastically scattered electrons are used for the structural analysis of matter. During inelastic scattering, the electron can lose its energy due to its interaction with the orbital electrons of the atoms in a matter. Inelastic scattering is responsible for the radiation damage of matter. The dissipated energy of the incoming electrons can be either converted into molecular vibrations (heat) and causes bond scission. According to the law of conservation of energy, mainly they can have the following effects as shown in Figure 3.11.[107-109]

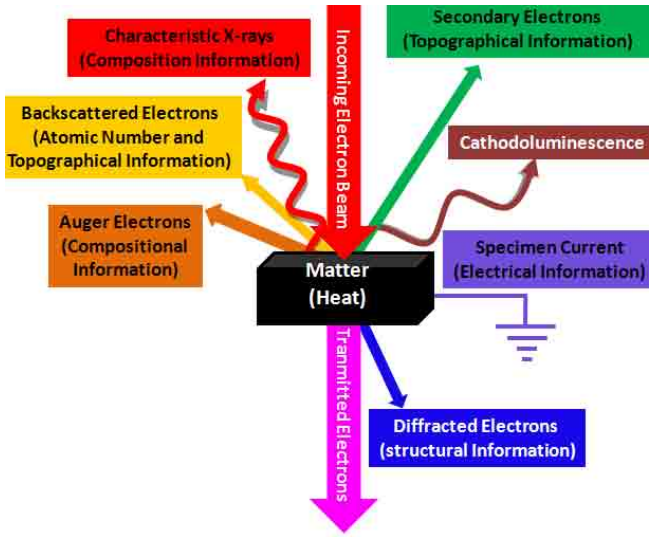


Figure 3.11: Illustrate the interaction of fast moving electrons with the matter and transformation of their energies into various forms

As we know that the electron has a dual nature (particle or wave), DeBroglie suggested that the electron could be thought of as wave with a characteristic wavelength (λ). The wavelength of an electron is a function of its mass (m) and velocity (v). The DeBroglie wavelength (λ) can be expressed as

$$\lambda = \frac{h}{p} \qquad 3.20$$

Here: $p = m_o v$

$m_o \rightarrow$ mass of an electron ($9.11 \times 10^{-28}$ g)

$h \rightarrow$ Planck's constant ($6.63 \times 10^{-34}$ J s)

$v \rightarrow$ Velocity of an electron and it can be obtained from the kinetic energy of an electron "$eV = m_0 v^2/2$"

Substituting the values of 'v' and 'p' in equation 3.20 implies

$$\lambda = \frac{h}{\sqrt{2m_0 eV}} \qquad 3.21$$

The equation 3.21 can be used to calculate the wavelength of an electron only for the non-relativistic case but it is not negligible in the electron microscope because the velocity of electron is nearly equal or higher than the half of the velocity of light. So, the equation 3.21 can be modified by replacing 'V' with '$V\left[1+\frac{eV}{2m_0c^2}\right]$ and it yields equation 3.22.[108]

$$\lambda = \frac{h}{\sqrt{2m_0 eV\left[1+\frac{eV}{2m_0c^2}\right]}} \qquad 3.22$$

Here: c → velocity of light (2.998 x $10^8$ m/s)

e → charge of an electron (1.602 x $10^{-19}$ C)

In this thesis, TEM was used to investigate the structure and morphology of P3AT thin films, operated with the voltage of 120kV (λ = 0.0335Å)

### 3.3.1 Transmission Electron Microscopy

TEM is one of the leading equipments which is used for the characterization of organic and inorganic nanostructures.[108, 110] A variety of signals generated by the electron beam passing through the specimen can be used to extract the useful information about their crystal structure, surface morphology, phases, chemical compositions, etc. In the advancement of materials science and engineering, it is an ultimate goal of the researchers to correlate the structure and morphology of materials with their optical and electrical performances. The electron optics of an electron microscope can be used to produce the images of electron density emerging from the back side of the sample. The ability to focus electrons in a tiny area is a key role of an electron microscope which can be used to study the individual nanoparticles. Actually TEM collects its data from the electrons that are transmitted (or diffracted) through the samples. Therefore, TEM specimens must be extremely thin, with optimal samples less than 50 nm thick and a maximum of about 200 nm. In thicker specimens, inelastic scattering will spread the beam and this reduces the resolution and clarity of the images.[108, 109]

The TEM can provide the information about the specimens in direct space (imaging) and also in reciprocal space (diffraction). Those two basic operations of a simple three lens TEM is schematically shown in Figure 3.12. A main thing to take care is that the

corresponding aperture must be inserted with respect to the mode of operation. For example, selected area electron diffraction (SAED) aperture must be inserted while performing the diffraction analysis as shown in Figure 3.12 (left side) and vice versa. The TEM investigations of nearly 40 nm thin P3AT films were carried out for the detailed investigation of in-plane stacking and the morphology of the crystallites by operating the TEM under electron diffraction (ED) and bright field (BF) imaging modes, respectively.

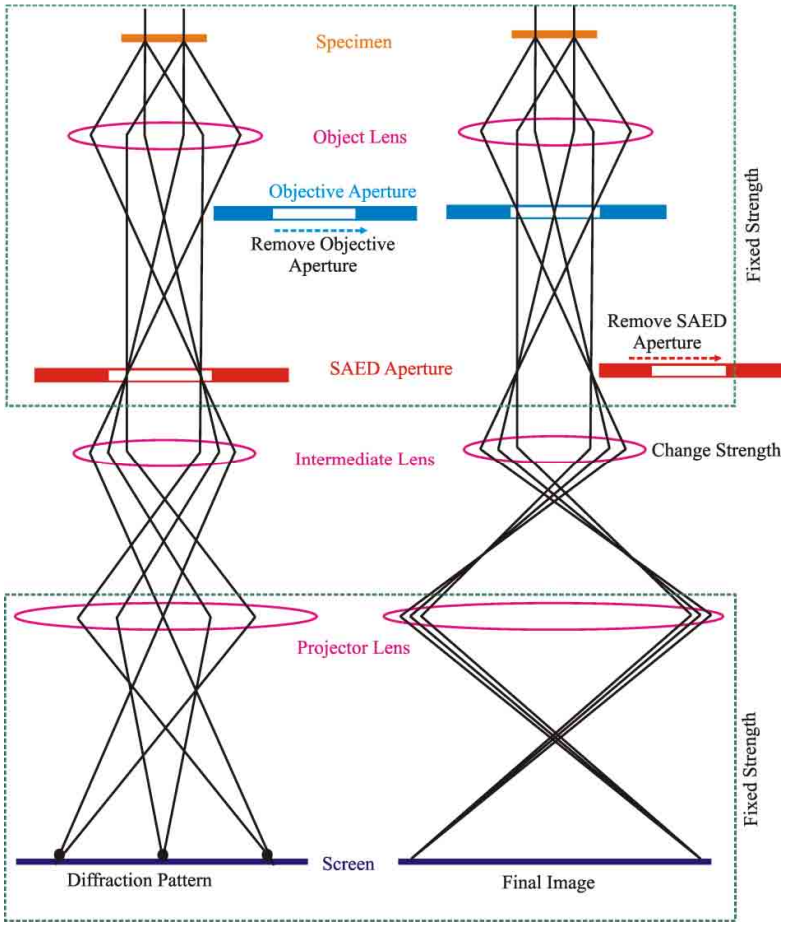


Figure 3.12: Depicts the formation of diffraction pattern and BF images on the TEM screen and the importance of apertures; this is a simple diagram of TEM which contains only three lenses

### 3.3.2 Electron Diffraction

Electron diffraction is a viable tool to understand the crystal structure of organic and inorganic specimens. The wavelength of an electron is much shorter than that of the X-ray mainly encountered in research labs. So, the decrease in wavelength of electrons can assist to cover the wider Q range. The lattice spacing of the crystallites can be calculated from the ED patterns by having the knowledge of electron wavelength and the Bragg angle. Since $\theta_b$ is

small, the 'sine' that occurs in the Bragg condition can be replaced by the 'tangent' in a first-order approximation. The lattice spacing can be estimated from the ED pattern using the equation 3.24[107]

$$\frac{\lambda}{\mathrm{d}} = 2\sin\theta_{\mathrm{b}} \simeq \tan(2\theta_b) = \frac{R}{Y} \quad 3.23$$

$$d \simeq \frac{\lambda Y}{R} \quad 3.24$$

Here: Y → Camera length

R → Radius of the Debye-Scherrer ring

X-rays can be focused in the range of 100 x 100 $nm^2$ in order to study the individual nanostructures, but the electrons can be used to study much smaller nanoparticles than what the X-rays do. X-ray diffraction is user friendly and one can use a lot of geometry which cannot be performed using TEM. The ED patterns can be recorded selectively from the individual nanostructure by focusing the electron beam on the nanoparticles via electron probe forming lenses and apertures. Mainly two diffraction modes are in use with respect to the illumination of parallel electron beams to the convergent beams using the electron optics, i) SAED and ii) convergent-beam electron diffraction (CBED).[108, 109]

#### 3.3.2.1 Selected Area Electron Diffraction

SAED analysis will be performed by impinging the electron beam perpendicular to the specimen. The SAED patterns can be obtained by placing a SAED aperture in the first imaging plane of the objective lens (Figure 3.12 (left)). In this case, we are really selecting an area of an image, but we always refer back to the volume of the diffracting specimen. Only the rays which are passing through the aperture will contribute to the diffraction pattern at the far field. The main drawback of SAED is that we cannot analyze the individual nanoparticles because the diameter of the spherical beam cannot be reduced to less than 1$\mu$m owing to the spherical aberration ($C_s$) of the objective lens. The Bragg angle can be reduced by reducing the wavelength of an electron but the spherical aberration increases with the operating voltage of the TEM.[107-109]

SAED technique can be used to distinguish whether the films are amorphous or crystalline. If, it is crystalline then it would be also possible to understand their crystalline phases, their long-range order, etc. For example, Lu *et al* have used SAED technique to separate the different crystalline phases like edge- and flat-on oriented crystallites present in the P3BT thin film.[55] This technique has been widely used by Brinkmann *et al* to probe the

MW dependent crystallinity and orientation of epitaxially grown P3HT thin films as well as to define the unit cell of P3HT nanocrystallites.[56, 59] It is a viable tool to analyze the formation of different crystalline phases and to study their growth processes.[67, 77]. In this thesis, SAED technique was used to analyze the in-plane stacking of ≈17 nm and 40 nm thin P3AT spin coated and drop cast films, respectively.

#### 3.3.2.2 Convergent-beam Electron Diffraction

During CBED analysis, the electron beam will be converged to relatively very small diameter (≈1 – 100 nm). The electrons will have a range of incidence vector because of converging, subsequently it results disk shaped diffraction patterns.[108, 109] This technique has some advantages and disadvantages as compared to the SAED technique. The advantages are; i) individual nanoparticles can be studied, ii) diffraction can be obtained from the well-defined areas, iii) defect analysis, iv) accurate determination of crystallite orientations, etc. The disadvantages are; i) weak scattering signals due to the small exposing volume and ii) less area of exposing is not suitable for analyzing the powder and amorphous materials. This technique is not widely used for the structural analysis of organic thin films because the focused electron beam can increase the radiation damage.

- *Rather than just doing the electron diffraction, combining it with the other imaging modes is an inevitable feature of TEM which can be used to analyze the lattice and defects present in the crystalline materials.*

### 3.3.3 High Resolution Transmission Electron Microscopy

Most of the crystallites are having unit cells which are larger than the resolution of the commercially available HRTEMs. The HRTEM images are directly interpretable in terms of projections of individual atomic-column positions by operating the TEM under defined conditions (which can reduce the image quality like astigmatism, spherical, and chromatic aberrations) and well-prepared samples. The HRTEM imaging technique is an indispensable tool in crystallography for the determination of defects, stacking faults, precipitates, grain boundaries, etc. The samples must be sufficiently thin in the order of 15 nm and it mainly depends on the composition of the specimens. Otherwise, multiple electron scattering effects become significant, and very fine details present in the images are not likely to be interpretable in terms of atomic arrangements.[108, 109]

During HRTEM imaging, the objective aperture will be opened enough for the transmitted and at least one diffracted beam to pass through. The phase of the diffracted

electron wave is preserved and it produces lattice images by interfering constructively or destructively with the phase of the transmitted waves. The transmitted beam is needed to provide a reference phase of the electron wavefront. The phase difference between the transmitted and diffracted electron waves arises mainly because of the path difference. As a result, interference fringes (a lattice image) appears in the image.[111] The contrast of the image is known as phase contrast and it is proportional to the diffraction amplitude. The distance between two fringes is proportional to the lattice spacing of the corresponding lattice planes which satisfies the Bragg condition.[112] Lattice imaging will be performed in the following manner; i) the diffracted electrons of corresponding reflections will be collected in the same spot of the back focal plane of the objective lens and ii) these spots become a new source so that the electrons starting here meet again at the image plane to form a lattice image as shown in Figure 3.13.[110, 111] The distance between the back focal plane and image plane (= b-f) is actually very large as compared to the extension of the diffraction spots.

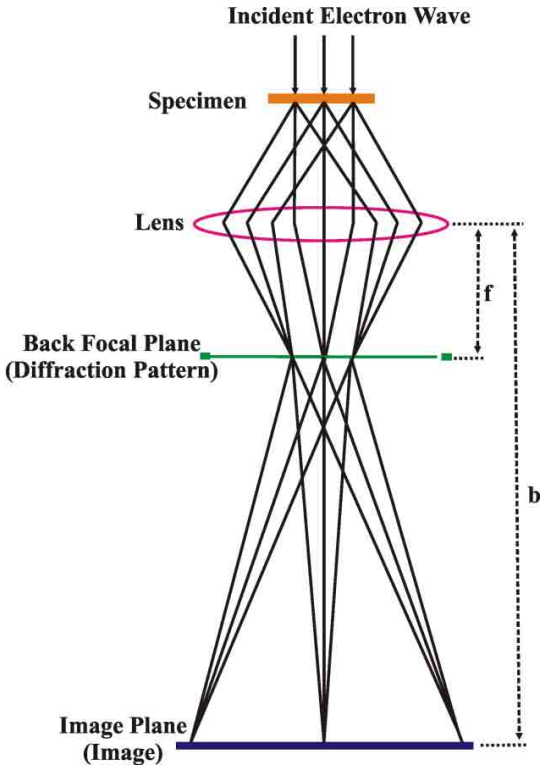


Figure 3.13: Schematic illustration of the interaction of electrons with the specimen and the formation of lattice images

HRTEM has more advantages over electron diffraction that the crystal structure and crystal shape or location information are incorporated in the same image. Compared to the other lattice imaging techniques like scanning tunneling microscopy (STM)[113], HRTEM is mainly used to study the P3AT crystalline lattices.[64] Brinkmann *et al* have used the

HRTEM technique to analyze the MW dependent chain packing, interconnections between the crystalline domains, the influence of film preparation technique on the size of the crystalline domains, etc.[64, 91] It is also used to separate the presence of P3HT crystallites in the amorphous matrix of P3HT thin films.[112] HRTEM imaging of spin coated P3AT thin films (≈17 nm) were performed for the determination of side chain length dependent crystallite orientations as well as the influence of annealing temperature on the anisotropic growth and plasticity of thiophene backbones.

### 3.3.4 Bright Field Imaging Technique

TEM will be operated in a BF imaging mode by inserting the corresponding objective aperture which can be used to filter the electrons which get deflected at greater angles (diffracted beams as well) and it only allows the transmitted beams to pass through (Figure 3.12 (right side)). A much smaller aperture is used in bright field imaging to collect only the transmitted electrons. In this case, images result from the weakening of the direct beam due to its interaction with the specimen. The contrast of BF image arises because of the scattering of incident beam by the specimen and it strongly depends on three main parameters such as mass-thickness, diffraction, and phase contrast.[108, 109] Therefore, the thickest areas as well as the areas where the heavy atoms are enriched will be darker because of their increased scattering. The probability of scattering of the electrons can be expressed by the equation 3.25.[108] Not only the thicker area, also the crystalline phases will results dark contrast in which the system contains both the crystalline and amorphous phases due to the diffraction of electrons. The contrast between the amorphous and crystalline phases can be enhanced by choosing a very small objective aperture in order to cut the maximum diffracted electrons. As a consequence, the crystalline part will be darker and the amorphous part will be brighter. So, care must be taken while interpreting the BF images.

$$\sigma_{total} t = \frac{N_0 \sigma_{atom} (\rho t)}{A} \qquad 3.25$$

Here: $\sigma_{total}$ → numbers of scattering events per unit distance

$\sigma_{atom}$ → the scattering cross section of an atom

A → atomic weight of the scattering atoms in the specimen (kg/ mol)

$N_0$ → Avogadro's number (in units of atoms/ mol)

ρ → density of the specimen (kg/ $m^3$)

t → thickness of the specimen

The bright field (BF) imaging is extensively used to analyze the different crystalline and amorphous phases present in the films, their morphologies, etc.[15, 56, 67] Brinkmann *et al* have reported that the presence of different crystalline phases like edge- and flat-on oriented P3HT crystallites in the films can be distinguished through the BF amplitude contrast by choosing a very small objective aperture.[56] Further, it has been widely used for the deep understanding on the formation of various P3AT crystalline morphologies such as fibrillar, spherulitic, and shish-kebab with respect to the preparation methods.[55, 56, 67, 77]

- *TEM is an inevitable tool as compared to the other techniques which are currently used in the field of material science and engineering because it can be used to study the crystal structure and morphology of the specimens where we are interested in. TEM has been operated under various modes in order to understand the influence of annealing, alkyl side chain length, and cast temperature on the structure and morphology of P3AT thin films.*

## 3.4 Experimental Details of Transmission Electron Microscopy Analysis

TEM analysis was carried out using a CM12 Philips microscope equipped with a MVIII (soft imaging system) charge coupled device (CCD) camera that contains pixels of 1376 × 1032. TEM has been operated under different modes like diffraction and imaging with the operating voltage of 120 kV. Prior to the TEM analysis, P3AT thin films were coated with few monolayers of amorphous carbon using an arc discharge technique in order to reduce the radiation damage.[108] Thin films were detached from the $Si/SiO_2$ substrate by dipping the samples in a 5 wt % HF (hydrogen fluoride) solution. The substrate has been dipped in such a way that the HF can diffuse and dissolve the $SiO_2$ which is sandwiched in between the P3AT thin films and Si substrate. The detached films were recovered on a 3.05 mm diameter copper grid that contains 200 square meshes. Prior to sliding the samples in a HF solution, the edges of the substrates were scratched with the blade followed by blowing with $N_2$ for the ease of HF solution to access the $SiO_2$.

As we know that the calibration of ED pattern is a crucial step for the determination of accurate lattice spacing using a well known crystalline specimens, it was performed using an oriented poly(tetrafluoroethylene) film.[108] For the comparison of scattered intensity, the intensity plot profiles were extracted from the ED patterns by angular averaging using an appropriate macro of imageJ. The extracted intensity profiles were plotted versus $Q_{x,y}$ after performing the proper conversion. The camera length (Y) has been varied in order to access

the higher orders of reflections that appears in the wider $Q_{x,y}$. Mainly the measurements were performed using two different camera lengths 2.05 and 1.4 meters. As we know that the distance between the camera and sample is fixed in the TEM but 'Y' can be increased by the magnifying lenses placed between the specimen and the viewing screen.[108] The lattice spacing of the corresponding reflections was calculated using the equation 3.24.

HRTEM images were recorded in a modified low dose mode. Focusing and astigmatism correction of the incoming electron beams were performed in the test area and then the samples were moved towards an unexposed area after blanking the beam. After about half a minute the HRTEM images were acquired in order to avoid the mechanical drift of the sample holder. The HRTEM images were acquired using <10 pA/cm$^2$ current with the magnification of 230 kX. The films weren't exposed more than a second. The image filtering and fast-Fourier transform (FFT) analyses were performed using the AnalySiS software. The contrast between the crystalline and amorphous areas of the polymer thin films was enhanced using a Bragg filter on the FFT. More than 10 HRTEM images were taken from each sample and the average length, width, and area of the nanocrystallites were extracted using the analysis software.

## 3.5 Mobility Analysis

The mobility of thiophene based OFETs are about to reach the value of amorphous silicon due to the evolution of new polymers, enhancement in their structural ordering, crystallinity of the films, etc.[2] The mobility of OFETs can be calculated from their output characteristic. There are two separate voltages applied to the source electrode of the OFET: i) the drain voltage ($V_{DS}$) is applied in between the source and drain and ii) the gate voltage ($V_{GS}$) is applied in between the gate and source electrodes as shown in Figure 1.6. The polarity of the applied voltages will be changed with respect to the channel type (p- or n-type semiconductor). When a gate voltage '$V_{GS}$' is applied in between the gate and the source, majority carriers accumulate at the insulator (dielectric)-semiconductor interface and it will form a conducting channel at the insulator-polymer interface with a width (W) and a length (L) (Figure 1.6a). The density of accumulated charges are not uniformly distributed in the channel, but it decreases while moving outwards from the insulator-semiconductor interface.[2, 114] The OFETs fabricated out of different P3HT layer thicknesses shows the increase in mobility while increasing the film thickness and it saturates at around 50 nm.[115] It clearly exhibits that the insulator-polymer interfacial ordering is mandatory for the enhanced performance of an OFET. The interfacial ordering probed by Kline *et al* through the

X-ray rocking scan exhibits that the SAM and annealing treatments increases the insulator-polymer interfacial ordering subsequently it improves the OFET performances.[8]

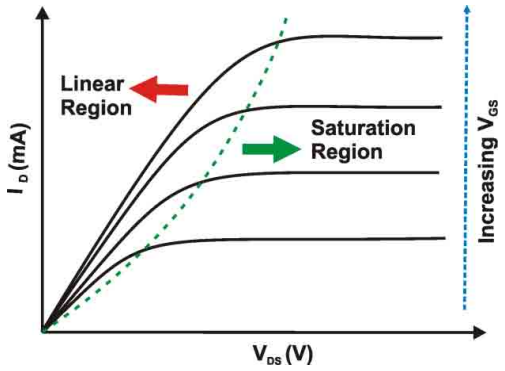


Figure 3.14: Shows the output characteristics of the organic thin film transistor with a well defined saturation and linear region

The mobility of electrons can be estimated by two ways either from the linear or the saturation regime by plotting $I_D$ (drain current) versus $V_{DS}$ as shown in Figure 3.14. In the linear regime, ($V_{DS} < V_{GS} - V_T$) the OFET mobility can be calculated using the equation 3.26. In the saturation region of operation ($V_{DS} \geq V_{GS} - V_T$), the mobility of OFETs can be extracted using the equation 3.27

$$I_{D_{lin}} = \frac{W\mu C_i}{L}(V_{GS} - V_T)V_{DS} \qquad 3.26$$

$$I_{D_{sat}} = \frac{W\mu C_i}{2L}(V_{GS} - V_T)^2 \qquad 3.27$$

Here: $C_i$ → capacitance per unit area of the insulating layer

$V_T$ → the threshold voltage

$\mu$ → the field effect mobility

The mobility of RT and -30°C cast P3AT OFETs were calculated from the saturation regime of the transfer characteristics. Bottom contact OFETs were fabricated by casting the films at RT and -30°C on the patterned test beds. The substrates were purchased from the company "Fraunhofer IPMS" which can be used to prepare 16 OFETs on one chip ($15x15mm^2$) which contains the same width (10 mm) but different channel lengths like 2.5, 5, 10, and 20 µm. The interdigitated source and drain electrodes (Au) were patterned on the 230 nm thick thermally oxidized heavily doped n-type Si substrate. The obtained Au patterned substrates were cleaned with acetone followed by isopropanol and dried under blowing $N_2$. Thin films were cast under $N_2$ ambient conditions and transported to our collaborators under

vacuum of around 1 Torr for the OFET analysis. The mobility of spin coated P3AT thin films was measured by spin coating them at ambient conditions in the home lab.

## 3.6 Optical Spectroscopic Analysis

The optical analysis such as photoluminescence (PL) and UV-Vis absorption spectroscopic analyses are the leading techniques used to calculate the free exciton bandwidth (W), band gap, orientation of P3AT polymers, etc. Especially, aggregates make a red shift in the emission spectrum by means of vibronic energy levels ($E_p \approx 0.17$ eV) caused by the C=C stretching vibration (1400 $cm^{-1}$) of the thiophene ring.[53, 90, 116, 117] The efficiency of solar cell increases when the crystallinity of the film increases because of the increased absorption of photons.[53]

### 3.6.1 Photoluminescence Analysis

PL spectroscopy is a viable technique for analyzing the luminescent properties of materials. In this technique, the electrons will be excited from the valence band to the conduction band by impinging them with photons having higher energy than the bandgap of the materials, this process is called photoexcitation. The absorbed energy can be dissipated through different ways when the electron returns from the conduction band like heat or emission of photons, the process of emission of light is usually called photoluminescence. The luminescent intensity and shape of the peaks can be used to study the properties of materials. Especially, the emission of P3AT polymer contains two parts, a lower energy dominates from the crystalline regions due to the weakly interacting H-aggregate states and the higher energy part is associated to the disordered regions (intrachain states) at T = 0K.[118] It is schematically shown in Figure 3.15, the lower energy part is marked in the PL spectrum by red colored box and the higher energy part is marked with black color.

The luminescent intensity of vibronic transition increases as the crystalline phase increases i.e. the intensity of 0-1, 0-2, 0-3, etc. transitions. The oscillator strength of the C=C stretching of thiophene ring increases relatively when the polymer chain goes from the twisted amorphous to the planar aggregated state.[117] The 0-0 transition is not allowed in a perfect crystalline P3ATs because of the symmetric reason but it is sensitive to the structural defects and temperature.[117, 118] In opposite, the 0-1 transition is independent of temperature. The intensity of (0-0) transition increases with the disorder parameter present in the films. So, the disorder parameter (α) present in the films can be calculated from the emission spectrum

using the modified model of Franck-Condon progression as reported by Clark *et al.*[119] The corresponding relation is given in equation 3.28.

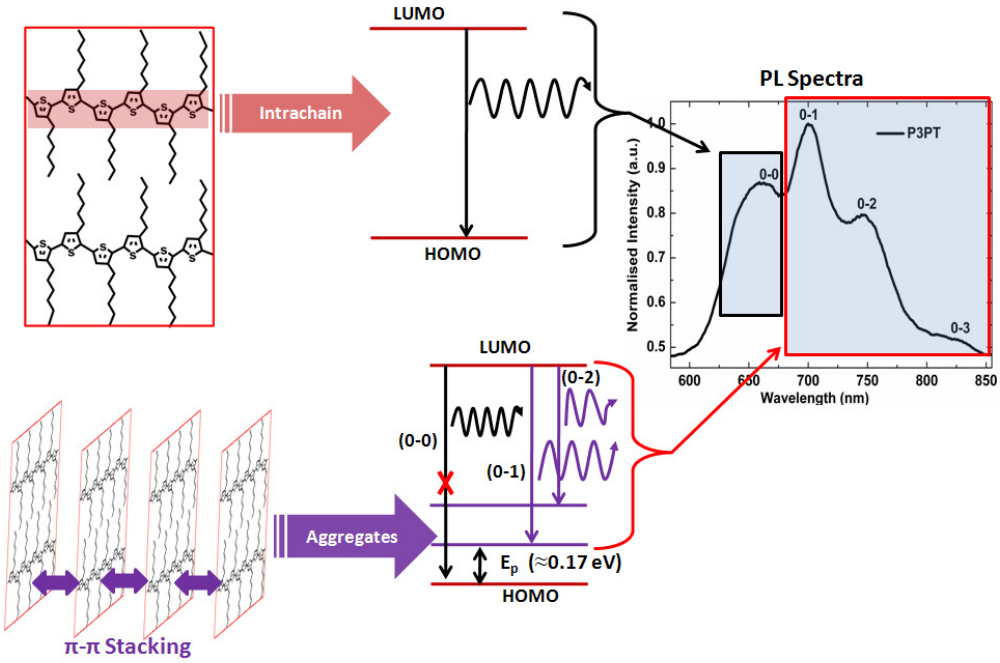


Figure 3.15: Schematic illustration of the formation of vibronic energy levels and their corresponding electronic transitions

$$I_{(\omega)} \propto (\hbar\omega)^3 {n_f}^3 e^{-s} * \left[\alpha\Gamma(\hbar\omega - E_0) + \sum_{m=1} \frac{s^m}{m!} \Gamma\left(\hbar\omega - \left(E_0 - mE_p\right)\right)\right] \qquad 3.28$$

Here : $n_f$ → real part of the refractive index (≈2 for P3HT)[120, 121]

ħω → Photon energy

I(ω) → 0-0 transition amplitude

m → denotes the vibrational levels

s → Huang-Rhys factor, which gives the measure of the coupling between the electronic transition and phonon mode (s≈1)

$E_0$ → 0-0 transition energy

$E_p$ → C=C symmetric stretching vibration coupling of electronic transition (≈0.17eV)

Γ → the line shape function (simplified to be purely Gaussian with constant width)

This technique has been widely used to separate the amorphous and crystalline phases present in the film. For example, Brinkmann *et al* have used PL analysis to separate the

amorphous and the crystalline phases present in the epitaxially crystallized film using the two distinct emissions of crystalline and amorphous P3HTs.[67] The cast temperature assisted enhancement in luminescent intensity of ≈400 nm thick P3AT films were analyzed using this technique. The measurements were carried out at ambient conditions using a Varian Cary Eclipse Fluorimeter. The excitation wavelength was fixed at 450 nm and the emitted signals were monitored. The slit of incoming beam was kept constant at 20 nm.

### 3.6.2 Ultraviolet-visible Spectroscopy Analysis

UV-Vis spectroscopy analysis is widely used to analyze the optical properties of organic and inorganic materials. During UV-Vis spectroscopic analysis, the transition from the ground state to the excited state will be monitored. In the UV-Vis spectrometer, the incoming beam will be split into two beams before it reaches the sample, as a reference and a probing beam. Both of them will be detected with different detectors. The intensity ratio between the reference and the transmitted (or reflected) beams will be plotted versus wavelength. It is a viable tool to determine the band gap and the optical quality of the materials.

*In situ* UV-Vis absorption spectroscopic analysis is widely used to understand the formation of P3AT crystallites in the mother phase.[68, 81] Crossland *et al* have used *in situ* UV-Vis absorption spectroscopic analysis to control the nucleation density during solvent annealing in a way to achieve bigger spherulites.[68] Rather than the formation of nucleation, UV-Vis spectroscopic analysis has been used to analyze the interchain stacking of the P3AT crystallites and their orientations.[65, 80, 116] As we have seen in the PL analysis, UV-Vis absorption spectrum contains two parts which are correspond to the aggregates and intrachain interactions.[116] So, the formation of crystalline phases in a mother phase or solutions can be understood through the evaluation of corresponding vibronic peaks.[68] The $\pi$-$\pi^*$ transition (absorption) is sensitive to the electric field vector of the incoming beam. The absorption of UV-Vis light is prominent when the electric vector of the incident light is parallel to the backbone of the conjugated polymers. Also, the degree of alignment of a $\pi$- $\pi$ conjugated system in an oriented P3AT nanostructures can be evaluated by measuring the polarization degree of UV–Vis absorption and PL spectra.[67, 80, 91]

As we have seen in the earlier text, UV-Vis spectroscopy is a viable technique for the analysis of aggregates present in the solutions. In the present work, UV-Vis spectroscopy analysis was carried out for the confirmation of complete dissolution of P3AT polymers in

$CHCl_3$. The UV-Vis absorption spectra of P3AT solutions (2mg of P3AT was dissolved in 1ml of $CHCl_3$) were recorded using a Cary 1 spectrophotometer by taking the solution in a square ($1mm^2$) shaped quartz cell (cuvette). The experiments were performed at ambient conditions.

## 3.7 Atomic Force Microscopy

Atomic force microscopy (AFM) is one of the leading equipment for the analysis of topography, roughness, and mechanical properties of conducting and non-conducting materials in the nanometer regime.[109] In AFM, the mechanical interaction between the sample and the probing tip has been used for surface imaging. It can be obtained via contact and noncontact modes. In contact mode, the cantilever is dragged across the surface of the sample and the deflection of cantilever will be monitored. In contrast to the contact mode, the cantilever is oscillating close to its fundamental resonance frequency in the noncontact mode of imaging. Rather than the contact mode, the noncontact tapping mode is widely used to analyze the material properties like adhesion, friction, viscoelasticity, etc. Here the cantilever will be oscillated with an amplitude greater than 10 nm.[109] The phase lag of the cantilever oscillation is related to the sample tip interactions i.e. adhesion and viscoelasticity of the materials. The phase lag of cantilever will be monitored simultaneously during topographic imaging.[72, 122] Phase images are used to separate the different phases present in the system. Differences in adhesion and mechanical properties of different components are responsible for various phase contrasts observed in the samples during imaging.[109] Phase imaging has started to play an important role in the growing material science field for the analysis of material properties in the nanometer scale. Especially the amorphous and crystalline phases present in the P3HT thin films can be distinguished via AFM phase imaging i.e. the harder regions correspond to the crystalline part and the softer regions correspond to the amorphous part.[56, 72]

The surface morphology and variation in phases (crystalline and amorphous) of P3HT thin films were characterized by AFM. Non-contacting tapping mode was used to obtain the detailed information about the topography, phase, and surface roughness of the films. The samples were probed with commercial tips of silicon nitrate featuring a tip radius of about 10 nm in a feedback controlled mode on all three x-, y- and z-axes. The images of having 10 x 10 $\mu m^2$ area with a pixel resolution of 512 x 512 were taken at different surface positions of each sample in order to drive the corresponding RMS roughness and phase contrast. In addition, the thicknesses of P3AT films were measured via the AFM scratching technique.

# Chapter IV

## 4 Influence of Cast Temperature on the Orientation of P3HT Crystallites

The P3HT thin films were cast at different temperatures like 23°C, 8°C, -12°C, and -30°C for the detailed understanding of growth temperature dependent enhancement in orientation of the crystallites. Thin P3HT films were cast on native and silanized substrates of $Si/SiO_2$. Two different HMW RR-P3HTs (76400 and 46500 g/mol; PDI is 1.52 and 1.47) were used for the structural and morphological analyses, but most of the analyses were performed using 76400 g/mol.

### 4.1 GIXD Analysis of P3HT Thin Films

The 2D X-ray diffraction pattern of different temperature cast P3HT thin films were recorded under grazing incidence geometry as schematically shown in Figure 3.5. The acquired 2D X-ray diffraction patterns of as-cast and 150°C annealed films are shown in Figure 4.1. Figures 4a-d shows the diffraction pattern of different temperature as-cast P3HT thin films. Qualitatively the 2D images of the films cast at - 30°C and -12°C exhibit similar scattering patterns (Figures 4.1c and 4.1d). All the diffraction patterns exhibit a series of (h00) reflection along Q and less intense (020) peak along $Q_{x,y}$ suggesting the growth of preferentially edge-on oriented crystallites, but a fraction of face-on oriented crystallites is observed in the RT and 8°C cast films (Figure 4.1a and 4.1b). The presence of (100) Debye-Scherrer ring in the RT cast film confirms the absence of preferential orientation of the crystallites on substrate and it became an elliptical spot while decreasing the cast temperature (Figure 4.1). It clearly exhibits the increase of edge-on oriented crystallites while reducing the cast temperature below RT. Those tendencies become much more pronounced after annealing the films at 150°C (Figure 4.1 right column). Thin films were annealed for an hour after optimizing the annealing time (Figure 3.10a). The in-plane (100) reflection gets weaker as the growth temperature decreases (Figure 4.1). A line profile was extracted along in-plane direction ($Q_{x,y}$) and shown in Figure 4.2.

The reduction in scattering intensity of in-plane (100) reflection while reducing the growth temperature confirms the series reduction of face-on oriented crystallites (Figure 4.2a). On the other hand, the (020) reflection is becoming narrower as reducing the cast temperature which concludes the formation of highly interchain stacked edge-on oriented crystallites (Figure 4.2a). The peaks become much narrower and more intense after annealing

the films at 150°C for an hour (Figure 4.2b). The appearance of (100) reflection along $Q_{x,y}$ even after the post growth annealing for the case of RT and 8°C cast film concludes that the face-on oriented crystallites cannot be completely removed by post growth annealing (Figure 4.2b). Increase of edge-on oriented crystallites together with the reduction of cast temperature can be explained by the controlled supersaturation and reduced evaporation rate of the solvent.

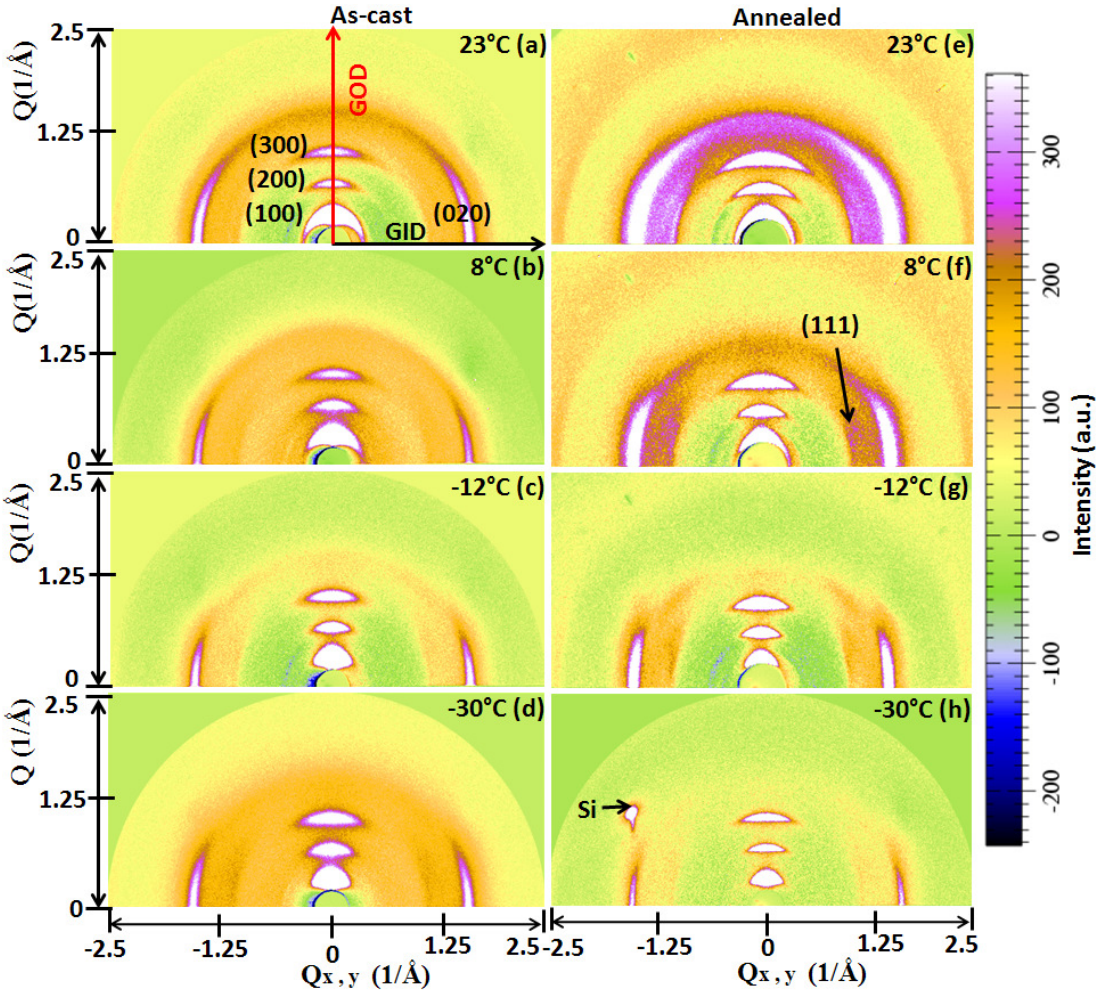


Figure 4.1: Shows the 2D X-ray diffraction pattern of 23°C, 8°C, -12°C, and -30°C as-cast (left column) and 150°C annealed (right column) P3HT thin films

Along with the in-plane stacking, the out-of-plane stacking of different temperature cast P3HT crystallites were probed by performing a point detector scan at home lab. The obtained GOD line profiles are shown in Figure 4.3. The as-grown and annealed films are displaying a series of (h00) Bragg peaks with a broad and ill-defined hump at the position of (020) peak. The (020) peak typically refers to the interchain stacking (π-π stacking) distance (here after it will be denoted by $d_{(020)}$ = 3.8 Å), whereas the interplanar distance (out-of-plane

(100); here onwards it will be mentioned as $d_{(100)}$ = 16.7 Å, it will vary with respect to the number of hydrocarbons grafted in the alkyl side chain) characterizes the stacking of hexyl side chains (Figure 1.5). Moreover, a broad hump centered at the (020) peak is only visible in the RT and 8°C cast and RT spin coated film, which corresponds to the amorphous as well as the face-on oriented crystallites (inset of Figure 4.3b).

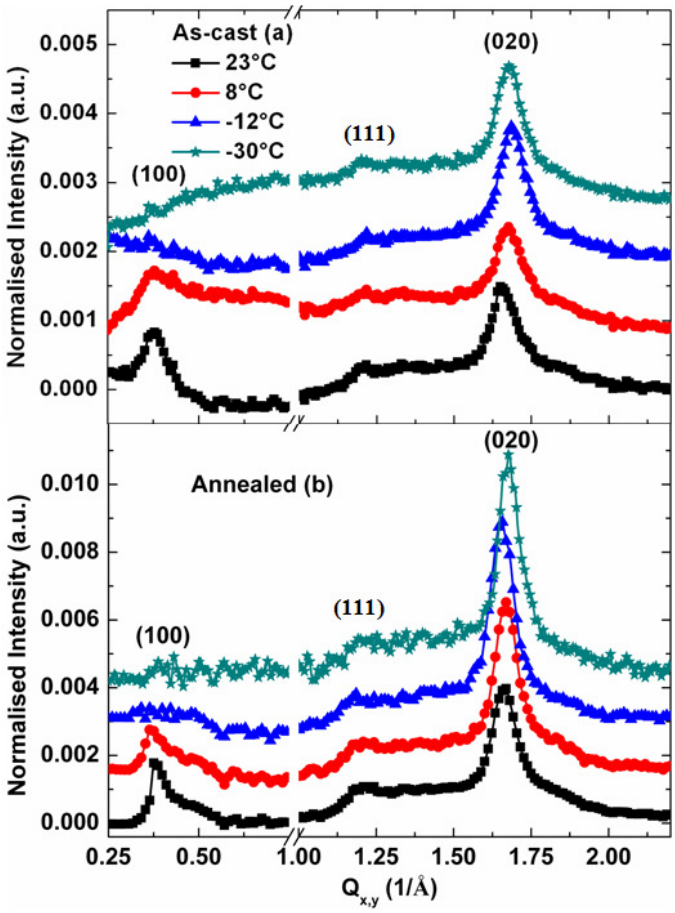


Figure 4.2: Depicts the in-plane line profile extracted from the 2D diffraction pattern of 23°C, 8°C, -12°C, and -30°C (a) as-cast and (b) 150°C annealed P3HT thin films; the profiles were shifted from the same baseline for clear presentation

Figure 4.3a reveals a strong increase of (h00) peak intensities while lowering the cast temperature. Thin films were spin coated out of the same solution in order to compare its structure and morphology with the cast films. The spin coated film produces non-thermodynamically stable crystallites without any preferential orientation. The Bragg peaks of as-spin coated films are not well separated from the background, but they are well pronounced after the post growth annealing (Figure 4.3). The formation of such non-thermodynamically stable crystallites during spin coating might be due to the rapid evaporation of the solvent ($CHCl_3$).[12, 16]

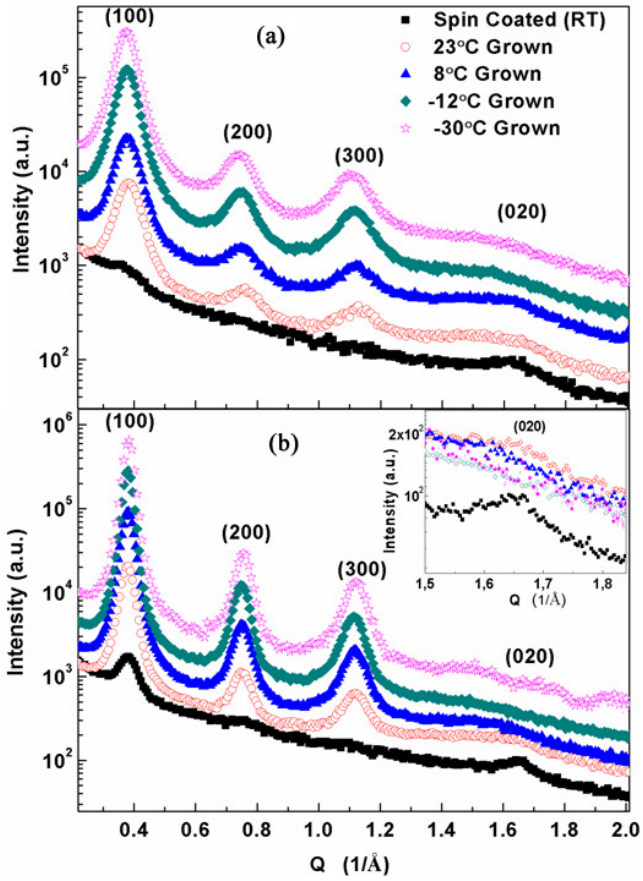


Figure 4.3: GOD profile of RT spin coated and cast P3HT films at 23°C, 8°C, -12°C, and -30°C (a) as-grown and (b) 200°C annealed; inset of b shows the (020) peak of annealed P3HT films; the profiles were shifted from the same baseline for clear presentation

Overall, the findings demonstrate that the highly crystalline P3HT thin films can be prepared by lowering the cast temperature. The FWHM of Bragg peaks are decreasing while reducing the cast temperature as well as after the post growth annealing. The FWHM of Bragg peak contains two important information; i) paracrystallinity (inhomogeneous in d-spacing) and ii) paracrystallite size. It can be mathematically expressed as stated in the equation 4.1.[123] The percentage of paracrystallinity can be quantified by plotting the Hosemann plot.[123, 124] The corresponding Hosemann plot of different temperature cast P3HT thin film is shown in Figure 4.4. It has been plotted integral breadth (δb) versus $h^2$. A plot of δb versus $h^2$ has an intercept ($1/N_{hkl}$) and slope ($(\pi gh)^2/d_{hkl}$) which can be used to extract the paracrystallite size and percentage of paracrystallinity, respectively. The δb can be obtained from the diffraction peak which has been plotted intensity versus b as shown in the inset of Figure 4.4a. Here, b is a scattering vector. In this thesis, I have used two different equations to represent the same physical quantity in order to make the calculation easier and

to follow the literature i.e. b and Q. The scattering vector 'b' can be converted into 'Q' by multiplying with 2π i.e. Q = 2π *b.

$$\delta b = \frac{1}{N_{hkl}} + \frac{(\pi g_{hkl} h)^2}{d_{hkl}} \quad 4.1$$

$$b = \frac{2sin\theta}{\lambda} \quad 4.2$$

Here: λ → wavelength of the X-ray beam

d → distance between the adjacent net planes

N → mean crystal size

h → (h00) (order of the peak)

$g_{hkl}$ → the relative paracrystalline distance fluctuation of the family net planes

In this thesis, two different models have been used to extract the crystallite size from the FWHM of (h00) reflection, they are, i) paracrystalline model proposed by Hosemann *et al* [123] and ii) Debye-Scherrer equation [125]. The crystallite size extracted using the paracrystalline model and the Debye-Scherrer equation will be named as paracrystallite size and effective crystallite size, respectively.

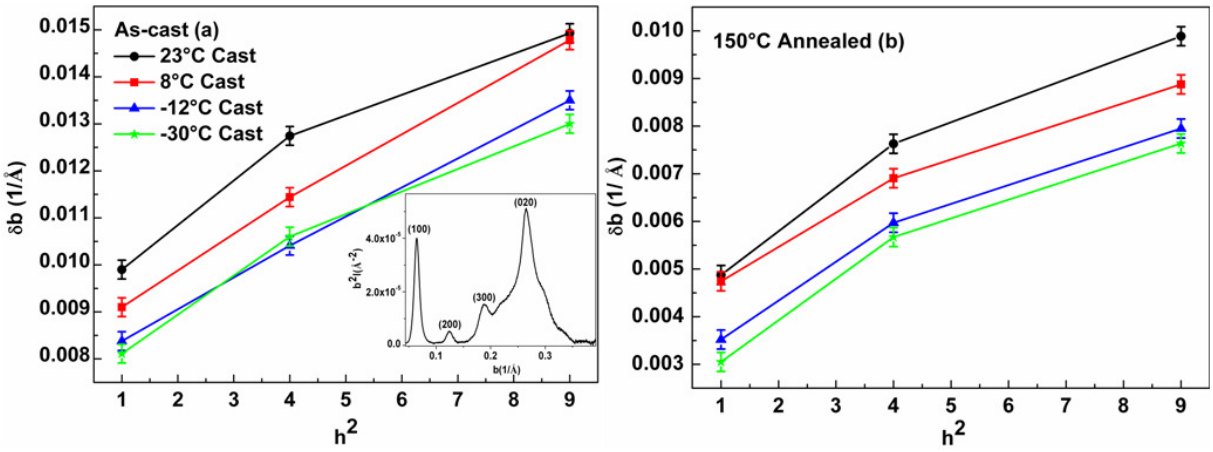


Figure 4.4: (a) Depicts the Hosemann plot of as-cast and (b) 150°C annealed P3HT thin films cast at different temperatures; inset of (a) shows the diffraction profile plotted b versus intensity for the extraction of δb

The percentage of paracrystallinity and paracrystallite sizes of different temperature cast P3HT thin films were extracted from the Hosemann plot (Figure 4.4) and presented in Table 4.1. Not much variation in fluctuation of P3HT lattices (paracrystallinity) were

observed while decreasing the cast temperature (Table 4.1). Rivnay *et al* have recently reported that the percentage of paracrystallinity of melt annealed film decreases with the cooling rate.[126] It clarifies that the reduction in FWHM of Bragg peak after the post growth annealing as well as decreasing the cast temperature is not associated to the reduction in paracrystallinity but it is completely due to the increased crystallite size.[126]

| Cast Temperature (°C) | Paracrystallite Size | | Paracrystallinity (±0.1) | | % of Crystallinity (As-cast) |
|---|---|---|---|---|---|
| | As-cast (±1nm) | Annealed at 150°C (±2nm) | As-cast | Annealed at (150°C) | |
| 23 | 10.3 | 21.6 | 3.2 | 3.2 | 35.2 |
| 8 | 11.8 | 22.3 | 3.4 | 2.9 | 40.1 |
| -12 | 12.8 | 31.2 | 3.3 | 3.0 | 45.6 |
| -30 | 13.1 | 35 | 3.2 | 3.1 | 44.3 |

Table 4.1: Summarizes the paracrystallite size, percentage of paracrystallinity and crystallinity of different temperature as-cast and 150°C annealed P3HT thin films

The crystallinity of different temperature cast P3HT thin films was extracted using Ruland's method (equation 4.3).[127, 128] The integrated intensity profile was extracted from the 2D scattering patterns using the appropriate fit2d software and the percentage of crystallinity was calculated. It was not able to use a simple line profile because the randomly distributed crystallites were started to orient while reducing the cast temperature from RT to -30°C (Figure 4.1). The following procedure has been undertaken before extracting the percentage of crystallinity; i) correction of polarization factor and ii) subtraction of incoherent scattering. Area under the Bragg peaks and the amorphous part was extracted using the Gaussian model from the diffraction profile plotted $b^2*I$ versus b.[127, 128]. For example, the Gaussian model of RT and -30°C cast P3HT films and the corresponding diffraction profiles are shown in Figure 4.5. The best way for obtaining exact percentage of crystallinity is by plotting $1/x'$ versus $b_2^2$ (intercept at $b_2^2 = 0$) which can be obtained by sectioning the diffraction profile.[128] But the calculation couldn't be done in that manner because only one amorphous halo could be observed. The crystallinity of P3HT thin film increases while reducing the cast temperature (Table 4.1). The crystallinity of RT cast P3HT is in agreement with the values reported for the other polymers like polyamide-6 and polypropylene.[127, 128] The crystallinity of low temperature cast P3HT is greater than the values reported by Zhokhavets *et al* for the different temperatures annealed P3HT film by considering the integrated intensity of the Bragg reflections.[129]

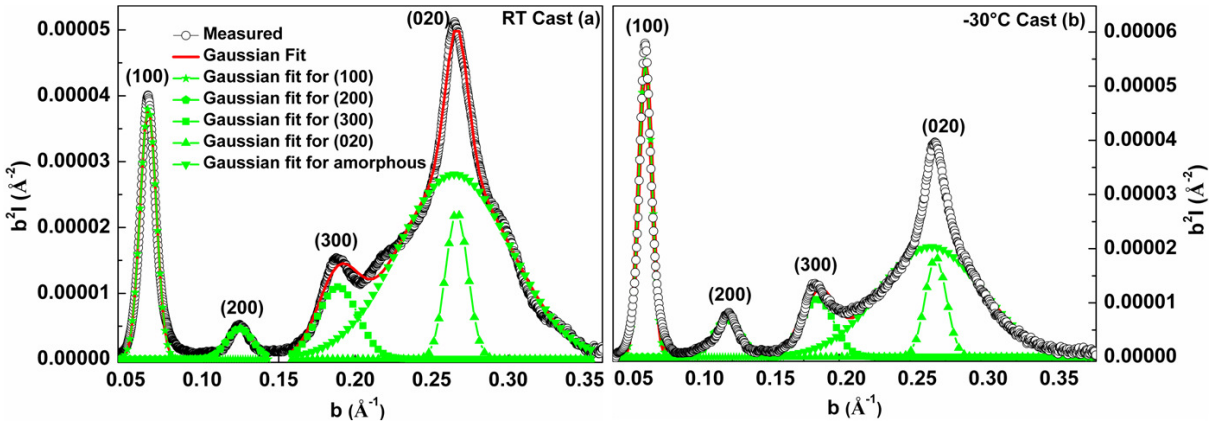


Figure 4.5: RT and -30°C integrated diffraction profile plotted $b^2I$ versus b and their Gaussian model

$$x' = \frac{\int_{b_1}^{b_2} b^2 * I_c(b) * db}{\int_{b_1}^{b_2} b^2 * I(b) * db} \qquad 4.3$$

In addition, the average crystallite size of different temperature cast and annealed P3HT thin films was extracted from the FWHM of (100) Bragg reflection using the Debye-Scherrer equation 4.4.[93] In addition to the cast temperature, influence of annealing on the crystallite sizes of the films were studied by annealing the films at various temperatures like 100°C, 150°C, and 200°C. The obtained values are presented in Table 4.2.

$$\tau = \frac{K\lambda}{\beta cos\theta} \qquad 4.4$$

Here: $\tau \rightarrow$ effective crystallite size

$\beta \rightarrow$ FWHM in radians

$\theta \rightarrow$ Bragg angle of the corresponding peak

K → constant (≈0.9)

| Cast Temperature (°C) | Effective Crystallite Size (±0.2nm) | | | |
|---|---|---|---|---|
| | As-cast | Annealing Temperature (°C) | | |
| | | 100 | 150 | 200 |
| 23 | 8.5 | 11.6 | 13.2 | 14.5 |
| 8 | 8.8 | 12.9 | 13.9 | 15.5 |
| -12 | 9.8 | 15.1 | 17.3 | 18.9 |
| -30 | 9.9 | 15.2 | 17.3 | 18.9 |

Table 4.2: Influence of annealing temperature on the effective crystallite size of the P3HT thin films cast at different temperatures

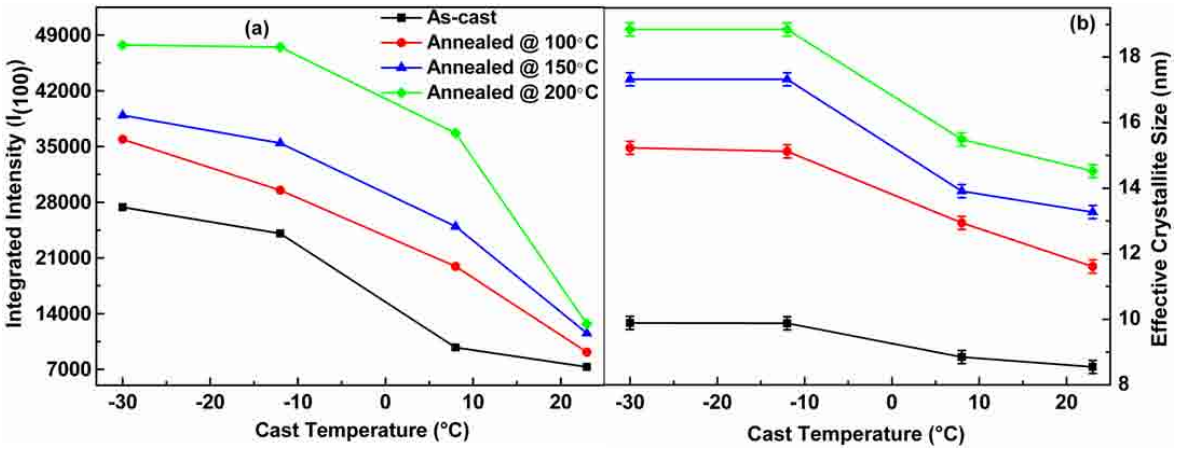


Figure 4.6: The growth and annealing temperature dependent enhancement in (a) integrated intensity of the first order Bragg peak ($I_{(100)}$) and (b) the effective crystallite size

The crystallite size does not increase much while casting at -30°C as compared to the RT cast one (increases by ≈1.5 nm). The obtained crystallite sizes of different temperatures as-cast P3HT is comparable with the values obtained from the Hosemann plot (Table 4.1). It increased by the factor of about two after annealing the film at 200°C for an hour. It is gradually increasing with the annealing temperature (Table 4.2). This result suggests that both the number of edge-on oriented crystallites, crystallinity, and the crystallite size are increased while decreasing the cast temperature (Figure 4.6). The influence of cast temperature on the crystallite orientation can be qualitatively estimated by comparing the integrated intensities of (100) Bragg peak because the thickness of the films used for the analysis are comparable. The thicknesses of the films are found to be independent of growth temperature and about 400 nm as measured by AFM. The (100) Bragg peak intensity of -30°C cast film is four-times higher than the RT cast film whereas the crystallite size does not increase much (Figure 4.6). The cast temperature T ≈ -12°C can be assumed as the optimum crystallization temperature because there is no major enhancement in either crystallinity or crystallite sizes were observed while reducing the cast temperature further down to -30°C (Figures 4.3 and 4.6). The enhancement in integrated intensity of (100) Bragg peak is not associated to the thickness but it is completely due to the enhancement in crystallinity, crystallite orientation, their sizes, etc. The cast temperature dependent enhancement in crystallite orientation was quantified via X-ray rocking and azimuthal ψ scan.

## 4.2 Cast Temperature Dependent Crystallite Orientation Analysis

X-ray rocking curve recorded for the (100) Bragg peak of different temperature cast P3HT films does not provide a sharp maximum but it depicts the random distribution of the

crystallites (not shown). Therefore, cast temperature dependent enhancement in orientation of the crystallites was quantified by performing the azimuthal ψ scan as schematically shown in Figure 3.7. Different temperatures as-cast P3HT films were azimuthally rotated '$\psi = \pm 45°$' at fixed Bragg condition ($\alpha_i = \alpha_f = \theta_b$) of the (100) peak. The obtained azimuthal profile (Figure 4.7) visualizes the inhomogeneous distribution of the crystallites with the FWHM of about 26° for the -30°C and -12° C cast films. There is a clear trend in increase of FWHM while increasing the cast temperature, i.e. 31° at 8°C, and 34° at 23°C. Increase of randomly oriented crystallites with increasing the cast temperature might be attributed to the fast evaporation of the solvent which can produce randomly oriented nucleates.[16] Yang *et al* reported that the film spin coated out of 40°C warm solution on the 40°C warm substrate produces much azimuthally distributed crystallites due to the latest initiation of nucleation than the one spin coated at RT using the same solution.[16] According to the equation 2.9, the size of a critical nucleus can decrease when the solution is over supersaturated, eventually it can produce randomly oriented multiple nucleates where the growth is thermodynamically trapped. The concentration of the RT and -30°C cast P3HT thin films were gradually varied in order to understand the influence of concentration on the crystallite orientation.

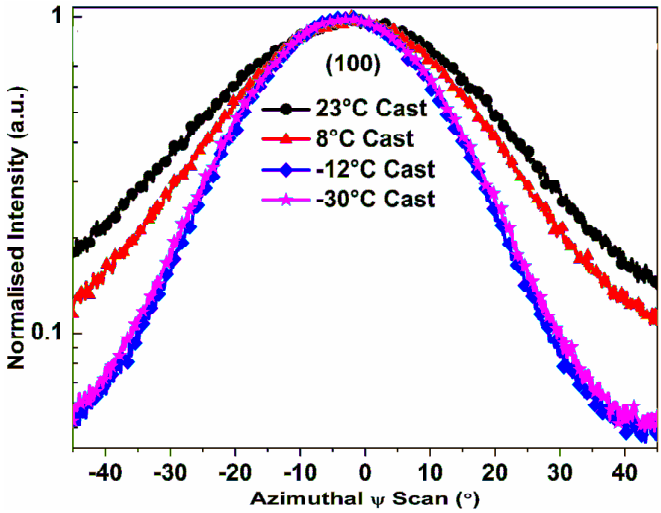


Figure 4.7: Azimuthal scattering profile of (100) Bragg peak for the P3HT thin films cast at 23°C, 8°C, -12°C, and -30°C, the measurement was performed under specular condition and normalized to one

### 4.2.1 Effect of Concentration on the Orientation of the Crystallites

The concentration of the solutions were gradually varied by keeping the amount of dropped solution, size of the substrate, and cast temperature as constant in order to understand the influence of concentration on the orientation of the crystallites. Most of the analyses

presented in this thesis were performed using the HMW P3HT (76400g/mol) except the results presented in the current subtitle (MW=46500g/mol) (chapter 4.2.1). X-ray measurements of both the MW P3HTs e.g. 76400 and 46500 g/mol provides the same $d_{(100)}$-spacing similar to the $CHCl_3$ fraction of deuterated HMW P3HT as observed by Zen *et al.*[57] The occurred azimuthal profiles and rocking curves are presented in Figure 4.8 and 4.9, respectively. The orientation of RT and -30°C cast films are increased while decreasing the concentration of the solution. The FWHM of azimuthal ψ profile as well as the X-ray rocking curve decreases with the concentration of the solution (Table 4.3). The FWHM of (100) azimuthal profile of RT and -30°C cast films are nearly the same while casting using the concentration 1 mg/14 ml. On the other hand, the -30°C cast film results Gaussian shaped profiles where the RT cast film shows Lorentzian shaped profiles, which confirms the presence of more randomly oriented crystallites in the RT cast films.[16]

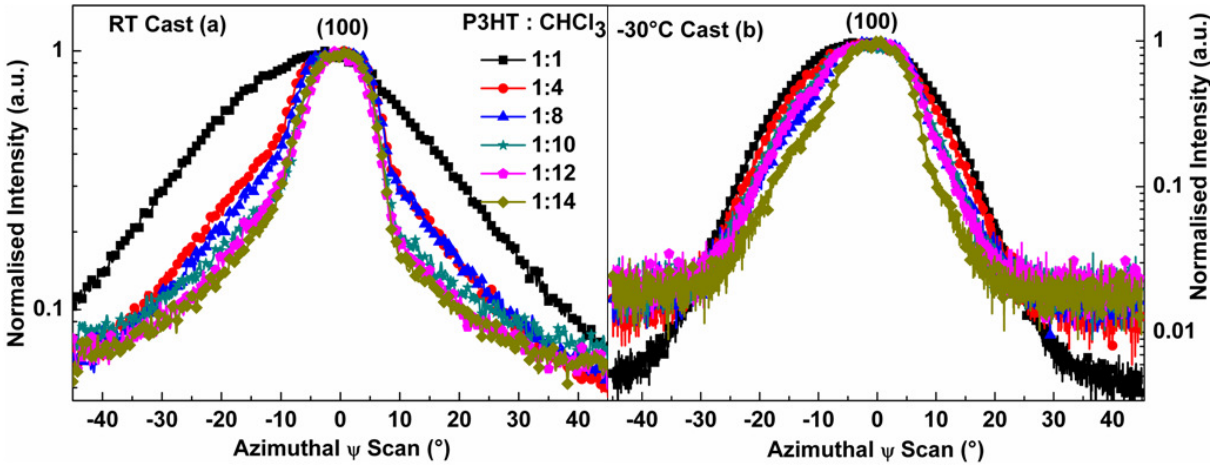


Figure 4.8: Azimuthal ψ profile of (a) RT and (b) -30°C cast P3HT thin films using different concentrations; the profiles were normalized to one

The surface roughness of RT cast film is increasing from ≈40 Å to 110 Å as the concentration decreases, but it does not vary much while casting at -30°C and lies in the range of 20 Å till 40 Å. The measured and simulated X-ray reflectivity (1 mg/14 ml) profile of RT and -30 °C cast films are shown in Figure 4.10 and the corresponding density profiles are shown in inset. The surface uniformity and surface coverage of RT cast films are getting worse while decreasing the concentration of the solution. Further reduction in concentration doesn't produce any uniform film while casting at RT and it covers a small area at the end of the growth because of lack in supersaturation. On the other hand, the -30°C cast film produces uniform thin films with good surface coverage and uniformity as reducing the concentration.

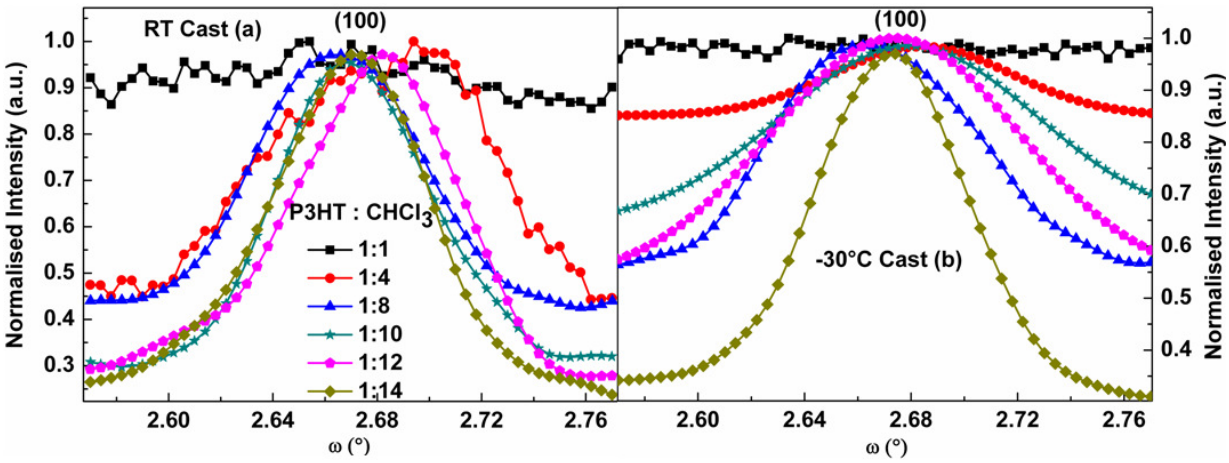


Figure 4.9: X-ray rocking curve of (a) RT and (b) -30°C cast P3HT thin films using different concentrations; the profiles were normalized to one

| Concentration (P3HT(mg)/ $CHCl_3$(ml)) | FWHM of Rocking Scan (±0.002°) | | FWHM of Azimuthal ψ Scan (±0.05°) | |
|---|---|---|---|---|
| | RT Cast | -30°C Cast | RT Cast | -30°C Cast |
| 1/1 | - | - | 28.87 | 19.69 |
| 1/4 | 0.086 | 0.066 | 17.43 | 17.86 |
| 1/8 | 0.059 | 0.07 | 15.87 | 14.45 |
| 1/10 | 0.058 | 0.095 | 12.85 | 15.23 |
| 1/12 | 0.056 | 0.091 | 11.75 | 14.91 |
| 1/14 | 0.055 | 0.054 | 12.1 | 11.2 |

Table 4.3: The FWHM of rocking and azimuthal ψ scans of P3HT film cast at RT and -30°C using different concentrations

The augment in orientation of the crystallites while reducing the concentration of the solution would be attributed to the reduction in formation of multiple nucleations (equation 2.10).[83] The rocking and azimuthal ψ scan analyses shows that the highly edge-on oriented films can be prepared by casting at -30°C but the random orientation of the crystallites increases with the concentration of the solution (Figure 4.9). Kline *et al* have reported that the orientation of the crystallites can be further increased by treating the substrate with the SAM. So, efforts have been taken to enhance the orientation of the crystallites via casting them at low temperature on the OTS treated substrate.[8]

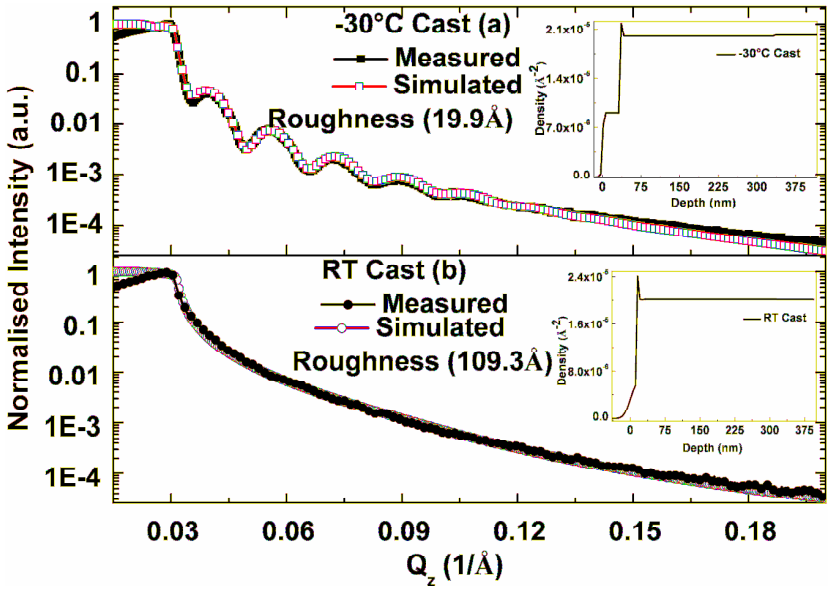


Figure 4.10: X-ray simulated and measured reflectivity profile of (a) -30°C and (b) RT cast thin films using the concentration 1mg/14ml and the corresponding density profiles are in inset

## 4.3 Influence of Substrate Silanization on the Orientation of P3HT Crystallites

Influence of substrate silanization on the enhancement in orientation of the cast and spin coated films were studied by depositing the films on the OTS treated and bare $Si/SiO_2$ substrates. It was not possible to use the same concentration (2 mg/ml) as used earlier because of the increased hydrophobicity of OTS treated substrates. Nearly 60 nm thin films were spin coated using the concentration of 5 mg/ml. For the RT and -30°C cast films, one observes a gain in diffracted intensity of the (100) Bragg peak by a factor 2 and 6, respectively as compared to the non-OTS treated substrate (Figure 4.11a). It reveals that the OTS treatment is also favorable for low temperature casting technique. The splitting of (h00) reflection is due to the presence of $CuK_{\beta}$ along with the $CuK_{\alpha}$ wavelength in the non filtered Cu tube X-ray source.[99] It has been proved by performing the measurement at DELTA synchrotron source using a monochromatic X-ray beam (not shown).

The appearance of an ill defined (020) peak at the position of $Q_z \approx 1.65$ $Å^{-1}$ in the spin coated and RT cast film envisages that the face-on oriented crystallites cannot be completely removed by depositing them on the OTS treated substrate, but it can help to increase the orientation of the crystallites at the substrate-film interface (Figure 4.11).[8] The azimuthal distribution of the crystallites was analyzed by performing the azimuthal $\psi$ scan and the corresponding scattering profile is shown in Figure 4.11b. Not much variation in the FWHM of azimuthal (100) reflection could be observed while comparing the film cast on OTS treated

substrate with the non-OTS treated one. On the other hand, the FWHM of spin coated film is reduced from 20.2° to 12.8° while spin coating on the OTS treated substrate (Table 4.4). It might be due to the formation of highly oriented crystallites at the substrate-film interface because of the increased substrate surface energy.[8, 75] The influence of substrate surface potential on the growth of the crystallites will decrease as moving away from the substrate-film interface, this can allow the formation of misoriented crystallites.[130] The increased surface potential of OTS treated substrates can produce more oriented crystallites at the buried substrate-film interface than the bare $SiO_2$ ((Figure 4.11c and 4.11d)). [8, 75]

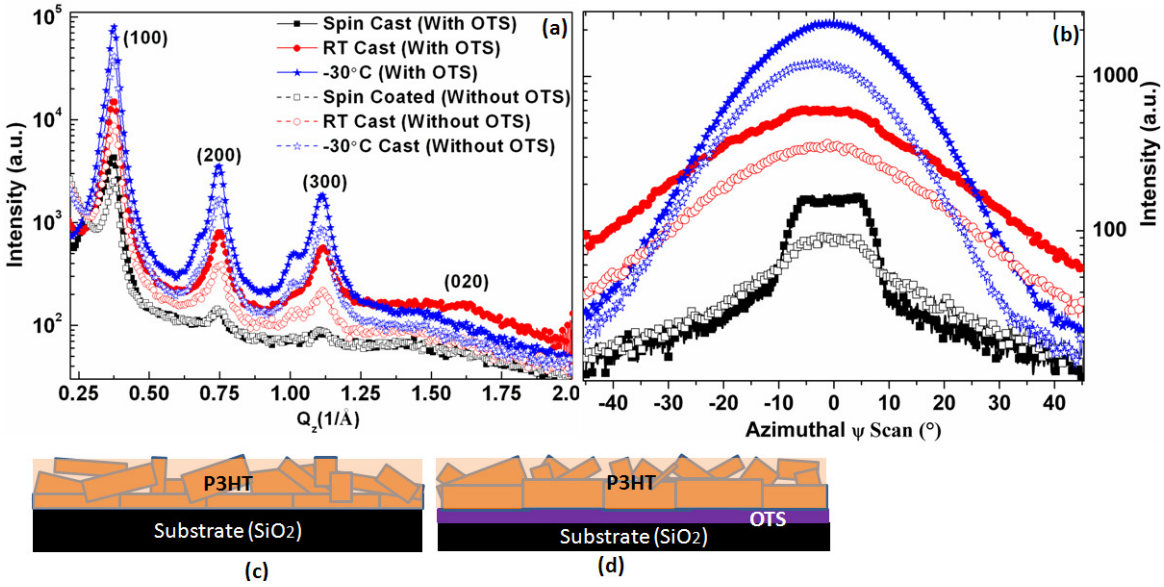


Figure 4.11: Influence of substrate silanization (OTS treatment) on the orientation of P3HT crystallites; (a) specular diffraction pattern, (b) the corresponding azimuthal ψ scan, and (c) and (d) illustrate the influence of substrate potential on the formation of oriented crystallites

| Growth Conditions | FWHM of Azimuthal ψ Scan (±0.1°) | |
|---|---|---|
| | OTS | Without OTS |
| Spin Coated (RT) | 12.8 | 20.2 |
| RT Cast | 30.9 | 30.2 |
| -30°C Cast | 22.9 | 22.8 |

Table 4.4: Variation in FWHM of azimuthal ψ scan measurment performed for the film cast at different temperature and RT spin coated

## 4.4 Electron Diffraction Analysis

Rather than the out-of-plane stacking of P3HT crystallites their in-plane stacking plays a vital role due to their incredible role in the charge transport.[7] In-plane stacking of P3HT

crystallites was analyzed via ED technique by casting ≈40 nm thin films at a concentration of 1 mg/14 ml. All the ED patterns are composed of a number of Debye-Scherrer rings with variable intensities (Figure 4.12). The integrated plot profiles were extracted from the ED patterns using the appropriate imageJ software and shown in Figure 4.12d. As observed through X-ray diffraction pattern (Figure 4.3 and 4.11a), the spin coated film (Figure 4.12e) exhibits weak (h00) (h=1,2 and 3) and (020) diffraction peaks confirming the absence of preferential orientation of crystalline domains on the $SiO_2$ substrate. The diffraction profile of -30°C cast film does not show any (h00) reflections and most of the observed reflections are indexed as (0k0) and (0kl). Presence of those mixed b- and c- reflections, especially (011) reflection at Q =1.18 $Å^{-1}$ is indicating the better in-plane perfection of P3HT domains in the -30°C cast films. The presence of weak (100) reflection in the RT cast film suggests the presence of few face-on oriented crystallites on the substrate (Figure 4.12d). All the diffraction peaks were indexed after constructing the unit cell of P3HT crystallites using the obtained reflections.

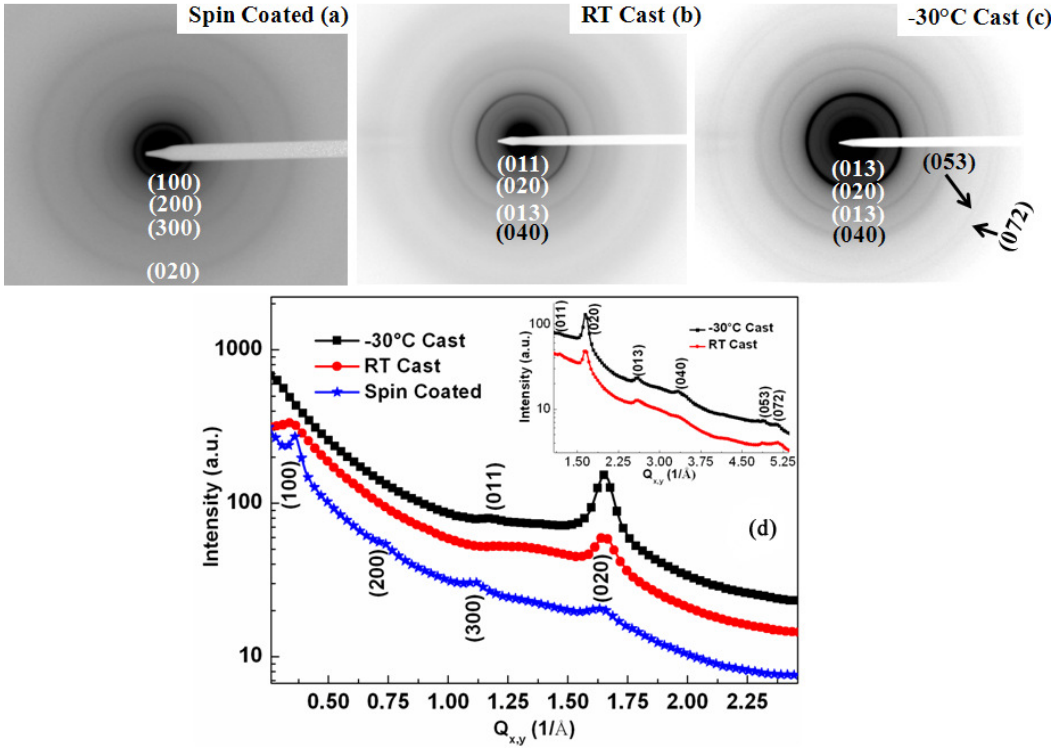


Figure 4.12: Shows the electron diffraction patterns of spin coated and cast P3HT films and their corresponding integrated intensity profile is shown in (d)

## 4.5 Unit Cell Construction of P3HT

Lattice spacing values obtained via electron and X-ray diffractions under various geometries were used to refine the structural model of P3HT crystallites. The obtained

d-values are presented in Table 4.5. The diffraction pattern of highly crystalline -30°C cast P3HT thin film was recorded under two geometries like reflection and transmission for the accurate determination of out-of-plane and in-plane lattice spacings. The diffraction pattern obtained through transmission geometry is shown in Figure 4.13a and the corresponding integrated intensity profile is shown in Figure 4.13b.

The $1/d^2_{hkl}$ has been calculated for the monoclinic system using the equation 4.4 [125] as well as with the Cerius2 program. All the observed reflections were indexed using the obtained structure model i.e. monoclinic unit cell with the unit cell parameters; a = 16.7 Å, b = 7.6 Å, and c = 7.8 Å; α = β = 90° and γ = 86.5°. The obtained lattice parameters are in agreement with the values reported by Tashiro *et al.*[58] The refined structure has a close agreement with the values reported by Kayunkid *et al*[59] and Joshi *et al*.[13] The calculated d-spacings as well as their corresponding planes are given in Table 4.5.

$$\frac{1}{d^2_{hkl}} = \frac{1}{sin^2\beta}\left(\frac{h^2}{a^2} + \frac{k^2 sin^2\beta}{b^2} + \frac{l^2}{c^2} - \frac{2hlcos\beta}{ac}\right) \qquad 4.4$$

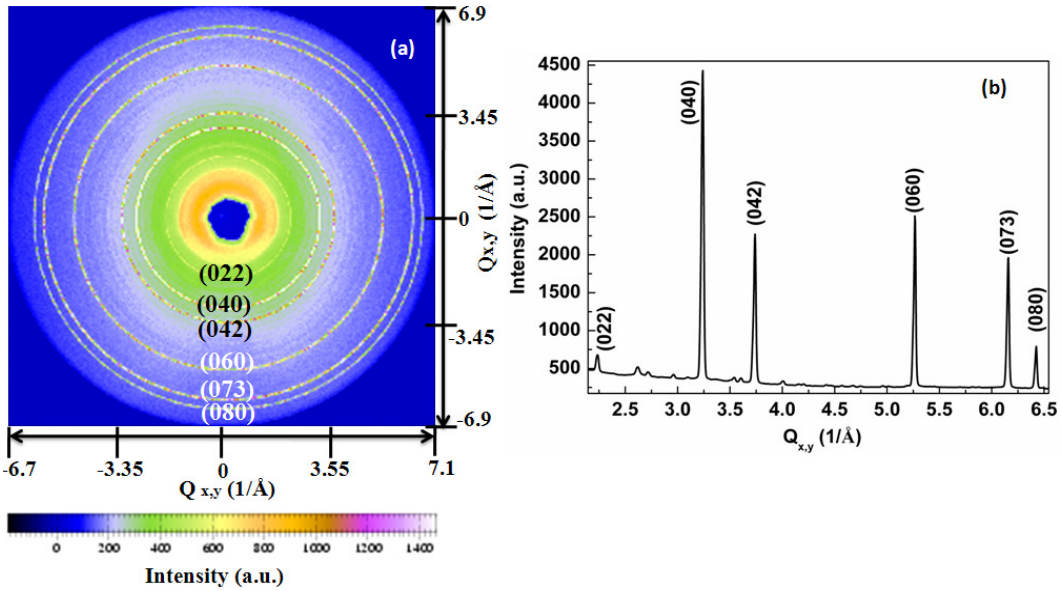


Figure 4.13: (a) depicts the 2D in-plane diffraction pattern of -30°C cast film measured at DELTA, and (b) its corresponding integrated intensity profile

| Miller indices (hkl) | Lattice-spacing (Å) | | |
|---|---|---|---|
| | Measured Values | | Calculated Values |
| | X-ray Diffraction (± 0.1Å) | Electron Diffraction (± 0.1Å) | a = 16.7, b = 7.6 and c = 7.8 Å; α = β = 90˚ and γ = 86.5˚ |
| 100 | 16.72 | 16.61 | 16.67 |
| 200 | 8.41 | 8.3 | 8.35 |
| 300 | 5.63 | 5.52 | 5.56 |
| 020 | 3.81 | 3.80 | 3.8 |
| 040 | 1.93 | - | 1.9 |
| 060 | 1.19 | - | 1.26 |
| 080 | 0.98 | - | 0.95 |
| 111 | 5.23 | - | 5.23 |
| 011 | - | 5.32 | 5.4 |
| 013 | 2.27 | 2.38 | 2.4 |
| 022 | 2.78 | - | 2.72 |
| 042 | 1.68 | - | 1.7 |
| 053 | 1.27 | 1.28 | 1.27 |
| 072 | - | 1.21 | 1.23 |
| 073 | 1.0 | - | 1.0 |

Table 4.5: Summarizes the measured and calculated lattice spacings and their Miller indices

## 4.6 Morphological Analysis of P3HT Thin Films

The morphology of semicrystalline P3HT thin films also plays an implausible role in the performance of the devices.[63, 76] The morphology of thick (≈400nm) and thin films (≈40nm) were analyzed using AFM and TEM, respectively.

### 4.6.1 Bright Field Imaging of P3HT Thin Films

The BF images of spin coated and different temperature cast (RT and -30°C) P3HT thin films were recorded to analyze the morphology of the crystallites (Figure 4.14). In order to visualize the nanomorphology by BF contrast, both a small objective aperture and adequate defocusing were used to enhance the contrast between the crystalline and amorphous phases coexist in the films. The RT cast film exhibits the distribution of long elongated nanofibrils with a characteristic length of around 200 nm and a typical width of 15 - 20 nm (Figure 4.14b). This morphology is reminiscent of the long nanofibrils observed by AFM in spin

coated and drop cast P3HT films.[16, 63, 65] On the contrary, the spin coated film shows ill-defined lamellae as observed in the case of HMW P3HT polymers.[56, 63]

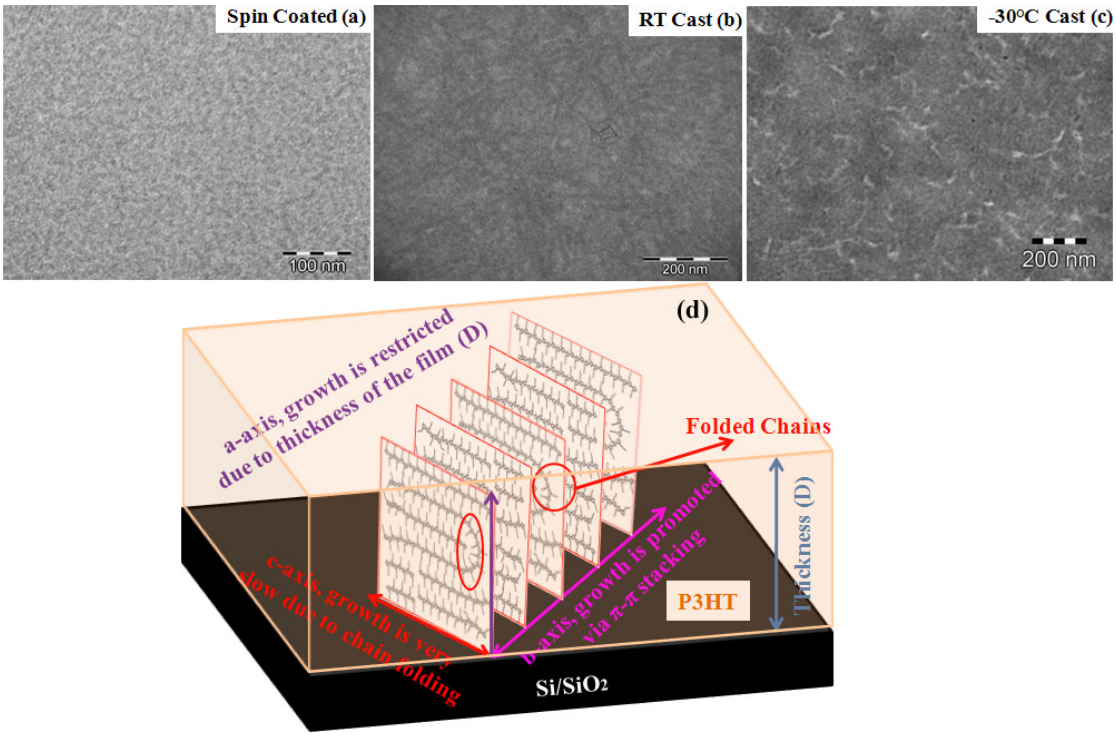


Figure 4.14: BF images of spin coated and RT and -30°C cast films, (d) depict the formation of fibrillar crystals due to the anisotropic growth of the polymers

The occurrence of nanofibrillar growth is attributed to the restriction of growth along ***a*** or ***b*** and ***c*****-**axis due to the thickness of the film and polymer chain folding, respectively.[131] When the crystallites are edge- or face-on oriented then they will have much freedom to grow along two directions because the **c**-axis is much restricted due to thiophene backbone, entanglement and folding. Chang *et al*[65] and Brinkmann *et al*[64] have reported that the increase in MW of P3HT does not help to increase the **c**-axis of the crystallites but it starts to fold. The BF morphological analysis performed by Liu *et al* for various MW P3HT depicts that the critical point of chain folding is around 10.2 kg/mol.[131] *In situ* STM analysis performed by Mena-Osteritz *et al* at the solution-substrate (highly oriented pyrolytic graphite (HOPG)) interface during the self-organization of P3AT visualizes the folded conformation of thiophene backbones with various angles.[113] While comparing the width of the nanofibrils with the contour length of the polymer chains used for the analysis (number of monomers present in the polymer unit) concludes the folded conformation of thiophene backbones (Table 2.1).[131] The growth of edge- and face-on oriented crystallites can be restricted along the substrate normal due to the reduced thickness (D) of the films. Ultimately, they will get

much freedom to grow along only one direction i.e. along the alkyl side chain stacking direction for face-on oriented ((h00)) crystallites and along π-π stacking direction ((0k0)) for the edge-on oriented crystallites. The growth of an edge-on oriented nanofibril is schematically shown in Figure 4.14d.

The morphology of -30°C cast film is entirely different from the RT cast film. Instead of nanofibrils, the BF image shows an assembly of lamellar crystals separated by the bright contour lines corresponding most presumably to the "grain boundaries" between the lamellae. Contrary to the highly oriented P3HT films grown by epitaxy on the substrates of potassium 4-bromo-benzoate, no clear nanomorphology corresponding to the amorphous/crystalline alternation could be observed in the domains of drop cast P3HT.[15] This observation supports the GIXD results i.e. -30°C cast film is composed of mainly edge-on oriented crystallites. In comparison to the X-ray findings, the variation in morphology may be due to the layer-by-layer growth of the films while casting at -30°C.

### 4.6.2 AFM Analysis

The height and phase images of spin coated (≈17 nm) and RT and -30°C drop cast (≈400 nm) films were recorded by operating the AFM under tapping mode (Figure 4.15). The topographic images shows higher surface roughness of drop cast films as compared to the spin coated one (Figure 4.16). The roughness of the film increases while decreasing the cast temperature from RT to -30°C because of the presence of valleys (Figure 4.15c). Similar to the BF images of -30°C cast thin film (≈ 40 nm) (Figure 4.14c), the -30°C cast thick film (≈400 nm) also contains holes (Figure 4.15c). The morphology of thick and thin film is entirely different i.e the BF image of RT cast film clarifies the growth of nanofibrils (15-20nm width and few $\mu$m long) (Figure 4.14b) but the AFM height image of RT cast thick film envisages the cloudy like pattern (Figure 4.15b). The phase images can be interpreted by associating the bright color with hard and dark color with soft areas present in the films.[72, 122] Having this in mind, the -30°C grown film (Figure 4.15f) has nearly a uniform distribution of bright color i.e. uniform crystalline phase.[72, 122] A small portion of dark color is visible in the phase image of -30°C cast film which is attributed to the valleys present in the film (Figure 4.15c). On the other hand, the phase image of RT cast film (Figure 4.15e) shows the coexistence of both the amorphous and crystalline phases. The phase image of spin coated film illustrates very small patches of bright parts within the dark region, i.e. existence of small crystallites in an amorphous phase.[72, 122]

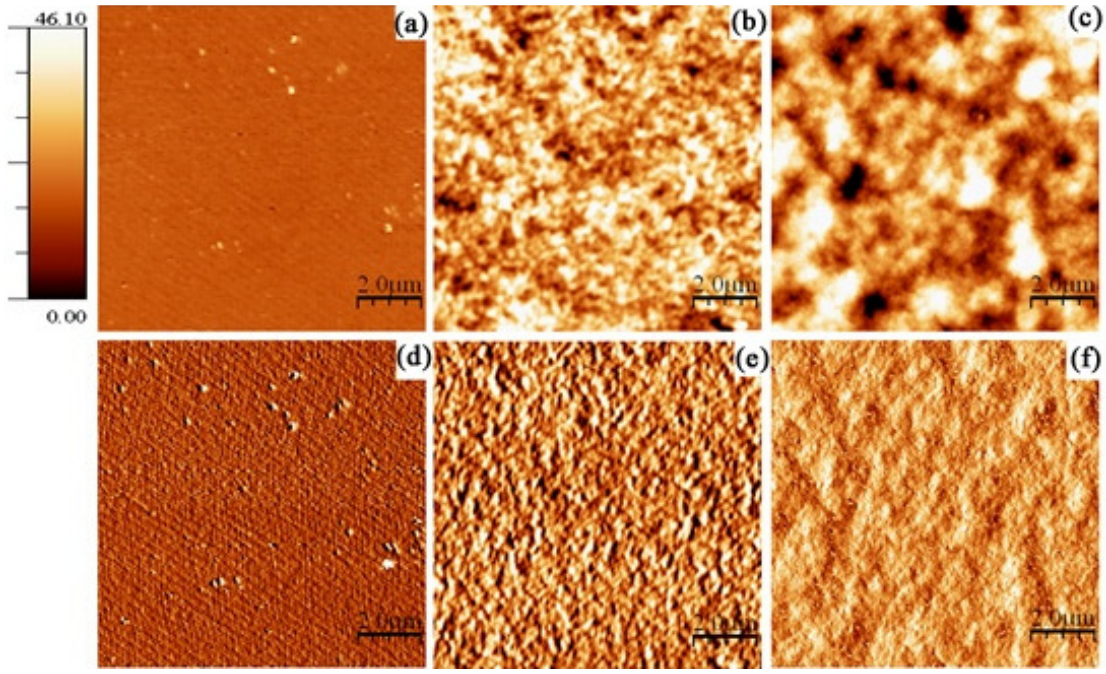


Figure 4.15: AFM tapping mode height (top row) and phase (bottom row) images of annealed films: (a, d) spin coated, (b, e) RT, and (c, f) -30˚C cast

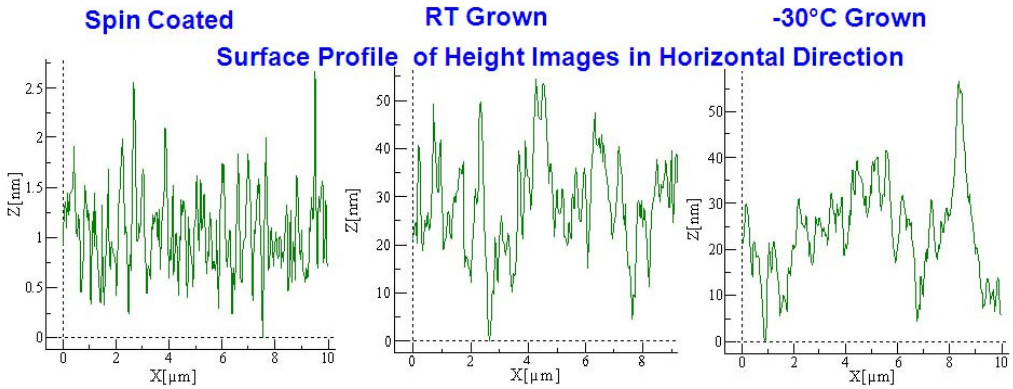


Figure 4.16: The extracted line profile from the AFM height image of spin coated, RT and -30°C cast P3HT along horizontal direction

## 4.7 Discussion

The detailed X-ray and electron diffraction analyses performed in this chapter concludes that the number of edge-on oriented crystallites can be increased by decreasing the cast temperature which has been identified as a prerequisite for the fabrication of efficient HMW P3AT OFETs. [1, 2, 7]

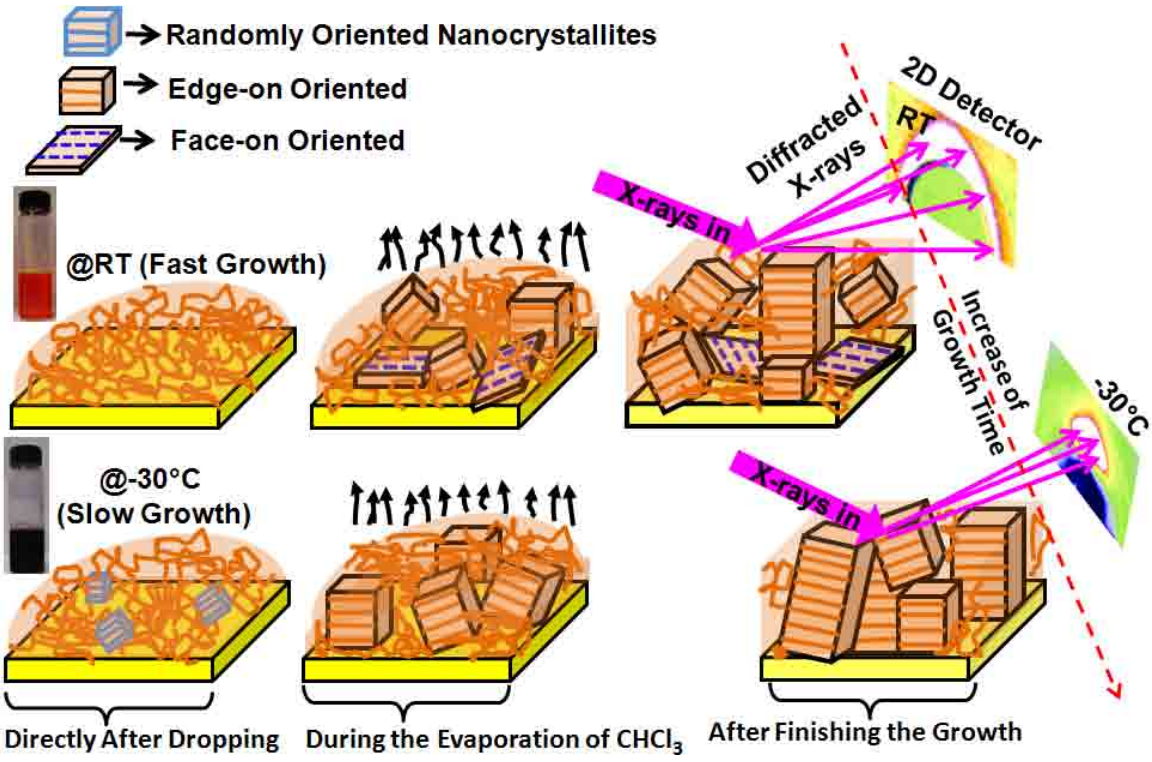


Figure 4.17: Schematically illustrate the formation of edge-on oriented crystallites due to the reduction in growth temperature

Among three ways of achieving supersaturation, cooling has two important effects i.e. i) slowing down the evaporation of $CHCl_3$ which can assist to reduce the formation of multiple nucleations and ii) to prolong the growth time. In other words, P3HT aggregates will set-in at a lower P3HT concentration in $CHCl_3$ as compared to RT while reducing the cast temperature. This should result in lower nucleation density and larger crystalline domains with enhanced crystallinity. For example, the evaporation of $CHCl_3$ is slower at -30°C (for example, 250 $\mu$l takes ≈300minutes to evaporate completely at 1bar pressure) than RT (≈10minutes for 250 $\mu$l at 1bar pressure), therefore the crystallization of P3HT will occur on a longer time scale and the polymer concentration in a solution will increase slowly allowing the aggregates to adopt the thermodynamically most stable orientation on the substrate (Figure 4.17).[12, 16, 83]. It is to note that the evaporation time of the solvent is also depends on the amount of solution that has been dropped. According to the equation 2.10, the formation of unwanted multiple nucleations can be controlled by two ways either by increasing the temperature or by reducing the concentration. We have seen that the increase of cast temperature can produce the unwanted face-on oriented crystallites (Figure 4.3) because of the fast evaporation of $CHCl_3$. X-ray rocking and azimuthal profiles recorded for the film cast using different concentration shows that the crystallite size and orientations are increased

as the concentration of the solution decreases (Figure 4.8 and 4.9). Not only the orientation, but it can also assist to decrease the thickness of the films. It has been reported that 20 - 50 nm thick active layers (organic semiconductor) are enough for the fabrication of OFETs.[114, 115, 130] It was able to prepare ≈40 nm thin films by reducing the concentration down to 1 mg/14 ml with less surface roughness and high surface coverage which cannot be obtained by casting at RT.

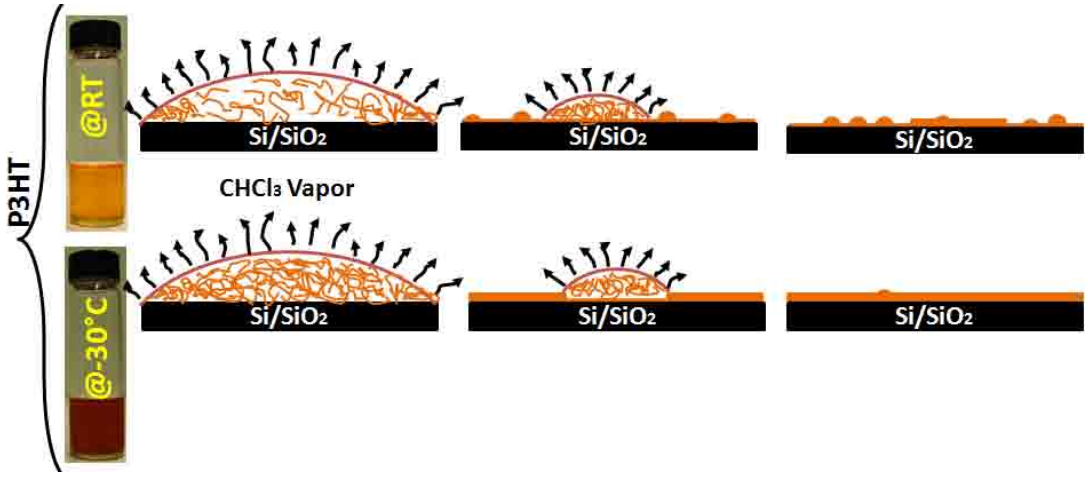


Figure 4.18: Influence of cast temperature on the roughness, thickness, and surface coverage of solution processable polymeric thin films

In 2009, Krebs stated that casting is one of the cheapest techniques for the fabrication of large scale devices but it is suffering from the fluctuation in density and layer thickness across the film.[10] As compared to the widely used spin coating and doctor blading techniques, low temperature casting can also provide comparatively uniform thin films. The X-ray reflectivity profiles depicts that very thin (≈40 nm) and smooth (≈20 Å) P3HT films with good surface coverage can be prepared by casting the films at -30°C using very diluted solution (1 mg/14 ml). On the other hand, the RT cast P3HT film does not produce thin films with uniform surface coverage cast using the same concentration. The non-uniformity in layer thickness across the RT cast film is associated to the contact angle dependent supersaturation of the solution.[80] It is schematically shown in Figure 4.18. The formation of uniform thin films while casting at -30°C can be explained using the equation 2.2. If the dropped solution is not supersaturated then it can supersaturate only when the solvent starts to evaporate.[83] Amundson *et al* reported that the polymers are not uniformly distributed whole over the droplets but it concentrates much on the foot of the droplets.[80] Ultimately, it will supersaturate first at the foot of the droplets and proceed to grow (Figure 4.18). It brings most of the polymers till the end of the growth stage because of lack in supersaturation and results a

thick film of around 60 nm at one place (measured by AFM). On the contrary, there will not be much variation in polymer concentration throughout the droplets in case of a supersaturated solution (Figure 4.18). This is the reason why the -30°C cast film produces uniform thin films because it can supersaturate directly after the dropping due to the reduction in cast temperature.[83]

It clearly shows that the selection of proper concentration, cast temperature, and very flat working surface are mandatory in order to achieve very thin and uniform films. Finally, the widely used spin coating technique for the fabrication of thin and uniform films can be replaced by low temperature casting to produce thin films with uniaxial orientation. Another point is that the polymer based devices are cheaper than the commercially used inorganic based devices because of their solution processability as compared to the cost of conducting polymers.[1, 2] Thickness of low temperature cast films can be reduced by reducing the concentration of the solution, but the proper casting temperature must be chosen at which temperature the undertaken solution can be supersaturated. The detailed analysis shows that the cast temperature maintains the crystallinity, orientation, crystallite size, surface coverage, and uniformity, so it can be varied according to the need of customer.

- *Polymer based devices are cheaper compared to the inorganic based devices because of their solution processability. The current chapter taught us that the highly crystalline polymeric thin films can be prepared by reducing the cast temperature of the solution processable polymers which have positive solubility. In addition, some of the other solution processable P3AT polymeric thin films have been prepared at below RT and it will be discussed in the upcoming chapter V.*

# Chapter V

## 5 Influence of Alkyl Side Chain Length on the In-plane Stacking of RT and Low Temperature Cast Poly(3-alkylthiophene) Thin Films

Among the P3AT family, P3HT is a working host for the fabrication of OFETs and solar cells.[2, 41, 132] In this chapter, the influence of alkyl side chain length on the in-plane stacking of P3AT crystallites and its importance on their electrical and optical properties will be discussed. Four P3AT polymers were used for the analysis by sequentially increasing the number of hydrocarbons from n-pentyl to n-octyl. Thin P3AT films with various thickness of around ≈400 nm and 40 nm were cast using two different concentrations like 2 mg/ml and 1 mg/14 ml, respectively. In the current chapter V, these films will be referred to as thick (≈400 nm) and thin films (≈40 nm).

### 5.1 X-ray Diffraction of P3AT Thick Films

Growth temperature of all the P3AT polymers such as P3PT, P3HT, P3HeptT, and P3OT were optimized by casting them at various temperatures like 23°C, 8°C, -12°C, and -30°C for a given concentration (2 mg/ml). The GOD profile of different temperature cast P3AT thick films are shown in Figure 5.1. The scattering intensity of (h00) reflection increases as the cast temperature decreases i.e. increase of edge-on oriented crystallites. The integrated intensity of (100) reflection is shown as a function of cast temperature in Figure 5.2a. As already observed in the case of P3HT film, the integrated intensity of (100) peak increases till -12°C and it is getting saturated. A marginal change in intensity was observed while reducing the cast temperature from -12°C to -30°C. The FWHM of the Bragg reflections are decreasing with the cast temperature. The effective crystallite size was extracted from the FWHM of (100) Bragg reflection using the Debye-Scherrer relation (equation 4.4). The obtained crystallite sizes are shown in Figure 5.2b as a function of cast temperature. The effective crystallite size increases with the alkyl side chain length. It could be attributed to the increase in solubility of P3AT polymers while increasing the alkyl side chain length which can increase the size of a critical nucleus (equation 2.9).[5, 6] The increase in crystallite size with decrease of cast temperature was already discussed in chapter 4.1. After optimizing the growth temperature, further analysis was performed only by casting the films at RT and -30°C in order to understand the influence of alkyl side chain length on the crystallite orientation of P3AT thin films.

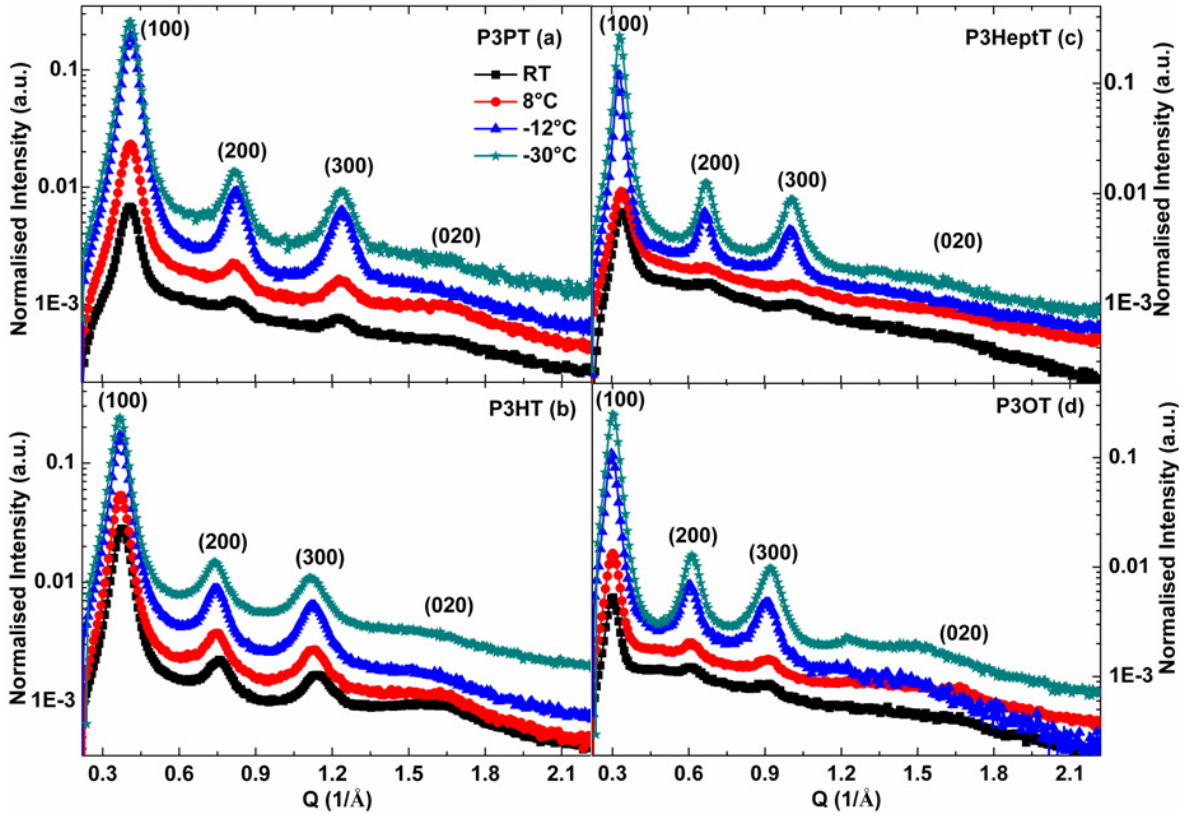


Figure 5.1: GOD line profile 23°C, 8°C, -12°C, and -30°C cast P3AT thin films extracted from the 2D diffraction patterns; the peaks were shifted from the same baseline by multiplying with a factor for better presentation

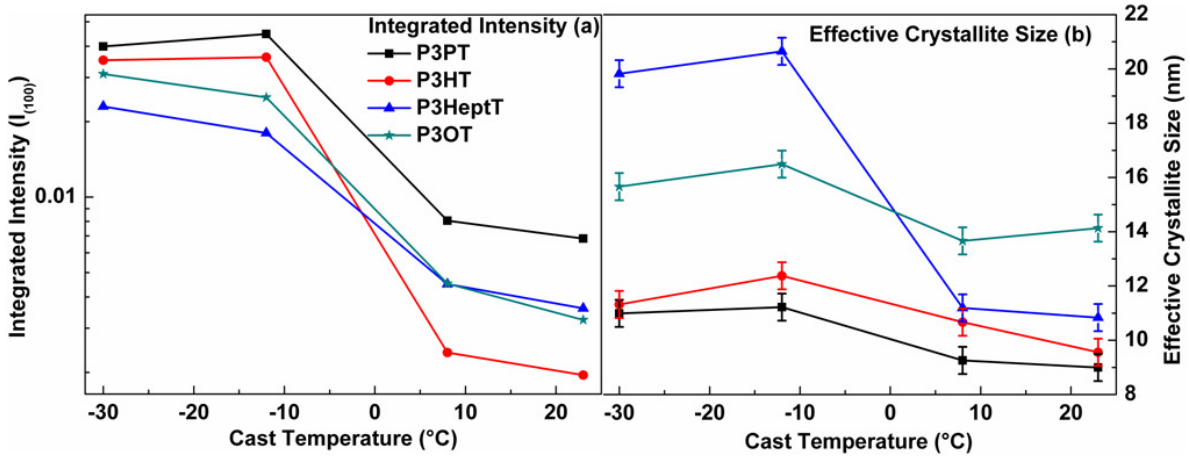


Figure 5.2: (a) Integrated of intensity of (100) Bragg peak cast at different temperatures like 23°C, 8°C, -12°C, and -30°C; (b) the effective crystallite size extracted from the FWHM of (100) Bragg peak

2D X-ray diffraction pattern of RT and -30°C as-cast P3AT thick films are shown in Figure 5.3. The RT cast P3AT thick films are composed of several Debye-Scherrer rings of (h00) and (020) reflections which confirm the absence of uniaxial orientation on the substrate

due to the fast evaporation of $CHCl_3$ (Figure 5.3 left columns). On the other hand, the -30°C cast films are resulting an elliptical (h00) spot along Q (out-of-plane) and more or less intense (020) reflection along in-plane direction (Figure 5.3 right column). That confirms the formation of only edge-on oriented crystallites while casting at -30°C (Figure 3.6) with pronounced in-plane stacking.

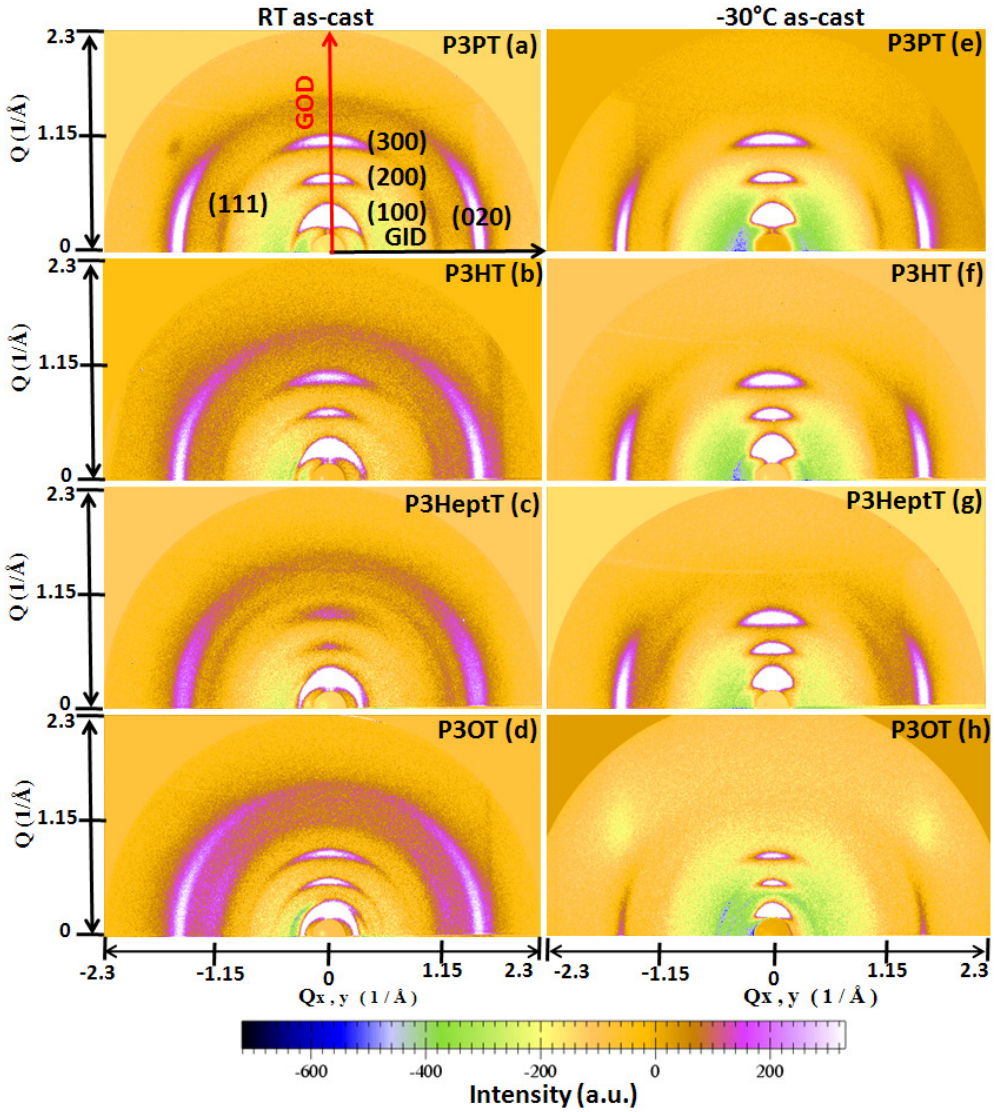


Figure 5.3: 2D X-ray diffraction pattern of RT (left column) and -30°C (right column) as-cast thick (≈400nm) P3AT films

The scattering intensity of (100) reflection along in-plane direction is increased by increasing the alkyl side chain length while casting the films at RT. A line profile has been extracted from the 2D diffraction patterns along the in-plane direction and shown in Figure 5.4. Figure 5.4a reveals an increase of face-on oriented crystallites while increasing the alkyl side chain length. There is no indication of any face-on oriented crystallites exists in the film

while casting at -30°C (Figure 5.4b). It depicts that the highly edge-on oriented and well in-plane stacked crystallites can be prepared by low temperature casting together with the reduction of alkyl side chain length. The weakening of (111) and (020) reflections while increasing the side chain length envisages the deterioration of in-plane perfection of P3AT crystallites (Figure 5.4). The interchain stacking of P3AT crystallites get better while casting at -30°C and it subsequently reflects it through the reduction in FWHM of (020) reflection (Table 5.1).

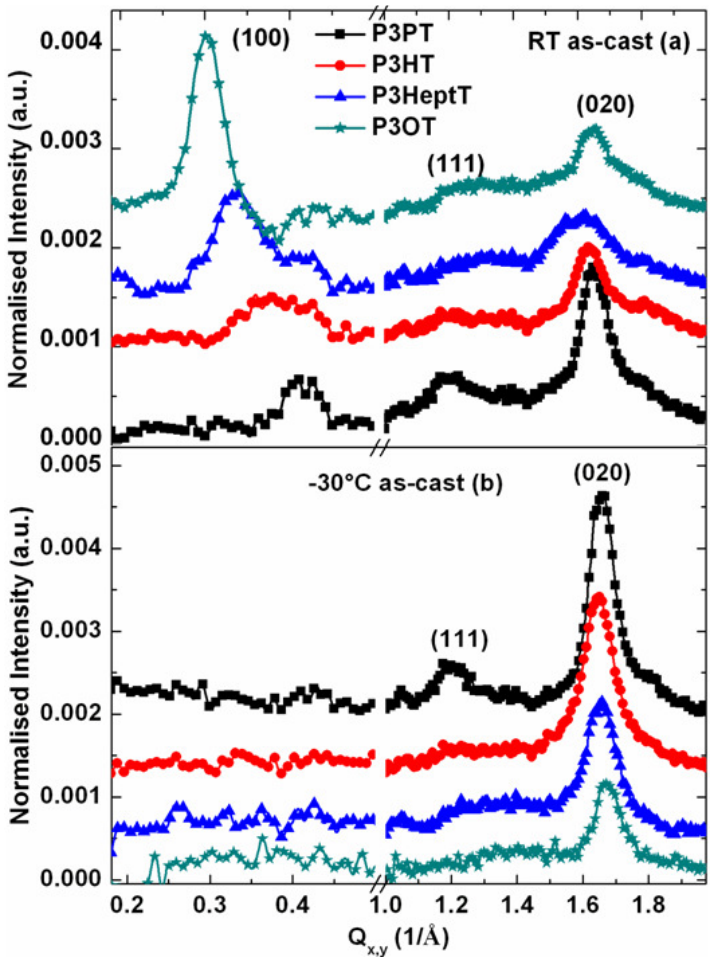


Figure 5.4: The GID line profile of RT and -30°C as-cast P3AT thick films which is extracted from the figure 5.3; the profiles were normalized by incoming flux and shifted from the same baseline

The scattering intensity of in-plane (100) reflection of RT cast film is gradually increasing with the alkyl side chain length. The azimuthal distribution of the crystallites were studied by extracting the azimuthal profile of (100) reflection from the 2D diffraction patterns of RT and -30°C as-cast P3AT thick films as schematically shown in Figure 3.7. The extracted azimuthal profiles are presented in Figure 5.5. It depicts that the azimuthal

distribution of the crystallites increases with the alkyl side chain length for the films cast at RT. The FWHM of (100) azimuthal profile is presented in Table 5.1, the FWHM of RT cast film is increasing with the alkyl side chain length, but it does not vary while casting at -30°C (≈22°). Overall results suggest that there is an increase of formation of non-thermodynamically stable crystallites while increasing the alkyl side chain length (Figure 5.4). Thick films were annealed at an undercooling of 45°C for the recrystallization of thermodynamically trapped crystallites.[11, 13] The melting temperature of the undertaken P3AT polymers is presented in Table 2.1. Annealing temperature of the undertaken P3AT polymers was optimized by performing an *in situ* GOD annealing analysis (Figure 3.10).

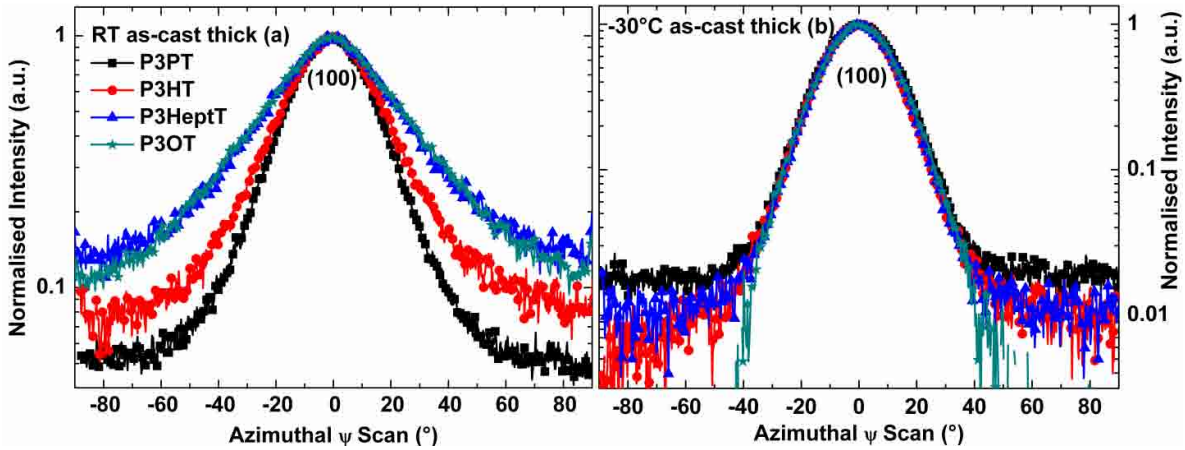


Figure 5.5: Azimuthal profile of (100) reflection extracted from the 2D diffraction pattern of as-cast RT (a) and -30°C (b) cast P3AT thick films; the profiles were normalized to one

| Polymers | FWHM of Azimuthal (100) Peak (±0.5°) | | FWHM of (020) peak (±0.05°) | |
|---|---|---|---|---|
| | RT as-cast | -30°C as-cast | RT as-cast | -30°C as-cast |
| P3PT | 28.5 | 23.1 | 0.97 | 0.61 |
| P3HT | 31.2 | 22.5 | 1.18 | 0.7 |
| P3HeptT | 38.9 | 22.3 | 1.22 | 0.82 |
| P3OT | 41 | 23.4 | 1.56 | 0.79 |

Table 5.1: Variation in FWHM of (100) azimuthal profiles and (020) peak of P3AT thick film cast at RT and -30°C

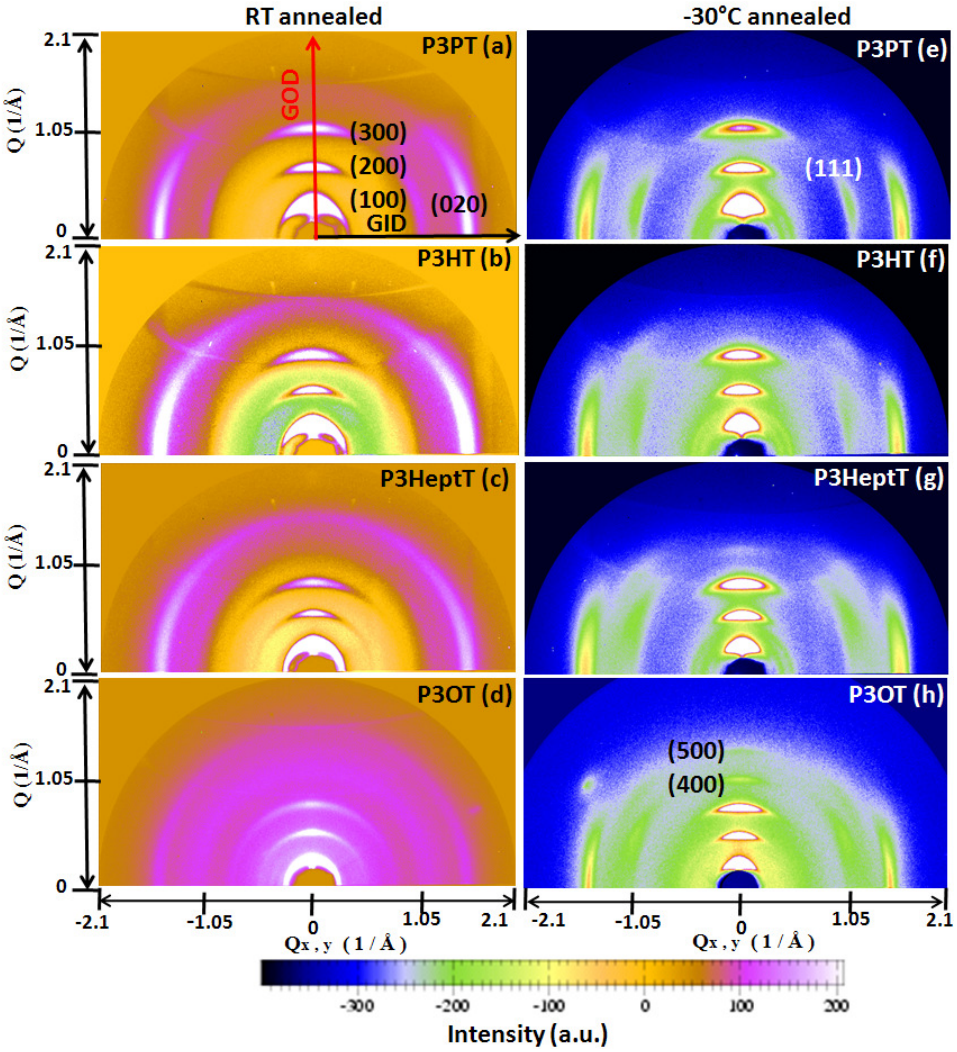


Figure 5.6: 2D X-ray diffraction pattern of annealed P3AT thick films cast at RT (left column) and -30°C (right column)

The ascribed tendencies become much more pronounced and elucidated after annealing the samples for an hour at 45°C below their corresponding melting point (Figure 5.6) i.e. increase of face-on and randomly oriented crystallites with poor in-plane perfection as increasing the alkyl side chain length while casting at RT. Increase in misorientation of the crystallites while casting at RT (Figure 5.4a and 5.6 left column) might be due to the delay in initiation of nucleation as the side chain length increases because of their enhanced solubility.[6, 16] After post growth annealing, the asymmetric reflections (h11) became much more pronounced and well defined for the case of -30°C cast films. The superior in-plane stacking of P3AT crystallites after the post growth annealing might be attributed to the reduction in plasticity of thiophene backbones and ripening of the crystalline domains. It will be discussed much more elaborately in chapter VI. The (h11) and (020) reflections start to fade while increasing the alkyl side chain length. That envisages the high

in-plane perfection of P3AT crystallites while casting at -30°C together with the reduction of alkyl side chain length.

## 5.2 X-ray Diffraction of P3AT Thin Films

Further, very thin films (≈40 nm) were prepared using a concentration of 1 mg/14 ml, it has been chosen after performing the concentration dependent orientational analysis of P3HT thin films (chapter 4.2.1). X-ray specular scan of -30°C and RT cast thin films are shown in Figure 5.7. There is a small variation in the intraplane stacking distance '$d_{(100)}$' of RT and -30°C cast film, that will be discussed later. The scattering intensity of the film increases with the alkyl side chain length and it can be observed in both the RT and -30°C cast films.

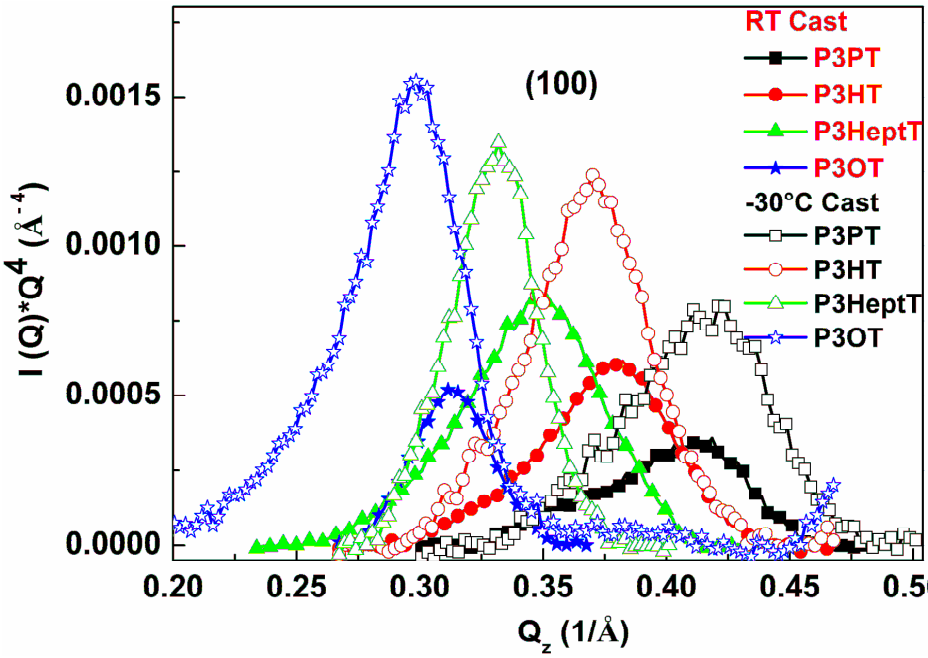


Figure 5.7: The specular diffraction profile of RT and -30°C as-cast P3AT thin films (≈40nm) (normalized to the incoming flux)

According to the scattering theory, the amplitude of scattering will add up at Q=0 because the X-ray waves scattered from different parts of the electron cloud in an atom are all in phase. As Q increases, the waves from different part of the atom develop more phase differences, subsequently the overall amplitude begins to decrease.[133] As per the Porod law, the scattering intensity "I(Q)" decreases rapidly by $Q^4$ as Q increases in small-angle X-ray scattering (SAXS) for the case of smooth surfaces and sharp boundaries. It can be explained with a simple mathematical equation 5.1.[134] The measurements were carried out at DELTA using the X-ray beam of having the wavelength of 0.82 Å. Eventually, the Bragg angle of (100) peak has shifted towards the lower scattering angle which lies in the range of

SAXS.[99] Therefore, the measured intensity profiles were multiplied by $Q^4$ in order to compare the scattering intensities of (100) reflections of four polymers which arises at different Q values. It clearly shows that the increase in scattering intensity of (100) reflection with the side chain length is not due to the reduction in scattering angle.

$$I(Q) = \frac{2\pi}{Q^4}(\Delta\rho)^2 S \qquad 5.1$$

Here: $\Delta\rho \rightarrow$ electron density difference between the domains and the matrix material

$S \rightarrow$ surface of the particles

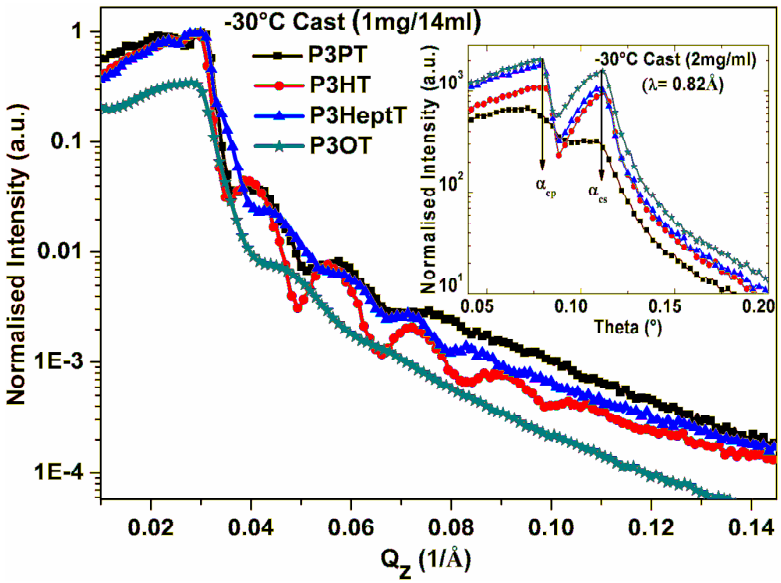


Figure 5.8: X-ray reflectivity graph of -30°C cast thin films and inset shows the critical angle of P3ATs (thick films)

According to the equation 3.13, the scattering amplitude of a crystal is depending on the product of two terms i.e. unit cell structure factor and the lattice sum.[92, 96, 99] Thickness and electron density of -30°C cast films were calculated using the X-ray reflectivity technique. The corresponding X-ray reflectivity profiles of thin and thick films are shown in Figure 5.8 and its inset, respectively. The calculated thicknesses and electron density values of -30°C cast P3AT thin films are given in Table 5.2. It confirms that the increase in scattering intensity of P3AT thin films upon increasing the alkyl side chain length is neither due to the thickness nor the variation in electron density.[92] Even the thickness of P3OT film is lesser than the thickness of P3PT film. The thickness of RT cast films were not able to measure through X-ray reflectivity technique because they were quite rough and they never produces uniform film because of the contact angle dependent supersaturation of the solution and formation of nucleations (chapter 4.7).[80] Thickness of RT cast films were measured by

AFM. Thickness of the RT cast film varies with respect to the places as discussed in chapter 4.7. The highest thickness value is about 60 nm. The analyses of RT cast films were performed on the thickest place. The difference in scattering intensity of RT and -30°C cast films is not due to the thickness but it is completely due to the enhancement in crystallite orientation and crystallinity of the films.[8, 96, 99] The enhancement in scattering intensity of P3AT films as increasing the number of hydrocarbons in the grafted alkyl side chain might be due to the solubility dependent growth of oriented crystallites.

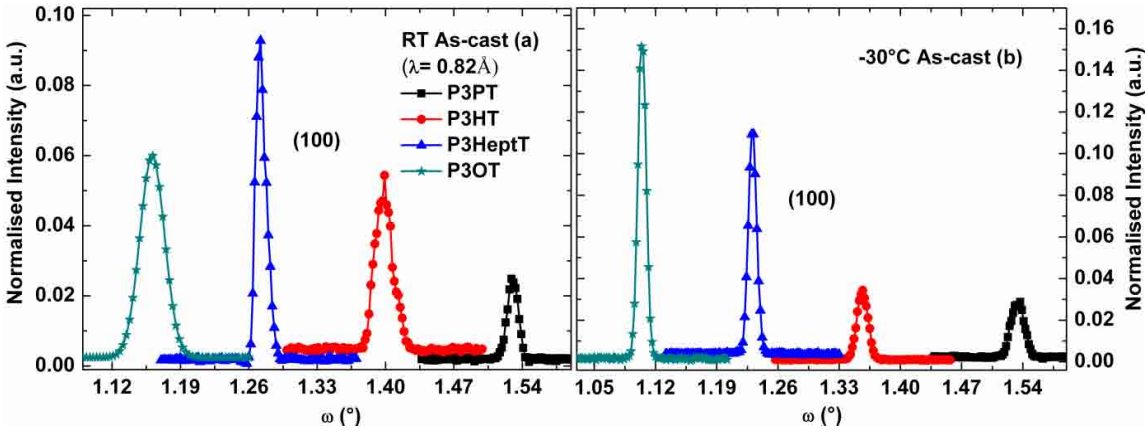


Figure 5.9: X-ray rocking profile of (100) Bragg peak; (a) RT and (b) -30°C cast P3AT thin films

X-ray rocking scan analysis was carried out in order to understand the mosaicity of P3AT thin films.[74, 99] The measurements were carried out using a monochromatic wavelength (λ=0.82 Å). The samples were rocked ±0.1° after fixing the detector and the incoming beam under Bragg condition of (100) peak as explained in chapter 3.1.4. The X-ray rocking profile also contains the beam reflected from the substrate because of small angle scattering. It has been subtracted by recording the reflected beam using a pure substrate ($Si/SiO_2$). The obtained X-ray rocking profile is shown in Figure 5.9. The rocking curve of -30°C cast P3OT covers the whole intensity of the specular scan where the RT cast P3OT fails to do that. The rocking curves of both the RT and -30°C cast films are sharper but they are slightly varying in FWHM (Table 5.2). The obtained FWHM is much smaller than the value reported for the spin coated films prepared on the OTS treated substrate.[8] The lateral crystallite size of RT and -30°C cast P3AT thin films were extracted from the FWHM of X-ray rocking curve and presented in Table 5.3.[105] The lateral crystallite size of -30°C cast film is comparatively higher than the RT cast one. The mosaicity of the crystallites can be extracted from the FWHM and the background scattering of X-ray rocking curve, but not much variation could be seen in the FWHM as well as the background scattering of RT and

-30°C cast films while varying the side chain length (Table 5.3 and Figure 5.9).[8, 96] So, it was rather difficult to explain the growth using the obtained rocking curves.

| Polymers | FWHM of X-ray Rocking Scan (±0.0001°) | | Electron Density ($1/Å^3$) (±0.01) | Average Thickness of the Films (±2nm) | |
|---|---|---|---|---|---|
| | RT As-cast | -30°C As-cast | | RT As-cast | -30°C As-cast |
| P3PT | 0.0112 | 0.0155 | 0.32 | - | 47.9 |
| P3HT | 0.0186 | 0.0126 | 0.33 | - | 39 |
| P3HeptT | 0.0108 | 0.0094 | 0.32 | - | 48.6 |
| P3OT | 0.0255 | 0.0092 | 0.32 | - | 38.2 |

Table 5.2: Summarizes the FWHM of X-ray rocking scan, electron density, and thickness (1mg/14ml) of P3AT thin films

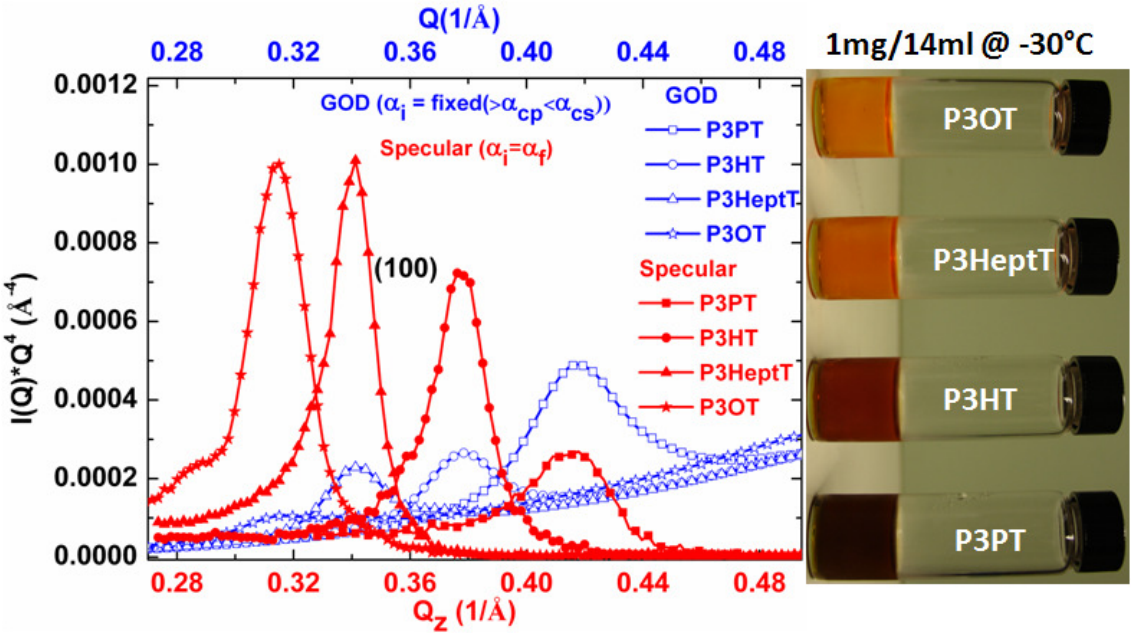


Figure 5.10: Depicts the GOD (blue color) and specular scan (red color) of thin P3AT films measured at the same place -30°C cast films after the post growth annealing; the right side vials depicts the increase in solubility of P3ATs as increasing the alkyl side chain length

Therefore, two scattering geometries such as GOD and X-ray specular scans were used to understand the orientation of the crystallites. The obtained diffraction profiles are shown in Figure 5.10. GOD and specular scans were performed at the same place of -30°C cast P3AT thin films after the post growth annealing. Increase of scattering intensity at higher Q of GOD scan might come from the multiple scattering.[135] The scattering intensity of (100) specular Bragg peak increases while increasing the side chain length. In opposite to the specular scan, P3PT polymer has more intense (100) reflection than the P3OT film while

performing the GOD scan and it is decreasing gradually as the alkyl side chain length increases (Figure 5.10 (blue color)). It helps us to explain the formation of randomly oriented nucleates due to the reduction in solubility of P3AT polymers while decreasing the alkyl side chain length.[5, 6] For example, the small vials showed on the right side of Figure 5.10 depict the decrease in solubility of P3ATs with the side chain length for a given concentration (1 mg/14 ml) at -30°C. The complete dissolution of P3OT at -30°C can supersaturate during the evaporation of $CHCl_3$ and it can nucleate at the substrate-solution interface in comparison to the P3PT and it can produce highly edge-on oriented bigger crystallites.[16, 83] It can be further proved by extracting the effective crystallite size along the vertical (from the specular scan) and lateral directions (from the rocking scan).[105] The crystallite sizes of -30°C cast films are increased in both the directions while increasing the alkyl side chain length (Table 5.3), it might be due to the reduction in multiple nucleations.[83] On the other hand, the crystallite size of RT cast films varies randomly. It might be due to the formation of trapped crystallites. Rather than the out-of-plane stacking of edge-on oriented crystallites their in-plane stacking plays a vital role because it governs the performance of OFETs and solar cells. It has been analyzed through ED technique.

| Polymers | Lateral Crystallite Size ($L_{lat}$) (±0.2$\mu$m) | | Vertical Crystallite Size ($L_{vert}$ (±1nm)) | |
|---|---|---|---|---|
| | RT As-cast | -30°C As-cast | RT As-cast | -30°C As-cast |
| P3PT | 13.2 | 10.2 | 25. 5 | 19.3 |
| P3HT | 9.3 | 14.3 | 23.4 | 23.4 |
| P3HeptT | 17.6 | 20.8 | 21.2 | 29.9 |
| P3OT | 8.2 | 23.6 | 29.1 | 30.0 |

Table 5.3: Lateral and vertical crystallite sizes extracted from the rocking scan and the specular scan, respectively

## 5.3 Electron Diffraction Analysis of Drop Cast P3AT Thin Films

The in-plane stacking of RT and -30°C cast P3AT thin films (≈40nm thick) were analyzed through the ED technique. The integrated ED plot profiles of as-cast (left column) and annealed (right column) films are shown in Figure 5.11. The intensity of (020) Bragg peak gets weaker while increasing the alkyl side chain length as observed in the X-ray diffraction pattern of thick films (Figure 5.4). The integrated intensity of (020) reflection was extracted from the diffraction pattern of RT and -30°C cast films and shown in Figure 5.12. The increase in integrated intensity of (020) peak while reducing the side chain length as well

as the cast temperature envisages the formation of highly interchain stacked crystallites. The appearance of well pronounced (011) and (031) reflections in P3PT as compared to P3OT concludes the formation of less disordered thiophene backbones while decreasing the alkyl side chain length.

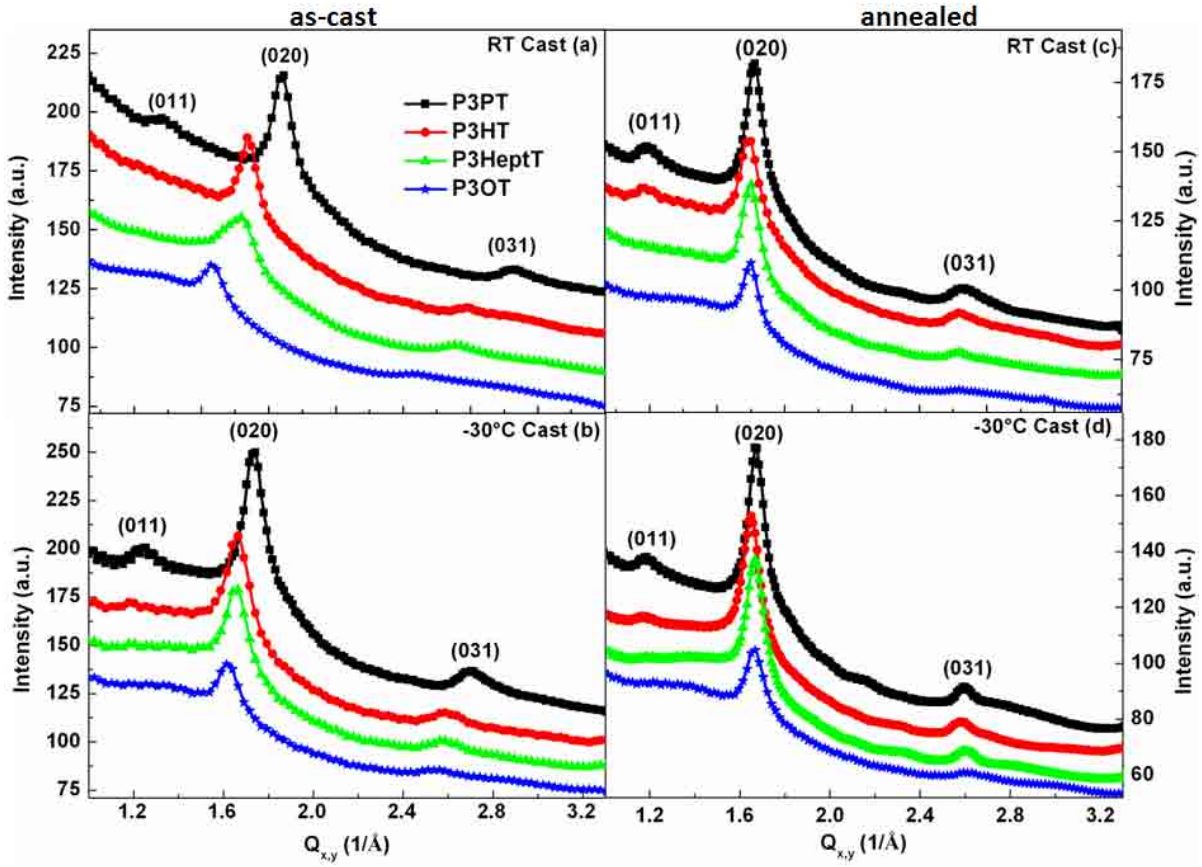


Figure 5.11: The ED integrated intensity plot profile of as-cast (left column) and annealed (right column) P3AT films cast at RT and -30°C; profiles were shifted by adding some values from the same baseline for better presentation

The interchain stacking distance '$d_{(020)}$' is increased while increasing the side chain length from n-pentyl to n-octyl but it was not observed in thick films (Figure 5.4). After the post growth annealing, the interchain stacking distance of all the P3AT polymers were the same (3.8 Å) (Figure 5.13b). The interchain stacking distance of RT cast P3PT film is increased from 3.4 Å to 3.8 Å after the post growth annealing. The same behavior was also observed for the spin coated P3PT film and it increased from 3.6 Å to 3.8 Å after annealing at 204°C (chapter VI). It clarifies the enhancement in π-π interaction while decreasing the alkyl side chain length due to the reduction in steric hindrance between the grafted alkyl side chains.[42]

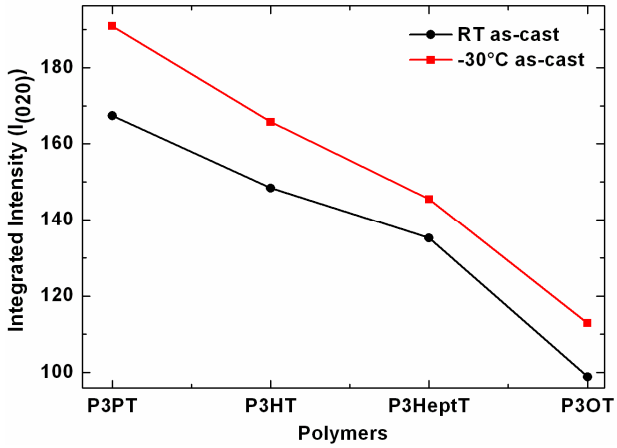


Figure 5.12: Integrated intensity of (020) peak versus polymers

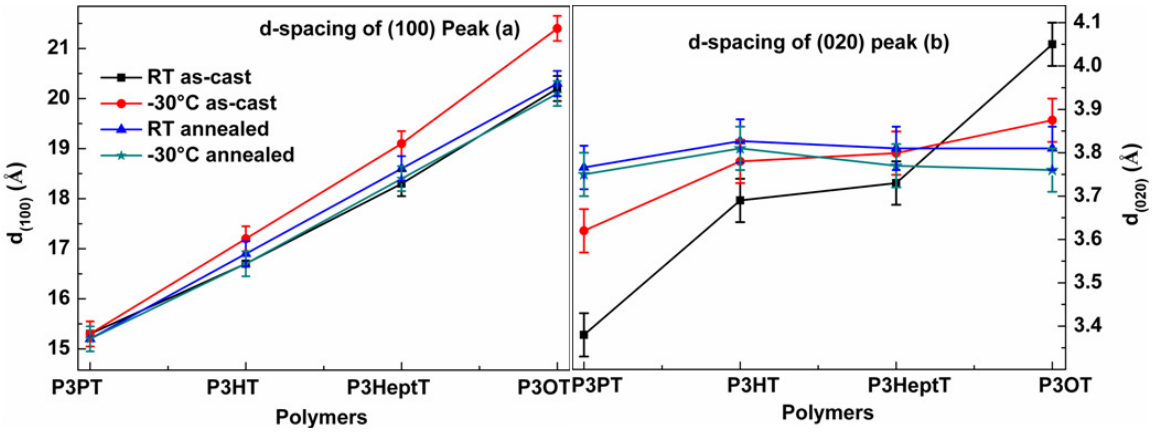


Figure 5.13: Influence of growth temperature and alkyl side chain on the variation in (a) $d_{(100)}$ and (b) $d_{(020)}$ lattice spacings

In addition to the interchain stacking, there is a difference in $d_{(100)}$ between the RT and -30°C cast films were observed (Figure 5.7 and 5.13a). The difference in $d_{(100)}$ of RT and -30°C cast film increases gradually with the alkyl side chain length (Figure 5.13a). Kawai *et al* [46] and Corish *et al*[45] reported that the $d_{(020)}$ is not affected by the alkyl side chain length when the alkyl side chain contains less than 10 hydrocarbon units and it is increased further while increasing the number of carbons grafted in the alkyl side chain through experimentally and computer based simulation, respectively. It might be due to the substrate surface potential. The substrate surface energy can hinder the formation of thermodynamically stable crystallites during the fast growth processes. They can reach their thermodynamically stable state by overcoming the substrate surface potential with the help of thermal energy. The shifts in $d_{(020)}$ is comparatively more in the case of RT cast films than the -30°C cast films (Figure 5.13b). It clarifies the growth of most thermodynamically stable crystallites while casting at low temperature. The $d_{(100)}$ of -30°C cast film is gradually reduced after the post growth

annealing (Figure 5.13a). The difference in $d_{(100)}$ of -30°C as-cast and annealed film is much higher for P3OT (1.3 Å) as compared to the P3PT (0.1 Å). It clarifies the increased flexibility of alkyl side chains while increasing the number of hydrocarbons in the grafted alkyl chain and their flexible conformations.[43] The increase in $d_{(020)}$ spacing can be explained by the augment in steric hindrance between the alkyl side chains upon increasing their length.[42] It will be explained elaborately in the discussion part.

## 5.4 Bright Field Images of RT and -30°C Cast P3AT Thin Films

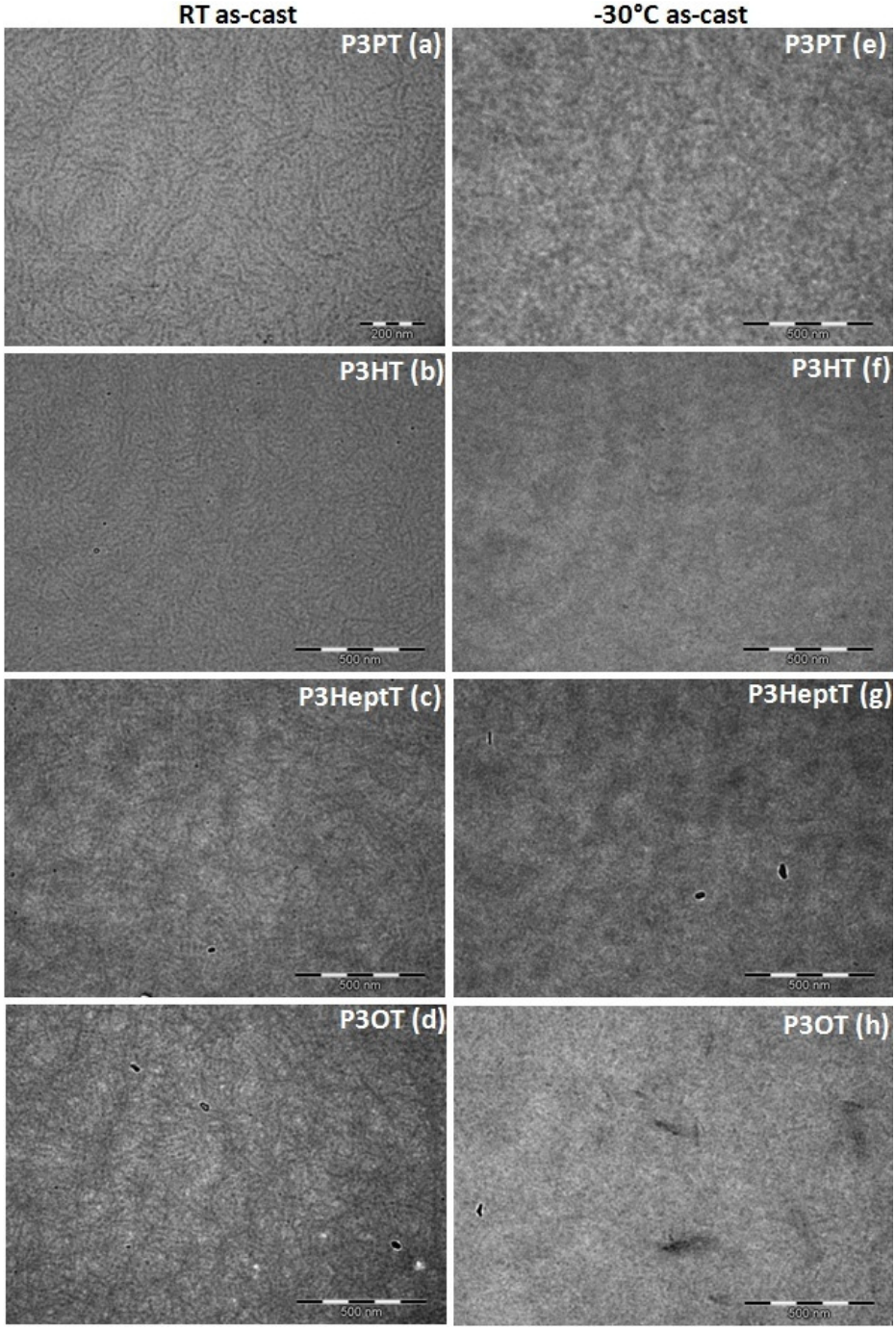


Figure 5.14: BF images of RT (left column) and -30°C (right column) as-cast P3AT thin films

The morphology of RT and -30°C cast P3AT thin films were analyzed via TEM. The RT and -30°C cast films have different morphologies as we have seen in chapter 4.6.1. The P3AT thin films cast at RT (Figure 5.14 left column) exhibits randomly distributed long elongated nanofibrils with the typical width of 15 - 20 nm and 200 - 300 nm in length as reported for the RT cast and spin coated P3HT films.[16, 65] Liu *et al* have reported that 10.2 kg/mol is a critical MW of P3HT where the thiophene backbone starts to fold.[131] The MW of undertaken P3AT polymers are given in Table 2.1. It clarifies the folded conformation of thiophene backbones while comparing the contour length with the width of the nanofibrils.[38, 131] It clearly shows that the growth of nanofibrils is due to the restriction of growth along the polymer backbone direction i.e. ***c-***axis because of thiophene backbone folding (Figure 4.14d).[64, 72] The morphology of -30°C cast films are entirely different from the RT cast films as discussed in chapter 4.6.1. All the -30°C cast films shows featureless smooth morphology (Figure 5.14 right column). In comparison with the X-ray findings, the variation in morphology of P3AT thin films while casting at -30°C as compared to the one cast at RT would be attributed to the layer-by-layer growth of the crystallites. It has been discussed elaborately in chapter 4.6.1.

## 5.5 Photoluminescence Analysis

PL analysis was carried out for the deep understanding of structural disordering on the optical properties of P3AT thick films (≈400nm) cast at RT and -30°C. The PL spectra of different temperature as-cast P3AT thick films are shown in Figure 5.15. The -30°C cast films contains three well pronounced emission peaks with defined linewidths which corresponds to the intrachain and interchain interactions i.e. 0-0 emission corresponds to the intrachain states and 0-1, 0-2, 0-3, etc. corresponds to the aggregates which can bring the vibronic energy levels in between the HOMO and LUMO bands.[117, 119] The formation of vibronic energy levels and its corresponding transition is schematically shown in Figure 3.15. The increase in aggregate concentration while casting at -30°C enhances the 0-1 luminescence peak intensity relative to the 0-0 emission (Figure 5.15).[117, 119] The appearance of well pronounced vibronic peaks together with the reduction of alkyl side chain length while casting at -30°C concludes the formation of highly interchain stacked crystallites (Figure 5.15b).[117, 119] As the side chain length increases, the 0-0 peak become more intense and the 0-1 transition reduces gradually (Figure 5.15). It can be well correlated with our in-plane structural findings obtained through X-ray (Figure 5.4) and electron diffraction (Figure 5.11) analyses. The decrease in luminescence intensity of 0-1 transition upon increasing the alkyl side chain

length might be attributed to the poor interchain stacking of thiophene backbones caused by the alkyl side chain flexibility (Figure 5.12).[117, 119] The 0-0 transition can increase relative to the 0-1 transition only when the disorder parameter or the temperature increases.[117, 119] The PL analysis was carried out at ambient conditions, so one can neglect the temperature factor.

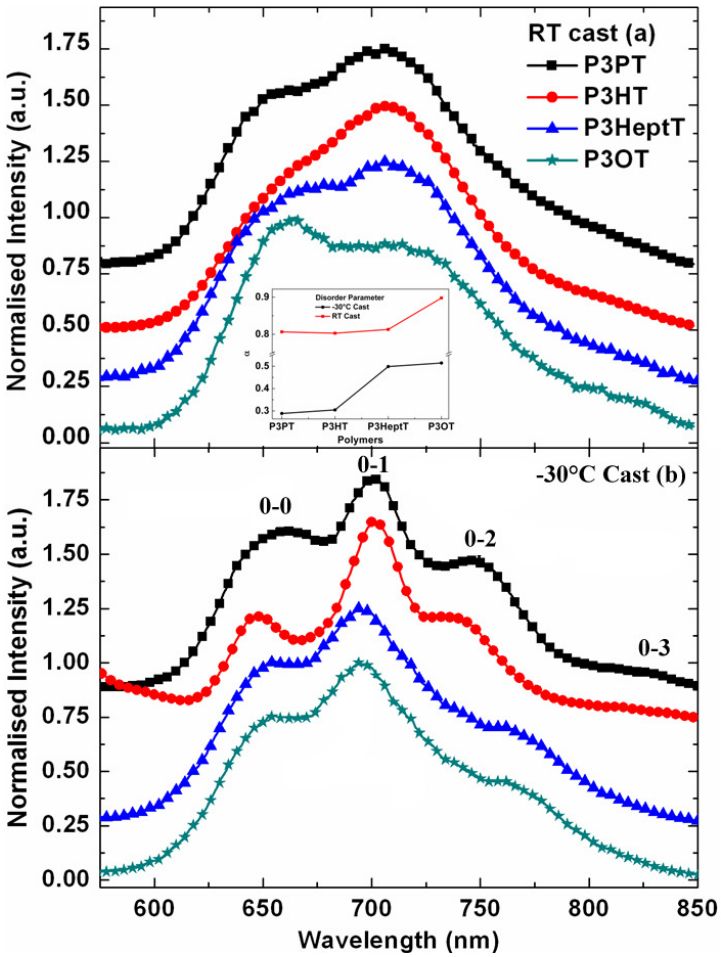


Figure 5.15: PL spectrum of (a) RT and (b) -30°C as-cast P3AT thick films (≈400 nm), the profiles were normalized to one and shifted for clear presentation; inset of (a) shows the decrease in disordering of the films while decreasing the alkyl side chain length

The reduction in cast temperature and side chain length dependent reduction in disorder parameter has been extracted from the PL spectra using the model proposed by Clark *et al.*[119] The disordering of P3AT polymers are decreased while decreasing the alkyl side chain length and cast temperature. It is in agreement with the X-ray findings but the values obtained from the X-ray and PL spectra are not exactly comparable (inset of Figure 5.15a). Even though, they have the same tendency i.e. decrease of disordering with the alkyl side chain length and the cast temperature.

## 5.6 Mobility Analysis of P3AT Thin Films

The field effect mobility of RT and -30°C cast P3AT thin films (≈40nm) were analyzed by fabricating bottom contact OFETs. Except of P3OT, the mobility of -30°C cast P3AT OFET is increased as the side chain length decreases (Figure 5.16). Kline *et al* have reported that the formation of highly edge-on oriented crystallites at the substrate-film interface is a key factor for the enhancement in mobility of P3HT OFET spin coated on the OTS treated substrate.[8] In this case, nearly a 40nm thin film prepared out of P3OT polymer produces more edge-on oriented crystallites than the P3PT one (Figure 5.7 and 5.10). On the other hand, P3PT provides highly in-plane stacked crystallites due to the reduction of in-plane disordering caused by the alkyl side chain flexibility (Figure 5.11). Eventually, the mobility of P3PT OFET (0.0041cm$^2$/Vs) is nearly twofold higher than the P3OT (0.0024cm$^2$/Vs). The enhancement in mobility of -30°C cast P3AT polymer as compared to the RT cast one is shown in the inset of Figure 5.16. The difference in mobility of RT and -30°C cast P3PT (0.0035cm$^2$/Vs) is an order of magnitude higher than the P3OT film (0.0009cm$^2$/Vs).

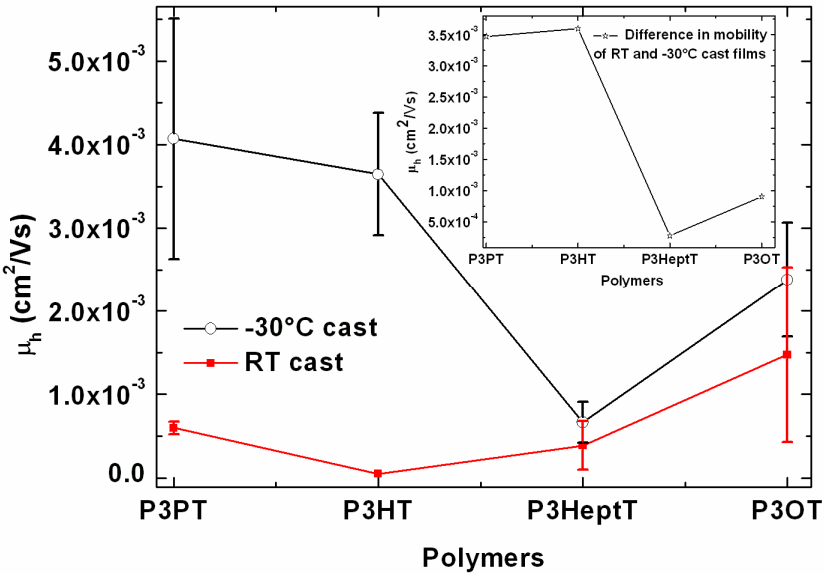


Figure 5.16: Influence of growth temperature and side chain length on the mobility of P3AT OFETs, inset shows the difference in mobility of RT and -30°C cast films

## 5.7 Discussion

Among the whole investigated P3ATs, n-hexyl has been found to be the optimum side chain length for the fabrication of OFETs and solar cells.[41, 132] The detailed X-ray and electron diffraction analysis performed in this thesis for the different temperature cast P3AT thin films clarifies that the highly edge-on oriented, very thin, and well in-plane stacked

crystallites can be prepared by reducing the cast temperature together with the reduction of alkyl side chain length. The reduction in growth temperature amplifies the formation of edge-on oriented crystallites as well as their in-plane perfections as compared to the RT cast one. It has been explained much more elaborately in chapter IV.

The face-on oriented crystallites of RT cast thick films are increased as the alkyl side chain length increases (Figure 5.4). It is similar to the findings of P3HT and P3DDT films drop cast on various substrates.[132, 136] Payerne *et al* have reported an increase of surface coverage of face-on oriented crystallites while increasing the side chain length from hexyl (≈25%) to dodecyl (≈75%) is due to the reduced glass transition temperature ($T_g$) of P3DDT (≈ -19°C) as compared to P3HT (≈23°C).[136] Even the annealing temperature of P3PT is 65°C higher than the P3OT which is greater than the difference between the $T_g$ of P3OT (-20°C)[137] and P3PT (37°C)[138].

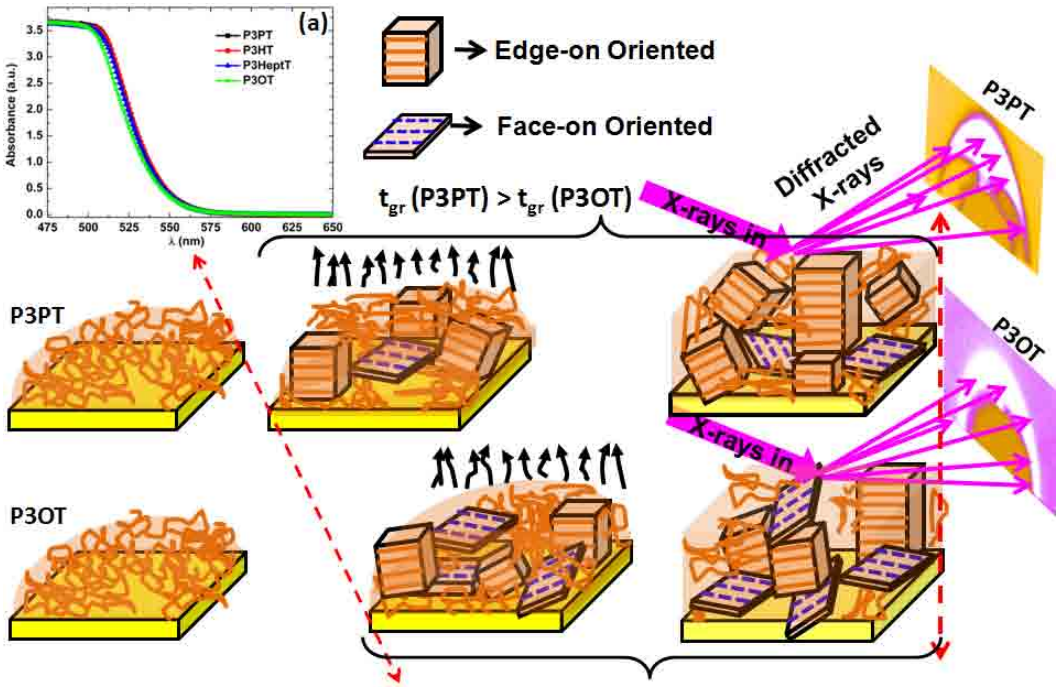


Figure 5.17: Schematic illustration of side chain length dependent growth of edge- and face-on oriented crystallites while casting at RT

The 2D X-ray diffraction pattern of -30°C cast film shows the absence of face-on oriented crystallites while casting at -30°C (Figure 5.4b). The increase of face-on oriented crystallites of RT cast films as increasing the alkyl side chain length might not be due to the decrease in $T_g$, but it might be due to the reduction in growth time.[17] Yang *et al* reported that the edge-on oriented crystallites can be initiated at the substrate-solution interface by spin coating at RT from the warm (40°C) solution because of the cooling assisted earliest

formation of nucleations as compared to the one spin coated on the 40°C warm substrate.[16] According to the equation 2.10, the enhanced solubility of P3OT as compared to P3PT can start to nucleate later than the P3PT and it can produce more face-on oriented crystallites because of the reduction in growth time ($t_{gr}$) where the other growth parameters such as pressure, cast temperature, concentration, amount of dropped solution, etc. were kept constant. It occurs due to the reduction in enthalpy of solution '$\lambda_{ss}$' as the side chain length increases. The enthalpy of solution of undertaken P3ATs were tried to calculate via differential calorimetric analysis (DCA), but it was not successful because of their poor solubility. For further details please refer appendix A. The UV-Vis absorption spectroscopic analysis shows that the increase of edge-on oriented crystallites while decreasing the side chain length is not due to the preexistence of any aggregate phase in the solution (Figure 5.17a).[14, 116] It clearly depicts that the formation of non-preferable face-on oriented crystallites of RT cast RR-P3AT thick films as increasing the side chain length is due to the fast growth process which can increase the nucleation of highly misoriented crystallites.[16, 17] It is schematically shown in Figure 5.17.

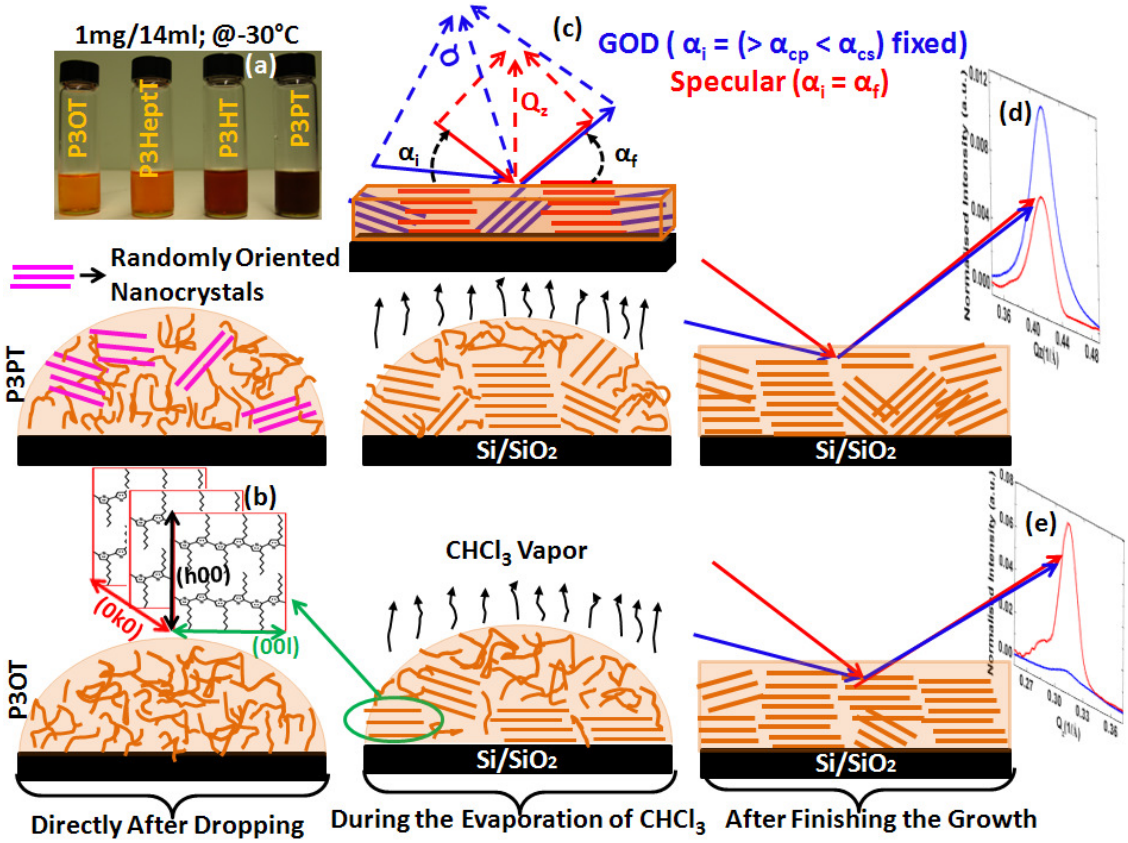


Figure 5.18: Schematic illustration of side chain dependent solubility on the growth kinetics of -30°C cast P3AT thin films

X-ray diffraction analysis carried out for very thin films cast at RT and -30°C shows the formation of well out-of-plane stacked edge-on oriented P3ATcrystallites as the alkyl side chain length increases (Figure 5.7). It might be due to the increase in solubility of P3AT polymers while increasing the alkyl side chain length (Figure 5.18a).[5] For example, decrease in solubility of P3PT can produce aggregates in the solution as compared to P3OT because of its solubility limit (Figure 5.18a) while cooling from RT to -30°C. The solutions were preserved at 0°C and brought to -30°C just 10 minutes before dropping the solution on the substrate. The solutions were dropped after reducing the substrate temperature down to -30°C. In such a case, the dropped P3PT solution can easily reach the substrate temperature and it can produce multiple nucleations directly after the dropping (Figure 5.18). The highest solubility of P3OT can start to nucleate during the evaporation of $CHCl_3$ only when the supersaturation is allowed. Ultimately, P3OT can nucleate on the surface of the substrate and it can grow slowly during the evaporation of $CHCl_3$ as schematically shown in Figure 5.18.

The complete dissolution of P3OT at -30°C than the P3PT can nucleate at the substrate-solution interface than the air-solution interface in a way to produce more out-of plane stacked edge-on oriented crystallites. Subsequently, it can scatter much more along $Q_z$ than the P3PT film (Figure 5.18e).[92] Such a formation of misoriented and multiple nucleates with the reduction of side chain length can ultimately reduce the effective crystallite size. The lateral and vertical crystallite sizes extracted from the FWHM of rocking and specular scans shows the reduction in crystallite sizes as decreasing the side chain length (Table 5.3). As per the equation 2.9, the size of the critical nucleus mainly depends on two parameters such as degree of cooling and enthalpy of solution per molecule. It clearly exhibits that the determination of appropriate concentration and growth temperature can help to control the nucleation rate as well as the growth rate of the crystallites. Further, it can assist to initiate the nucleation at the substrate-solution interface rather than the air-liquid interface and to produce thermodynamically more stable edge-on oriented crystallites. The P3AT films prepared at various temperatures suggest that the highly edge-on oriented crystallites can be prepared by casting at low temperature. On the other hand, the in-plane analysis performed for the same films through ED depicts the formation of poorly interchain stacked crystallites while increasing the alkyl side chain length (Figure 5.11).

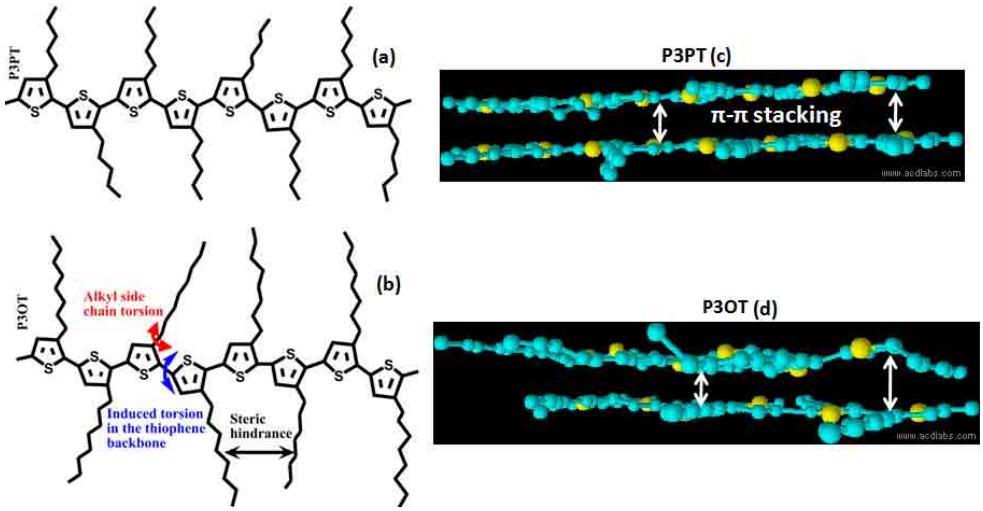


Figure 5.19: A schematic illustration of side chain flexibility on the flexibility of thiophene backbone (b) and its influence on π-π stacking (c)

Prosa *et al* reported that the flexibility of alkyl side chain increases when the number of hydrocarbons in the grafted alkyl side chain increases (Figure 5.19a and 5.19b).[43] The gradual reduction in $\boldsymbol{d_{(100)}}$ of -30°C cast film after the post growth annealing confirms the increase in flexibility of alkyl side chains as the side chain length increases (Figure 5.13a). Xie *et al* documented the evolution of torsion in the thiophene backbone caused by the torsion evolved in the alkyl side chains.[44] It is schematically shown in Figure 5.19. The induced torsion in the thiophene can increase the plasticity of thiophene backbones, subsequently it can lose its coplanarity with the adjacent thiophenes.[42] When the coplanarity of c-axis reduces due to the tilting and twisting of thiophene backbones then it can suppress the π-π interaction between the adjacent molecules and it can lead to non-coherence in $\boldsymbol{d_{(020)}}$ (Figure 5.18d).[42] Such a fluctuation in lattice spacing can directly influence the FWHM and scattering intensity of the in-plane reflections such as (020), (h11), (011), (031), etc. (Figures 5.4 and 5.11).[123] Such a non-coplanarity must be reduced because in-plane stacking especially interchain stacking plays a vital role in the conduction of charge carriers through hopping.

The key role of crystallinity and interchain stacking in the electrical and optical properties of P3AT thin films were analyzed by fabricating OFETs and recording the PL spectra, respectively. The luminescence intensity of the vibronic peaks (0-1, 0-2, 0-3, etc transitions) is increased while decreasing the alkyl side chain length (Figure 5.15). The augment in PL intensity while reducing the side chain length and cast temperature is due to the reduction in disordering in the films.[117] The enhanced luminescence intensity and

OFET mobility of P3AT thin films together with the reduction of alkyl side chain length depicts the inherent role of interchain stacking on the optical and electrical performances. Sauve *et al* recently reported that n-hexyl is an optimum alkyl side chain for the fabrication of high throughput OFETs.[132] In this case, the mobility of -30°C cast film is increased while decreasing the alkyl side chain length. The X-ray diffraction analysis shows that the P3OT film has more edge-on oriented bigger crystallites at the substrate-film interface than the P3PT (Figure 7) even though the mobility of P3PT is twofold higher than the P3OT (Figure 5.16) because of the formation of highly in-plane stacked crystallites (Figure 5.11). The structural analysis shows that the in-plane stacking can be enhanced further by reducing the alkyl side chain length to n-pentyl or even lesser. Kline *et al* reported that the formation of edge-on oriented crystallites at the dielectric-film interface is necessary for the fastest charge transport.[8] The detailed analysis performed in this thesis using various techniques concludes that, not only the edge-on oriented crystallites but their interchain stacking is also important for the fast charge transport via hopping between the molecules where the growth along the polymer chain axis is restricted due to polymer chain entanglement and folding of thiophene backbones (Figure 4.14d) (chapter VI).

- *The anisotropic growth of P3AT crystallites was analyzed by annealing them at various temperatures using HRTEM. It will be presented in chapter VI*

# Chapter VI

## 6 HRTEM Investigation of Annealing Temperature and Alkyl Side Chain Induced Anisotropic Growth of P3AT Crystallites

It is key to understand the preferential growth directions of P3AT crystallites because of their anisotropy in electrical and optical properties which can be used to orient them uniaxially by applying the proper growth methodologies. The HRETM is an inevitable tool which is widely used in the organic electronics field for studying the plasticity, orientation, the interconnections between the crystalline lamellae, etc.[64, 110] I have systematically analyzed the influence of annealing temperature on the plasticity and anisotropic growth of P3AT crystallites by recording the lattice images. Besides, I have also analyzed the influence of alkyl side chain length on the rate of formation and orientation of the crystallites. The HRTEM findings have been further substantiated with X-ray and electron diffraction analyses as well.

### 6.1 Nanomorphology of as-spin Coated P3AT Films as Observed by HRTEM

Influence of alkyl side chain length on the rate of formation and orientation of P3AT crystallites were analyzed by collecting the HRTEM images of ≈17 nm thin as-spin coated films. More than five HRTEM images have been collected on various places of the films. The HRTEM images are allowing to distinguish the amorphous (featureless) zones and the crystalline nanodomains of P3ATs. The crystalline P3AT domains show fringed patterns corresponding to regular π-stacked chains with a characteristic lamellar period ($a_{P3AT}$ axis). The contrast in the HRTEM images is related to the presence of sulfur atoms in the stacks of polythiophene backbones versus carbon/hydrogen atoms in the layers of alkyl side chains. These nanocrystals show a preferential face-on orientation on the Si (100) substrate. The areas not showing any periodic lamellar patterns correspond either to the amorphous zones or to the P3AT domains whose orientation to the electron-beam prevents their observation by HRTEM i.e. as soon as the π-π stacking direction of P3HT chains is no longer normal to the film substrate. This indicates that the HRTEM provides only a lower limit of domain size along the $a_{P3AT}$ axis as the contrast can be lost for a slight misorientation of the crystalline domain to the substrate normal. More generally, attempts to observe edge-on oriented P3AT crystallites by low dose HRTEM were not successful (presumably because of the monoclinic unit cell of P3ATs as evidenced for form I of P3HT).[59]

It is not possible to observe any face-on oriented crystallites in the P3PT film (not shown). In contrast to this, as the length of the alkyl side chains increases, a higher fraction of face-on oriented nanocrystallites is evidenced. This is particularly true for the P3OT films showing well defined nanocrystallites with face-on orientation. The as-grown P3OT film is showing sufficient crystalline domains, it was possible to perform a statistical analysis of the domain sizes. The length i.e. along the alkyl side chain stacking direction ($l_a$) and width of the crystalline domains i.e. average stem length ($l_c$) were extracted from the HRTEM images using the AnalySIS software. The direction of $l_c$ and $l_a$ are shown in 6.1d. The statistical average area, length, and width of the crystalline domains are presented in Table 6.1. It was not able to measure the length and width of the P3HT and P3PT as-grown films because of the presence of tiny crystallites with weak phase contrast (Figure 6.1a). It reveals that the spin coated P3OT film composed of ≈10 nm long face-on oriented crystallites and it reduces gradually with the side chain length (Figure 6.1). The same tendency can be observed in the X-ray and ED patterns as well and it will be explained latter in detail.

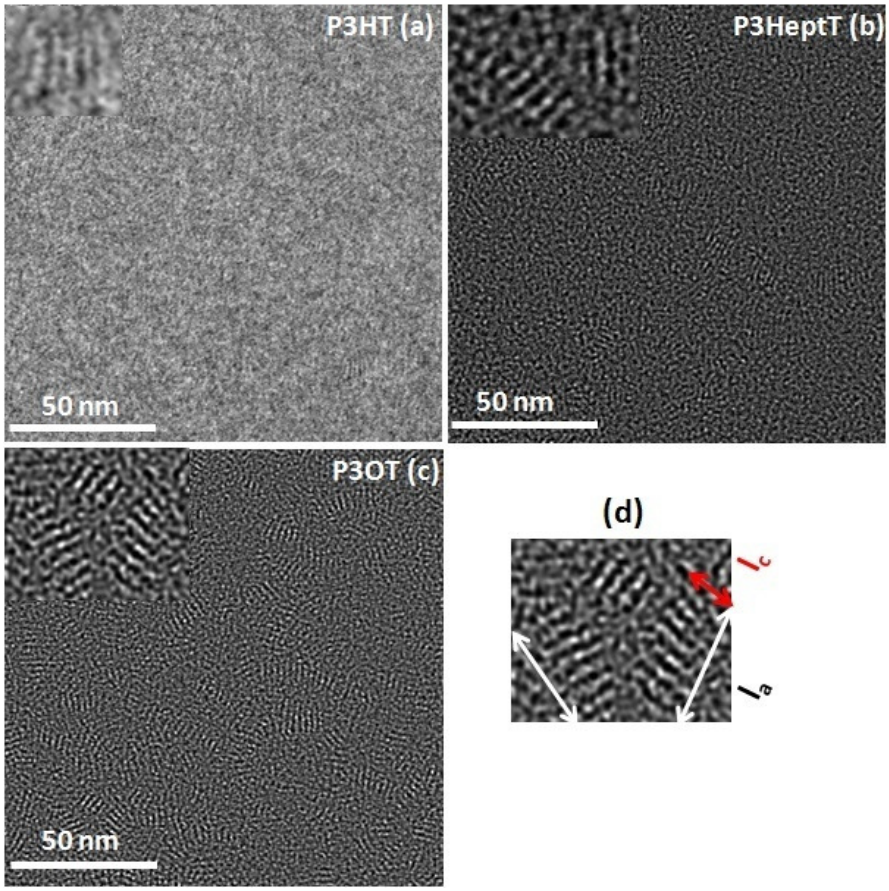


Figure 6.1: The HRTEM images of as-grown P3AT spin coated polymers. (d) illustrates the definition of $l_a$ and $l_c$ (see text) for P3OT nanocrystals

| Polymers | Average crystallite size along the alkyl side chain ($l_a$) (nm) | | Average stem length in the crystallites ( $l_c$) (nm) | | Mean area of the crystallites ($nm^2$) | | Percentage of face-on oriented domains | |
|---|---|---|---|---|---|---|---|---|
| | As-grown | Annealed | As-grown | Annealed | As-grown | Annealed | As-grown | Annealed |
| P3PT | - | 11 | - | 6.8 | - | 98.1 | - | 2.6 |
| P3HT | - | 12.4 | - | 7.8 | - | 144.7 | - | 5.9 |
| P3HeptT | 7.5 | 15.9 | 5.7 | 8.6 | 57.8 | 207.2 | 0.8 | 15.2 |
| P3OT | 10.4 | 21.6 | 7.1 | 9.4 | 91.1 | 261.2 | 3 | 20.4 |

Table 6.1: Average nanocrystal dimensions ($l_c$ and $l_a$) obtained from the statistics on HRTEM micrographs on spin coated RR-P3AT thin films. For all samples, the annealing corresponds to an undercooling $\Delta T$=45°C

## 6.2 Impact of Isothermal Annealing: Effect of Alkyl Side Chain Length

The spin coated films were annealed at 45°C below their corresponding melting point (Table 2.1). Respective HRTEM images of annealed P3AT thin films are shown in Figure 6.2. The crystallites are ripening unevenly after the post growth annealing. The length along $a_{P3AT}$ '$l_a$' and width $l_c$ of the crystalline domains were extracted by recording few HRTEM images and the average values are given in Table 6.1. The statistical analysis of domains sizes after annealing demonstrates a preferential growth of the crystallites along the $\mathbf{a_{P3AT}}$ axis i.e. along the alkyl side chain stacking direction. For instance, in the case of P3OT, $l_a$=10 nm before annealing whereas after annealing $l_a$= 22 nm. Similarly, for P3HeptT, $l_a$ increases by a factor of almost two after annealing. Contrary to $l_a$, the stem length $l_c$ increases only marginally which is most important for fast charge transport. For P3OT, $l_c$ increases from 7 nm to 9.4 nm upon annealing. A similar trend is observed for P3HeptT and P3HT. The restriction of growth along $l_c$ might be attributed to the folding and entanglement of thiophene backbones.[38, 91]

The percentage of face-on oriented crystallites was extracted by calculating the area of the whole visible crystallites and the area of HRTEM images. The percentage of face-on oriented crystallites of annealed P3PT film (2.6%) is far less than the P3OT film (20%) and it increases as the side chain length increases (Table 6.1). This result is further in agreement with the observations of Payerne *et al* obtained for P3ATs grown on HOPG graphite: an increasing fraction of face-on oriented crystallites is observed while increasing the alkyl side chain length from hexyl (P3HT ≈ 25%) to dodecyl (P3DDT≈75%).[136] The increase of

kinetically trapped face-on oriented crystallites as increasing the side chain length might be due to the latest initiation of nucleation during spin coating as compared to the P3PT as discussed in chapter 5.7. These observations suggest that both the kinetics of P3AT nanocrystal growth and the interactions with the $SiO_2$ substrate are determined by the length of the n-alkyl side chains.[132]

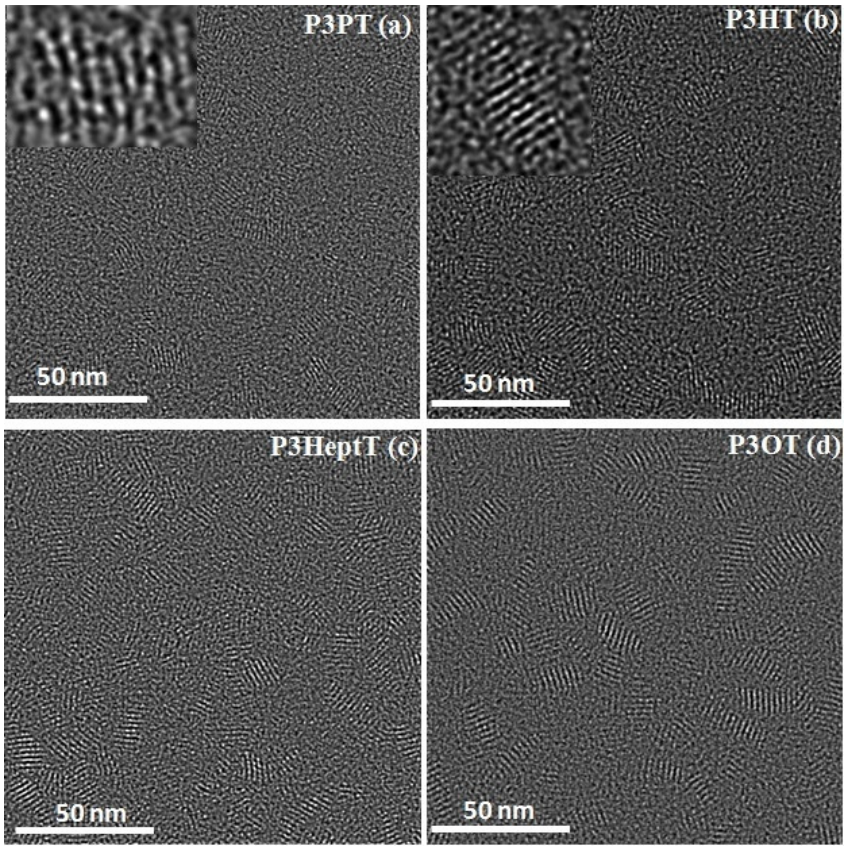


Figure 6.2: HRTEM images of P3AT spin coated films (≈ 17 nm thick) annealed at 45°C below from their corresponding melting point

The HRTEM images in Figure 6.2 show that the adjacent nanocrystals with a face-on orientation show high-tilt grain boundaries as evidenced for instance in the case of pentacene nanocrystals.[139] Such high-tilt grain boundaries are known to be detrimental to the charge transport in thin films of semiconducting materials.[139] This observation implies also that there is apparently no orientational correlation between the stem directions in adjacent P3OT nanocrystals in the spin coated films. This is a major difference with respect to the P3HT films oriented by DEC in 1,3,5-TCB that shows a periodic arrangement of oriented lamellar crystals sharing a common in-plane orientation of the polymer stems.[64, 91]

The lamellar periods $\lambda_a$ were extracted from the FFTs of the HRTEM images for the different P3AT samples. As expected, $\lambda_a$ increases linearly with the number of carbon atoms

in the alkyl side chain i.e. 15.1Å (P3PT), 16.7Å (P3HT), 18.5Å (P3HeptT), and 20Å (P3OT). These periods correspond well with the ones extracted from the angularly averaged ED line scans as well as the lamellar periods reported in the literature for form I P3ATs.[46, 66] These values are also in agreement with the values obtained from the drop cast films (Figure 5.13a). It concludes that the alkyl side chains are not interdigitated as observed in the case of P3AT films cast on the HOPG substrate.[113, 136]

## 6.3 Evolution of the Semicrystalline Nanomorphology in P3OT and P3PT Films upon Increasing the Annealing Temperature

A more detailed analysis of the impact of annealing temperature $T_a$ on the nanomorphology of the spin coated films was performed for P3OT and P3PT.

The nanomorphology of the as-grown, and annealed P3OT thin films for different values of $T_a$ are shown in Figure 6.3 (first column) as well as the corresponding histograms obtained from the statistical analysis of the domain sizes $l_a$ and $l_c$ (Figure 6.3 second and third column). Here one cannot take the number of nanodomains into account because few HRTEM images were used to obtain more than 150 nanocrystallites for the better statistics. The hardly visible crystallites present in the as-grown films (Figure 6.3a) are well developed after the post growth annealing. While comparing the HRTEM images of as-grown and annealed films, the crystallites are growing much along the alkyl side chain stacking direction while increasing the annealing temperature. The length of the crystallites '$l_a$' is increased by ≈3nm when the annealing temperature of P3OT is increased from 130°C to 150°C, but the $l_c$ does not vary much even after annealing the as-grown film at 150°C. The contour length extracted from the HRTEM images of different temperature annealed P3OT film is in the order of 7 till 9 nm and it does not vary much with respect to the polymers (Table 6.1), it is similar to the values reported by Brinkmann *et al* for different MW P3HT.[64] In addition, the HRTEM images show that the boundaries of the P3OT nanocrystals are sharp but indicate some characteristic tapering as was observed for instance in the case of poly(9,9-di-n-octyl-2,7-fluorene) (PFO) and poly(9,9-bis(2-ethylhexyl)fluorene-2,7-diyl) (PF2/6) lamellar crystals.[140, 141] In most of the nanocrystals, the domain boundary is not orthogonal to the stem direction. The same observation was made in the case of epitaxied thin films and it was interpreted in terms of specific crystallographic fold planes.[64]

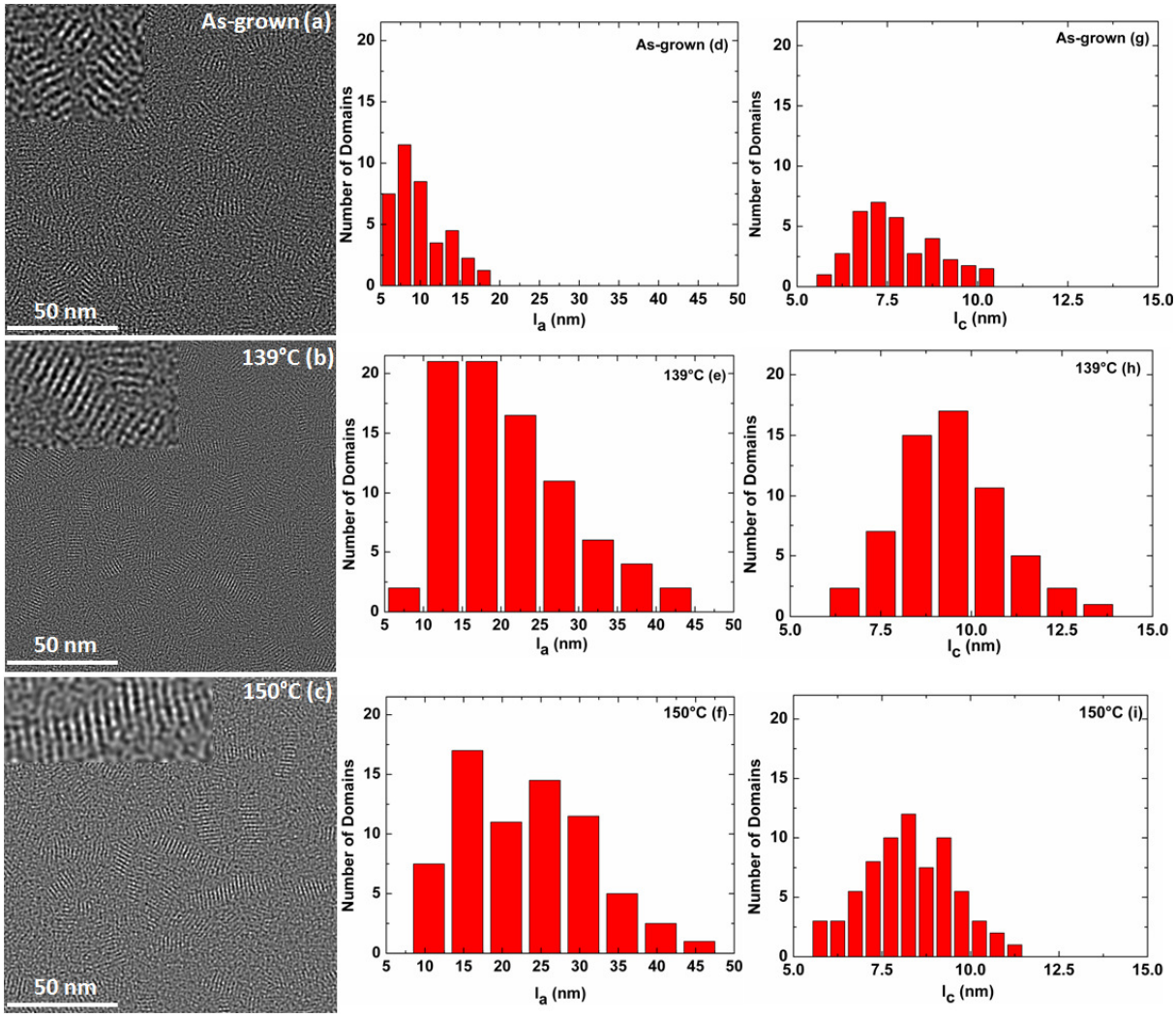


Figure 6.3: HRTEM images of 139°C and 150°C annealed and as-grown P3OT films (first column); the bin diagrams shows the difference in growth rate of P3OT crystallites along $\boldsymbol{l_a}$ (second column) and $\boldsymbol{l_c}$ (third column)

The same analysis has been carried out for P3PT by annealing at 150°C, 204°C, and 220°C for an hour. Figure 6.4 depicts the nanomorphology of the P3PT films after annealing at different temperatures $T_a$ as well as the corresponding histograms of the domain size in the direction perpendicular to the stems i.e. $l_a$ (Figure 6.4 right column). The sizes of P3PT crystallites are comparatively smaller as compared to P3OT. Despite the higher annealing temperatures for P3PT, the increase in domain size is limited to ≈4 nm along the $a_{P3PT}$ axis in the best case ($T_a$= 220°C). This observation indicates that the increase of domain size is favored along the side chain direction for longer side chains. However, for both the P3PT and P3OT, the increase of domain size along the chain axis direction is limited. In other words, the long alkyl side chains are favorable for the growth of the crystalline domains along the side chain stacking direction i.e. along the $a_{P3AT}$ axis whereas lamellar thickening along the

polythiophene chain direction is limited regardless of the length of the alkyl side chains (*n*-pentyl to *n*-octyl).

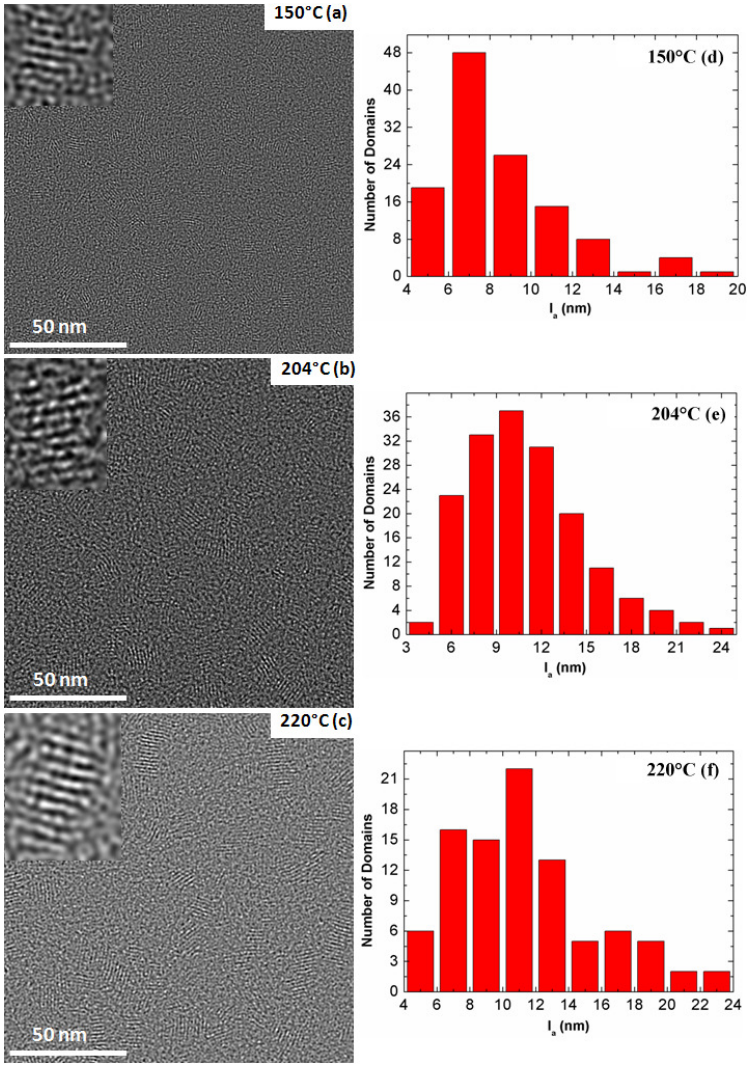


Figure 6.4: HRTEM images of different temperature annealed P3PT films (first column) and the corresponding bin diagram of $l_a$ versus number of domains (second column) of spin coated films (≈ 17 nm thick films)

## 6.4 Electron Diffraction Analysis of Spin Coated Films

The electron diffraction analysis was performed by choosing the camera length 2.05m which can cover both the (100) and (020) reflections that are correspond to the face- and edge-on oriented crystallites. The integrated plot profiles were extracted using an imageJ software and plotted with respect to the momentum transfer vector $Q_{x,y}$. The obtained integrated intensity profiles of as-grown and annealed P3AT spin coated films are shown in Figures 6.5a and 6.5b, respectively. The ED patterns are concurrent with the HRTEM findings. The first order (h00) reflection is visible in the as-cast P3OT film and it starts to

diminish as the alkyl side chain length decreases. On the other hand, the as-spin coated film does not provide any (h00) reflections but a small hump is visible at around ($Q_{x,y} \approx 1.73 Å^{-1}$) which corresponds to the π-π stacking distance (edge-on oriented crystallites) (inset Figure 6.6). It depicts the formation of non-thermodynamically stable crystallites during spin coating due to the fastest evaporation of $CHCl_3$.[2, 16]

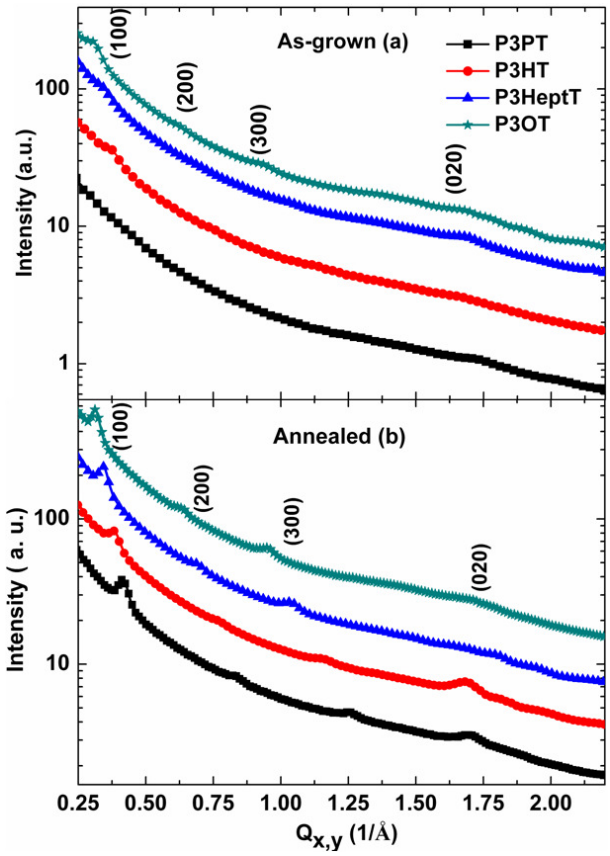


Figure 6.5: ED integrated line profile of as-grown (a) and annealed (b) P3AT films (≈ 17 nm thick), the curves were shifted from the same baseline by adding some factor for better presentation

The scattering intensity of (h00) and (020) Bragg reflections are increased after post growth annealing. The diffraction profile of annealed P3PT (Figure 6.5b) film envisages the presence of both the face- and edge-on oriented crystallites. On the contrary, the annealed P3OT has an ill defined hump at the position of (020) which corresponds to the edge-on oriented crystallites. The (020) peak is diminishing as the alkyl side chain length increases. It clearly supports the HRTEM findings of annealed P3AT thin films (Figure 6.2) i.e. longer side chain length favors the formation of non preferable face-on oriented crystallites.[132] The increase of face-on oriented crystallites upon annealing might be due to the growth of

pre-existing kinetically trapped face-on oriented crystallites. It will be discussed more elaborately in the discussion part.

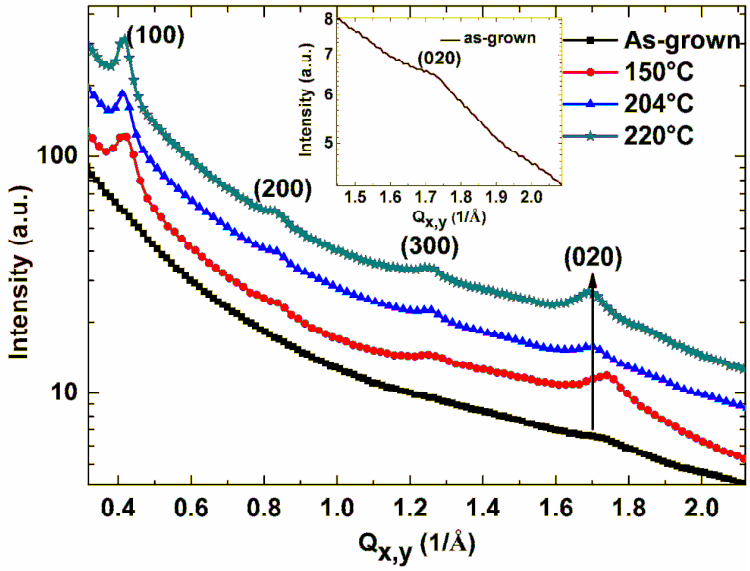


Figure 6.6: ED integrated line profile of P3PT film annealed at different temperatures, (020) Bragg peak of as-spin coated P3PT is in inset; the profiles were shifted by adding some factor for clear presentation

The influence of annealing temperature on the recrystallization of P3PT thin film was studied by annealing at various temperatures like 150°C, 204°C, and 220°C. The corresponding diffraction profile is shown in Figure 6.6. The amount of face- and edge-on oriented crystallites are increased as the annealing temperature increases which can be explained from the continuous growth of (h00) and (020) reflections. The (020) peak of as-grown P3PT has shifted towards the lower Q value (1.65 $Å^{-1}$) i.e. the increase of π-π stacking distance from 3.6 Å to 3.8 Å after annealing the film at 204°C. It might be due to the formation of thermodynamically trapped crystallites because of substrate surface potential. The same behavior has been observed in the RT cast P3AT films as well, and it has been explained more elaborately in chapter 5.3. It depicts that the high annealing temperature is necessary for the recrystallization of spin coated films which can suppress the fabrication of devices on the low thermal resist plastic substrates.

## 6.5 Bright Field Imaging of Spin Coated P3ATs

The morphology of P3AT thin films were analyzed via BF imaging. The morphology of spin coated P3AT films is entirely different from the cast films. The HRTEM images shows that the spin coated P3AT polymers are having very tinny nanofibrils and their sizes are

decreasing with the alkyl side chain length. Such a small nanofibrils were not able to resolve through BF imaging, but it depicts the wavy like pattern as observed by Brinkmann *et al* and Kline *et al* for the HMW P3HTs.[56, 63] The corresponding BF images are shown in Figure 6.7. The non-visibility of these nanocrystallites might be due to their reduced size and weak phase contrast.

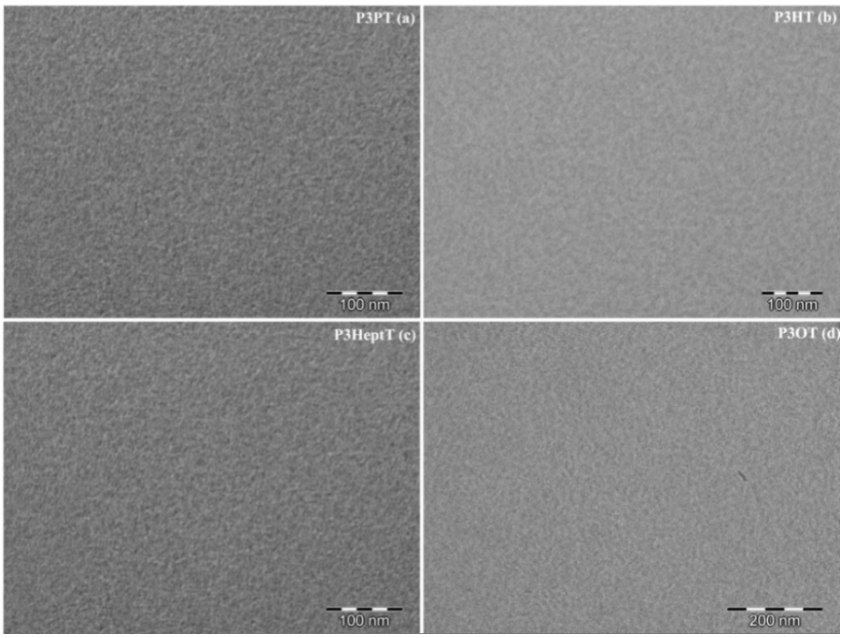


Figure 6.7: BF images of as-spin coated P3AT thin films

## 6.6 X-ray Diffraction Analysis of Spin Coated P3AT Thin Films

The obtained 2D X-ray diffraction patterns of as-spin coated P3AT films are shown in Figure 6.8. No Bragg reflections for the as-grown P3PT film could be observed. On the other hand, P3OT film composed of several Debye-Scherrer rings which depicts the random distribution of the crystallites. The (020) peak of P3OT film along out-of-plane direction is much more pronounced and more intense than the other polymers which depicts the presence of more face-on oriented crystallites (Figure 6.8d). The (020) reflection is diminished while decreasing the side chain length. On the contrary, the scattering intensity of (100) reflection along Q increases as the side chain length decreases which confirms the increase of edge-on oriented crystallites while decreasing the side chain length (except P3PT). The same films were annealed at the undercooling of 45°C and analyzed at DELTA synchrotron source. The corresponding 2D diffraction patterns are shown in Figure 6.9.

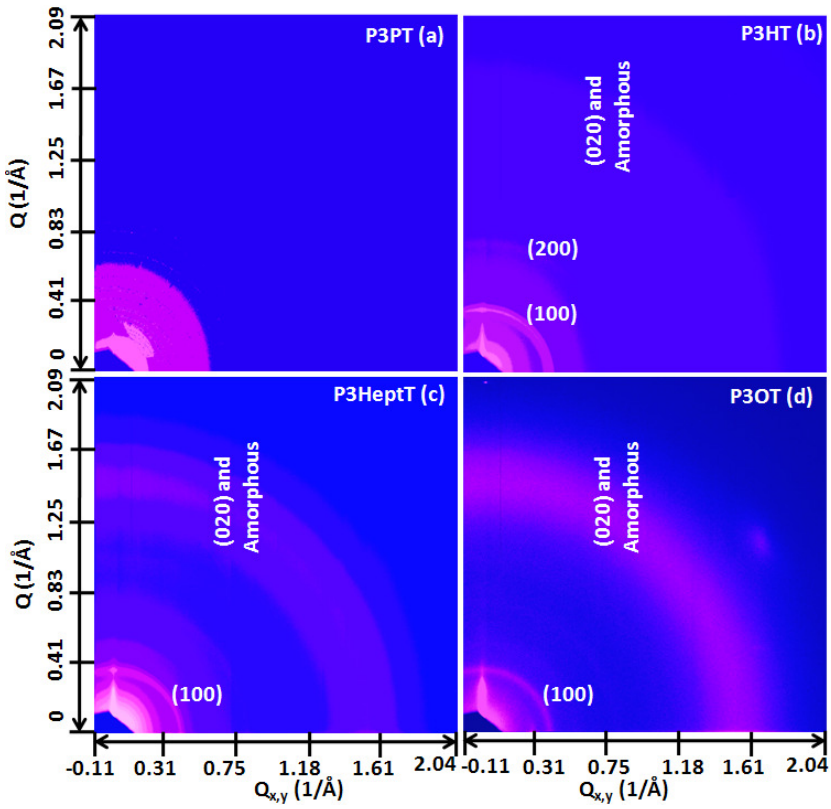


Figure 6.8: 2D X-ray diffraction pattern of as-spin coated P3AT films (≈ 17 nm thick)

The Debye-Scherrer ring of (100) and (020) reflections observed in the as-grown film has changed to diffraction spots after post growth annealing because of the texturing of crystalline domains (Figure 6.9). It concludes the coexistence of both face- and edge-on oriented crystallites in the films (chapter 3.1.2.2). The scattering intensity of (100) reflection along in- and out-of plane directions are not the same for all the polymers and it varies with respect to the polymers. The GOD and GID line profiles were extracted from the 2D scattering patterns of annealed P3AT films and shown in Figure 6.10a and 6.10b, respectively.

The scattering intensity of out-of plane (100) reflection is increased as the alkyl side chain length decreases (Figure 6.10a). On the other hand, the scattering intensity of (100) Bragg peak along in-plane direction decreases with the alkyl side chain length (Figure 6.10b). The augment in scattering intensity of P3AT thin films along in-plane direction together with the side chain length is not associated to the thickness. Thicknesses of the P3AT spin coated films were calculated using X-ray reflectivity technique, it will be discussed later. The increase in scattering intensity of (100) reflection along the in-plane direction while increasing the alkyl side chain length clarifies the formation of more face-on oriented crystallites (refer Figure 3.6). The X-ray findings are comparable with the HRTEM findings

(Figure 6.2) i.e. increase of face-on oriented crystallites as increasing the alkyl side chain length. The in-plane and out-of plane crystallite sizes of annealed P3AT thin films were extracted from the corresponding line profiles using the Debye-Scherrer relation. The obtained crystallite sizes are presented in Table 6.2. The lateral crystallite sizes ($l_a$) are increasing with the alkyl side chain length but they are slightly varying from the values extracted from the HRTEM images.

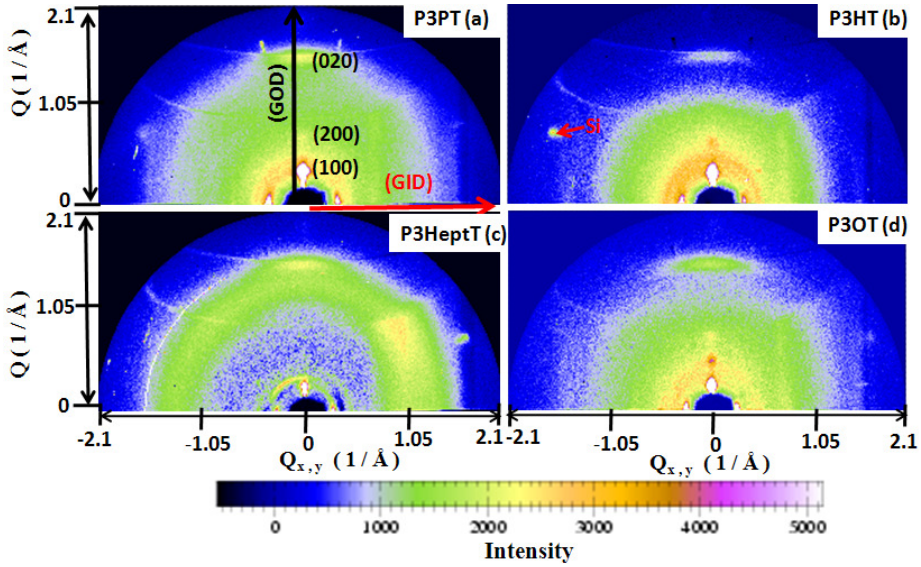


Figure 6.9: 2D X-ray diffraction pattern of spin coated P3AT polymers annealed 45°C below their corresponding melting point for an hour

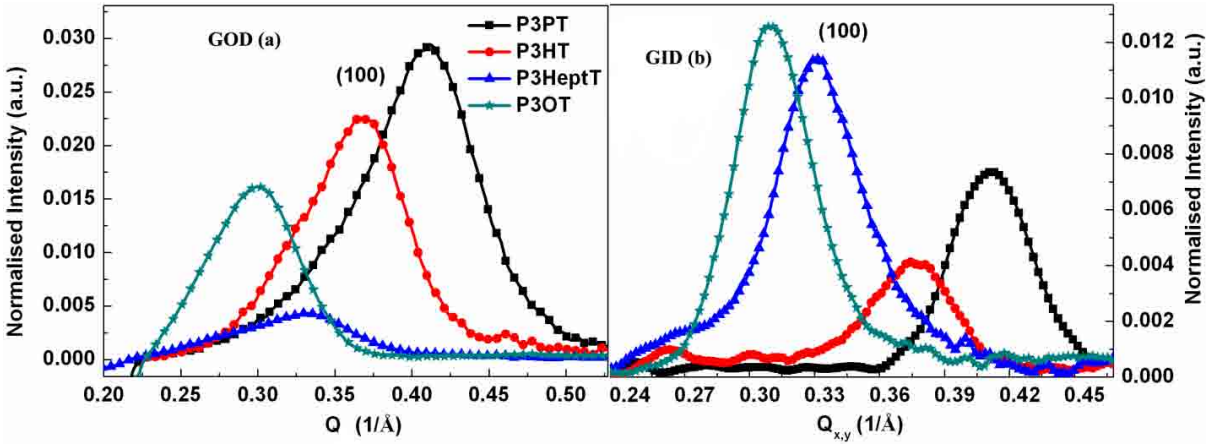


Figure 6.10: The GOD (a) and GID (b) line profile of P3AT annealed spin coated films; the scattered intensity is normalized to the incoming flux

| Polymers | Effective Crystallite Size of Annealed Films (±0.2nm) | |
|---|---|---|
| | Out-of Plane | In-plane |
| P3PT | 8.3 | 15.9 |
| P3HT | 8.8 | 16.8 |
| P3HeptT | 7.9 | 14.2 |
| P3OT | 9.9 | 16.5 |

Table 6.2: Effective out-of-plane and lateral crystallite sizes of annealed P3AT thin films extracted from the FWHM of GOD and GID profiles, respectively

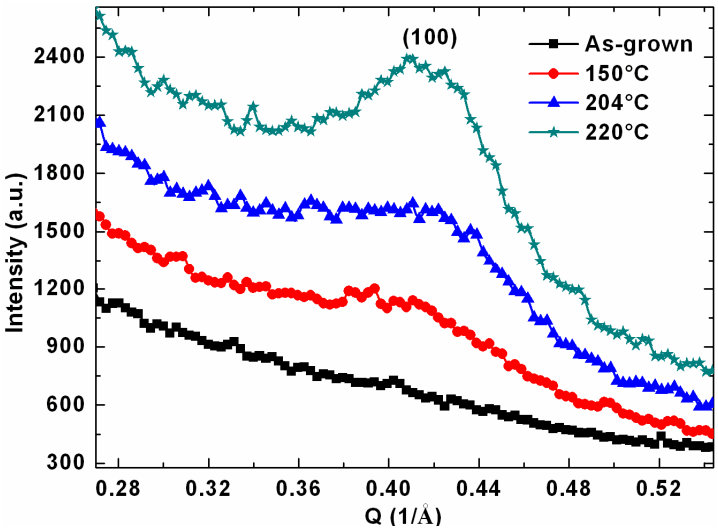


Figure 6.11: GOD line profile of different temperatures annealed nearly ≈17 nm thick P3PT spin coated film; the curves were shifted for clear view from the same baseline

The GOD diffraction profile of different temperature annealed (150°C, 204°C, and 220°C) P3PT thin films has been recorded for the detailed understanding of annealing temperature dependent enhancement in edge-on oriented crystallites (Figure 6.11). The integrated intensity of (100) reflection increases while increasing the annealing temperature $T_a$ i.e. 144 (150°C), 383 (204°C), and 462 (220°C). The overall results suggest that a higher annealing temperature is necessary for the recrystallization of P3AT polymers while correlating the difference in annealing temperature with the enhancement in scattering intensity of the films.

## 6.7 X-ray Reflectivity Analysis of Spin Coated Films

The thicknesses of the spin coated P3AT films were calculated from the X-ray reflectivity profile (Figure 6.12) and presented in Table 6.3. It does not vary much with respect to the polymers. The roughnesses of the films were extracted by simulating the

measured X-ray reflectivity profile using the Parratt32 software. The surface roughnesses decreases with increasing the alkyl side chain length (Table 6.3). The X-ray and electron diffraction pattern collected for the same film concludes the augment in edge-on oriented crystallites while decreasing the alkyl side chain length. The alkyl side chains will stay perpendicular to the substrate plane when they are edge-on oriented as compared to the face-on oriented crystallites (parallel to the substrate) (Figure 1.5). Eventually, such long alkyl side chains can increase the surface roughness when they are staying perpendicular to the substrate.

| Polymers | Thickness (±0.2nm) | Roughness (Å) |
|---|---|---|
| P3PT | 16.9 | 10.5 |
| P3HT | 15.6 | 8 |
| P3HeptT | 15.5 | 5 |
| P3OT | 17.3 | 6 |

Table 6.3: The thickness and roughness of P3AT spin coated annealed films

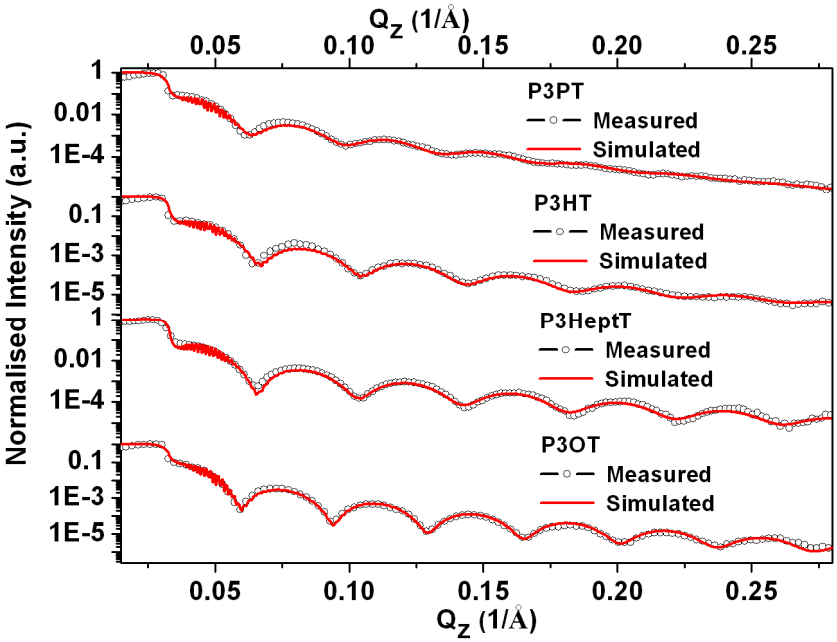


Figure 6.12: The measured and the simulated X-ray reflectivity profile of annealed P3AT spin coated films; the intensity profile is normalized to one

## 6.8 Influence of Alkyl Side Chain length on the Field Effect Mobility of Spin Coated Films

In order to correlate the structural information gathered by HRTEM and GIXD with transport properties, the field effect mobility was measured for P3AT samples before and after

annealing using the same undercooling (ΔT=45°C). The influence of alkyl side chain length on the mobility of annealed and as-spin coated P3AT films are shown in Figure 6.13. The mobility of annealed and as-spin coated P3AT films tends to decrease with increasing length of the alkyl side chain from $3.6*10^{-4}$ $cm^2/Vs$ (P3PT) to $6.3*10^{-5}$ $cm^2/Vs$ (P3OT). In other words, the mobility of annealed P3PT and P3HT film is an order of magnitude higher comparative to the P3OT films. The overall trend observed with alkyl side chain length is similar to that reported by Park *et al.*[142] and Babel *et al.*[143]. It suggests that the mobility of P3AT films annealed in the same conditions (same ΔT) tend to decrease as increasing the side chain length. Moreover, the GIXD and TEM data collected for the same samples show that the proportion of face-on oriented crystallites becomes larger while increasing the side chain length from *n*-pentyl to *n*-octyl. This effect of the side chain length might be the reason why the mobility of P3AT crystallites increases as the side chain becomes shorter.[2, 8] Accordingly, the observed decrease of charge mobility may reflect the decrease of proportion of edge-on oriented domains in the films when the alkyl side chain length increases. The mobility of P3PT is slightly lesser than the P3HT ($5.9*10^{-4}$ $cm^2/Vs$) even though P3PT contain more edge-on oriented crystallites. It might be due to the increased grain boundaries because of the reduction in growth rate of the crystallites while decreasing the side chain length as observed through HRTEM.[2, 78] The decrease of field effect mobility after the post growth annealing could be attributed to the increased face-on oriented crystallites with sharp grain boundaries.[[2, 78]]

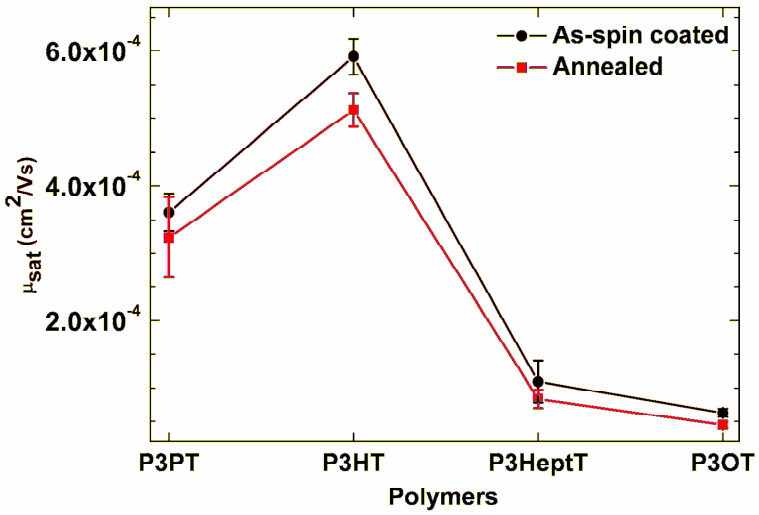


Figure 6.13: Influence of alkyl side chain length on the field effect mobility of annealed P3AT OFETs

## 6.9 Discussion

This important observation indicates that lamellar thickening of the P3AT domains is strongly limited in spin coated films after annealing. Lateral growth of the crystalline lamellae in the directions of the soft alkyl side chains is the predominant process induced by thermal annealing. One can accordingly define a fast growth direction along the $\mathbf{a_{P3AT}}$ axis and a slow growth direction along the $\mathbf{c_{P3AT}}$ axis as illustrated in Figure 6.14. In other words, post growth annealing leads to an anisotropic coarsening of the crystalline domains.[131]

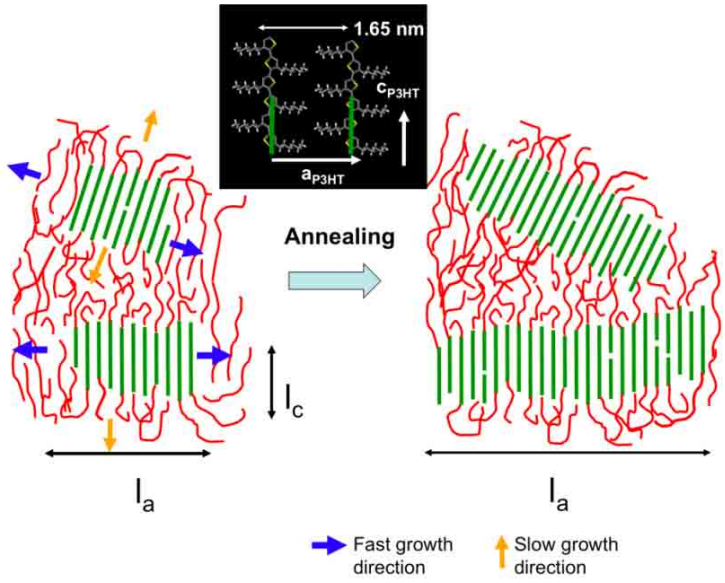


Figure 6.14: Schematic showing the anisotropy of P3AT lamellar growth. Annealing promotes fast growth along the side chain direction whereas lamellar thickening remains limited

Various groups have evidenced the importance of macromolecular parameters (RR and MW) of P3ATs on the formation of edge- and face-on oriented crystallites and the correlations with the performances of solar cells and OFETs.[2, 9, 53, 63] Regarding morphology of spin coated P3HT films, nanofibrils are most often observed via AFM.[16, 63, 65] Various authors evidenced the growth of long P3HT nanofibrils upon annealing.[72, 131] Cho *et al* reported a two-fold increase of charge carrier mobility upon annealing a P3HT (MW=40kg/mol) dip coated film at 150°C for 15 minutes.[144] Zen *et al* found a similar increase of mobility for the $CHCl_3$ fraction of P3HT after annealing at 150°C.[145] However, AFM does not allow to map the structure of the domains down to the individual stacks of polymer chains. Nanofibrils observed by AFM may be polycrystalline to a certain extent. In this context, HRTEM provides a complementary view of the nanomorphology in spin coated

and annealed layers for various P3ATs. In the following, I will discuss the main findings using the frame of polymer crystallization established for more classical systems e.g. polyolefins.

In most of the semicrystalline polymers e.g. PE, annealing can result in lamellar thickening (increase of the stem length in the lamellae) or lateral growth (increase of the number of stems in the direction perpendicular to the chains). Lamellar thickening occurs via reorganization of polymer chains within stacked lamellae i.e. a process of secondary crystallization. In other words, during thickening, no new crystalline chains are introduced in the crystal from the surrounding melt. As opposed to this, lateral growth implies the incorporation of new chains in a crystal. The experimental data gathered in this study show that both lamellar thickening and lateral growth depend on the length of the alkyl side chains.

More generally, annealing of P3AT films does not induce a substantial thickening of the crystalline domains along the PT backbone direction, at least within the frame of annealing times used in this study. Moreover, thickening is not substantially augmented with increasing the annealing temperature $T_a$. As a matter of fact, the maximum of the stem length measured in annealed films of P3OT are comparable to those observed for P3HT films grown by DEC (9 nm).[64] Only the films grown very slowly by DEC at 20 µm/s show a higher average stem length of 13 nm as measured by Hartmann *et al.*[91] This result suggests that the slide-diffusion of polythiophene backbones within the existing nanocrystals is particularly difficult during the thermal annealing which results in limited lamellar thickening. This is not unexpected as the π-π interaction between the P3AT stems are much stronger than the van der Waals interactions between PE chains in a corresponding PE crystal. Accordingly, the energetic barrier to the sliding of a PT chain in a P3AT nanocrystal is most presumably much larger as compared to PE.

However, the present study has shown that the extension of the nanocrystals dimensions along the $\mathbf{a_{P3AT}}$ axis is preferred, especially for the P3ATs with longer alkyl side chains. The HRTEM results demonstrate that *n*-octyl side chain favors the lateral growth of P3OT lamellae as opposed to the shorter *n*-pentyl side chains for which annealing induces only limited lateral growth even for high annealing temperatures (up to 220°C). Although significative, the two-fold increase in hole mobility reported in the literature after annealing remains moderate.[144] From the point of view of charge transport, it is the extension of the domains along the chain ($\mathbf{c_{P3AT}}$ axis) and π-π stacking directions ($\mathbf{b_{P3AT}}$ axis) that is expected to lead to an improved charge transport in the crystalline domains. However, the present

results show that annealing promotes mainly the growth of along the $\mathbf{a_{P3AT}}$ axis (direction of the side chains), i.e. along the direction of poor charge transport in P3ATs whereas the stem length in the crystalline domains increases only by a few nanometers. In addition, more face-on oriented domains are observed for P3OT after annealing, indicating that the nanocrystals are well ordered along the π-π stacking direction i.e. along the substrate normal. This means also that ordering along the $\mathbf{b_{P3AT}}$ axis is also promoted by annealing as could be evidenced by GIXD (see Figure 6.9). The origin of the efficient lateral growth of P3AT lamellae as increasing the number of carbon atoms in the side chain can be twofold: (i) it might be due to an easier folding ability to the P3AT chains, (ii) a higher overall plasticity of the crystalline lattice.

As demonstrated by several authors, P3HT crystallized from solution shows an onset of folding for a MW around 10 kg/mol.[131, 136] For all investigated P3ATs in this study, the MW of the sample implies the possibility for folding of the PT backbone. First, it may indicate ease of folding for P3ATs with longer side chains. This is not unexpected if one considers the chain packing and the $\mathbf{a_{P3AT}}$ parameter of the lattices. Indeed, as indicated earlier, in order to fold, the P3AT chain must show a sequence of about 8 thiophene units in *cis* conformation. The tightest fold would imply a folding diameter of approximately 20 Å. In P3PT, two chains are separated by 15.1 Å along the $\mathbf{a_{P3PT}}$ axis versus 20 Å for P3OT suggesting that tight folding is easier for P3OT as compared to P3PT.

A second reason explaining the improved lateral growth for higher number of carbon atoms in the side chains is certainly related to the overall plasticity of the crystal conveyed by the side chains. For the annealing temperatures used in this study, the lateral side chains are in a disordered "molten" state whereas the strong π-π interactions maintain the structural cohesion of the lamellae made of π-π stacked PT backbones.[13] Lateral growth of P3AT lamellae occurs via addition of chains at the growth front of the lamellae i.e. at the two terminal (b,c) planes of the lamellae. Mobility of chains in the vicinity of the growth front is expected to be higher for P3AT's bearing long side chains. Along the same line, Causin *et al* reported that P3DDT is crystallizing faster than the poly(3-butylthiophene) because of the increased molecular mobility in the melt as the side chain length increases.[146] This explains also the observation of a lower overall crystallinity in as-spin coated films of P3ATs for shorter side chains. On the other hand, the amount of edge-on oriented crystallites are increasing while decreasing the alkyl side chain length which can be evidenced from the continuous increase of (100) reflection along the out-of-plane (Figure 6.10a) and (020)

reflection from the ED pattern (Figure 6.5b). It consequently increases the mobility by an order of magnitude while decreasing the side chain length from n-octyl to n-pentyl. The decrease of charge carrier mobility as increasing the alkyl side chain length might be due to the increase in amount of lying insulating alkyl side chains along the substrate plane even though the crystallite sizes are increased (Table 2).[2, 9]

- *The overall results suggest that the annealing has mainly three important effects on the polymeric thin films; i) ripening of crystalline domains, ii) reduction in plasticity of thiophene backbones, and iii) crystallization of amorphous phase. The reduction in FWHM of in-plane and out-of plane diffraction peaks of P3AT thin films after the post growth annealing observed in chapter IV and V is also attributed to the reduction in plasticity of thiophene backbones as well as the ripening of crystalline domains.*

# Chapter VII

## 7 Conclusions and Outlook

The ultimate goal of this research is to develop a low-cost thin film preparation method for the fabrication of cheap and flexible electronic devices via solution processing techniques. Among the thiophene family, RR-P3AT is a widely used semiconducting polymer due to its solubility in common organic solvents, promising electrical and optical properties, satisfactory environmental stability, self-organization, and formation of microstructures. In addition to the crystallinity of semicrystalline P3AT polymers, interconnection between the crystalline domains was found to be a crucial factor for the enhancement of OFET performances. The currently used techniques like spin coating and epitaxial growths are much more favorable for the LMW P3HT than the highly tie-chain interconnected HMW P3HTs. Coexistence of both the face- and edge-on oriented crystallites and poor crystallinity of RT spin coated and drop cast P3AT thin films are due to the rapid evaporation of solvent ($CHCl_3$). These problems can be overcome by decreasing the cast temperature of the film. The conclusion remarks of low-temperature casting and the importance of future work for further improvements are presented in the following subchapters.

### 7.1 Conclusion

The crystallinity and orientation of HMW P3AT polymers were enhanced by casting them at low temperature (below RT). The percentage of edge-on oriented crystallites is increased from about 75 to 100 percent while reducing the cast temperature from 23°C to -30°C and it varies with respect to the polymers. A phase diagram of well studied P3HT has been constructed in order to represent the increase of edge-on oriented crystallites while reducing the cast temperature by plotting $I_{(100)}$ of GOD and GID Bragg peak (which are corresponding to the edge- and face-on oriented crystallites) versus cast temperature (Figure 7.1). For this purpose the diffraction pattern of P3HT film cast using the concentration of 2 mg/ml was used. The phase diagram can vary with respect to the concentration as well as the physical properties of the polymers and solvents such as solubility, molecular-molecular interactions, etc.

In addition, the trend in crystallinity of P3AT thin films cast at different temperatures was evaluated by Ruland's method. The crystallinity of P3AT thin films is increased as the cast temperature decreases (Figure 7.2). However, the crystallinity of P3AT thin films is

decreased as the alkyl side chain length increases. The crystallinity and crystallite sizes of P3AT thin films are not increased while decreasing the cast temperature from -12°C to -30°C. Therefore, -12°C can be assumed as an optimum crystallization temperature for the concentration of 2 mg/ml for the four P3AT polymers investigated in this thesis. Very thin films cast at RT and -30°C shows that the out-of-plane stacking of P3AT crystallites are increased as the side chain length increases, but the in-plane stacking and crystallinity of the polymers are getting worse because of the augment in steric hindrance between the alkyl side chains.

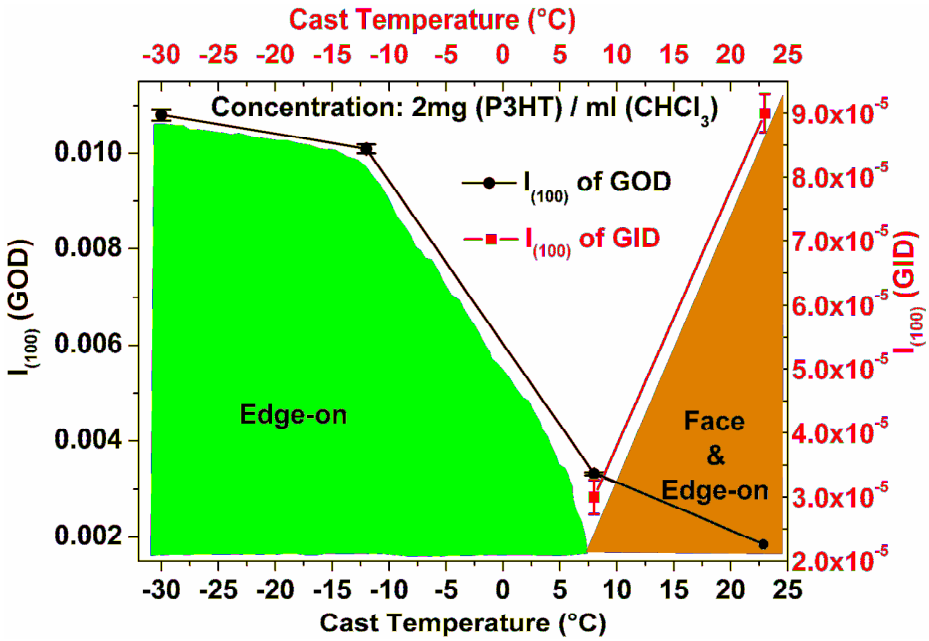


Figure 7.1: Phase diagram of P3HT which depicts the formation of face-on and edge-on oriented crystallites with respect to the cast temperature for a given concentration of 2mg/ml

The enhanced interchain stacking as well as the crystallinity of P3AT thin films while casting at -30°C together with the reduction of alkyl side chain length enhances the luminescent intensity as well as the field effect mobility of OFET by an order of magnitude in comparison to the RT cast one. The appearance of well pronounced vibronic transition in the PL spectra clarifies the formation of highly ordered P3AT crystallites (aggregates) while casting at -30°C. The HRTEM and morphological analysis carried out for the spin coated and RT drop cast films, respectively concludes that the growth of the crystallites along the chain axis (c-axis) is restricted due to the reduction in slide diffusion of π-π stacked PTs, chain entanglement, and thiophene backbone folding. It can hamper the charge transport by increasing the grain boundaries as well as by bringing the insulating alkyl side chains parallel to the direction of charge flow. So, it is necessary to increase the interchain stacking of P3AT

polymers and it can be done only by reducing the alkyl side chain length with the cast temperature.

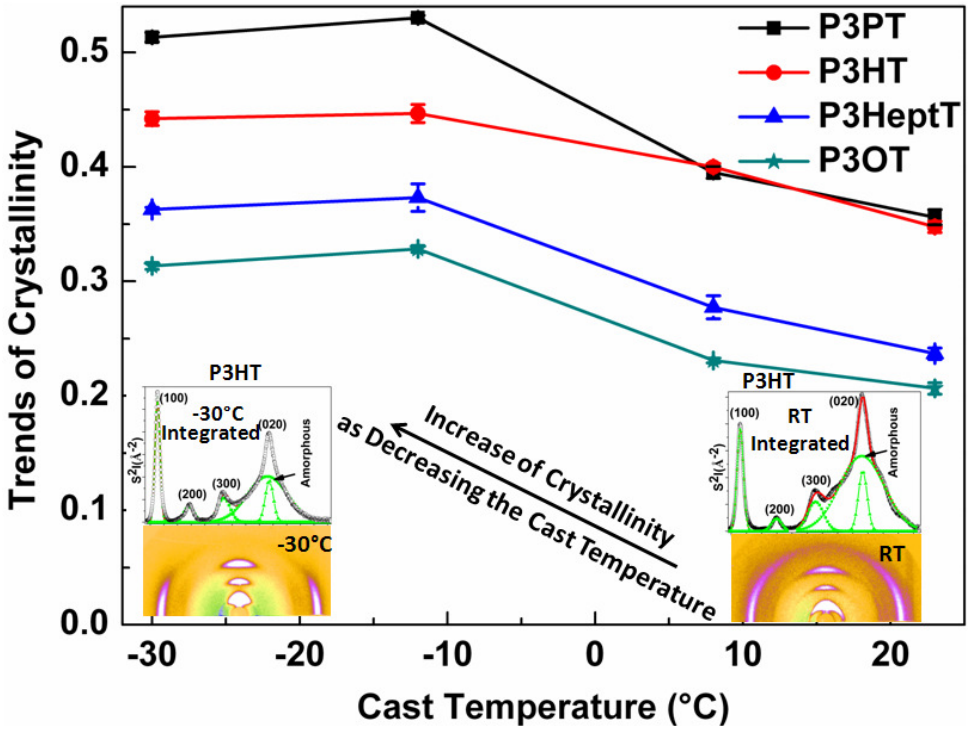


Figure 7.2: Depicts the trend in crystallinity of P3AT thin films cast at different temperatures using the concentration of 2mg/ml

The reduction in cast temperature does not only improve the crystallinity and orientation of polymer crystallites, in the same time, it also reduces the cost of device fabrication. As we know that the polymer based devices are cheaper because of their solution processability as compared to the cost of conducting polymers. The low temperature casting can be more attractive than the normal processing techniques which are widely used in the industries like doctor blading and spin coating because (much) diluted solutions can be used to produce very thin, homogeneous, and uniform films. As compared to casting, spin coating technique produces uniform thin films but engenders large wastes of polymers and does not allow for the precise control of face-on versus edge-on orientation of the crystallites.

In 2009, F.C. Krebs stated that “Casting is one of the cheapest techniques which are widely used in the industries but it is suffering from the surface roughness”. Besides the crystallinity, reduction in cast temperature is assisting us to increase the surface coverage and to reduce the surface roughness of the films. The proper selection of concentration, growth temperature, and uniform deposition surfaces are mandatory for the fabrication of highly uniform thin films with less surface roughness. For example, by dissolving 1mg of P3HT in

14 ml of $CHCl_3$ can provide ≈40 nm thin film of area ≈30×30 $cm^2$ with the surface roughness of ≈20 Å while casting at -30°C, which cannot be achieved by casting at RT (surface roughness =110 Å). However, from the technological point of view, low-temperature casting protocol might be advantageous because it is cheaper (economical) due to low consumption of polymers and more environmental friendliness. Low temperature casting protocols may be integrated with printing and doctor blading techniques in order to produce low cost electronic devices with enhanced performances. In particular, low temperature casting method would be suitable for the fabrication of OFETs on the flexible polymeric substrates which cannot undergo high temperature annealing steps. The only one drawback of this technique is that, it takes more processing time as compared to the spin coating as well as the RT casting, but it can be varied by varying the cast temperature. Overall studies conclude the following:

1. Increase of favorable edge-on oriented P3AT crystallites upon decreasing the cast temperature
2. The ratio of face- versus edge-on oriented crystallites can be well controlled by choosing the appropriate cast temperature for a given concentration
3. -12°C is an optimum cast temperature for the chosen concentration of 2 mg/ml
4. Crystallite size of the films can be controlled by reducing the formation of multiple nucleations and increasing the growth time
5. Thickness of the films can be adjusted by controlling the concentration and amount of solution being dropped
6. Roughness of the films can be controlled by choosing the appropriate concentration, cast temperature, and a flat working surface
7. The growth of nanofibrils is due to the restriction of growth along the thiophene backbone axis because of the entanglement and folding of thiophene backbones and increased π-π interaction between the molecules that can hamper the slide diffusion of the molecules

It would be possible to prepare epitaxial P3AT layers by controlling the nucleation via choosing the proper concentration and cast temperature. The HRTEM analysis carried out for the various temperatures annealed HMW P3ATs depicts that the 3D growth of the crystallites are restricted due to the restriction of growth along thiophene backbone axis. The anisotropic

growth and conductivity of P3AT crystallites are needed of further work in order to improve their interchain stacking in a way to produce efficient devices.

## 7.2 Outlook

The detailed analysis performed for the P3AT thin films cast below room temperature shows that the face-on oriented crystallites can be completely removed by reducing the cast temperature. This demands further work in order to reach the industry level.

P3AT thin films prepared at RT and -30°C envisages that the in-plane stacking of the crystallites are increased as the number of hydrocarbons in the grafted alkyl chain decreases, which is most important for the fabrication of high throughput OFETs and solar cells. It would be interesting if one can continue the structural and device analysis of P3ATs which contain less than 5 and higher than 8 hydrocarbons in the grafted alkyl chains. Especially at low temperature, because fast growth processes like spin coating is favorable for the long side chains (e.g n-octyl) due to the ease of thiophene backbone folding. The P3HT thin films cast and spin coated on the OTS treated substrate shows that the substrate-film interfacial ordering can be increased by increasing the substrate surface potential. The orientation of the crystallites can be further enhanced by casting them at low temperature on the various SAM treated substrates.

The processing temperature mainly controls the formation of nucleation, so this method can be applied to the other solution processable polymers which of them are having positive solubility e.g. poly(3,3’’’-didodecyl quarter thiophene), poly(2,5-bis(3-alkylthiophen-2-yl) thieno[3,2-b]thiophene), etc. The low temperature casting can be integrated with widely used printing and doctor blading techniques in order to increase the crystallinity, orientation and crystallite size of the films in a way to enhance the device performance.

# Appendix A

## A.1 DCA Analysis

Calorimetry is used to measure the heat of chemical reactions or physical changes.[147, 148] It is possible to determine the rate of heat generation with respect to the time with the rigid control of a computer control system. The calorimeter is designed with a steel housing to protect the samples from the environmental heat fluctuation as well as specimen-to-specimen heat transfer. In calorimetry, the sample and the calorimetric cell temperature is kept constant before starting the reactions. Absorption or the evolution of heat during the reactions can be quantitatively measured by comparing it with the reference sample which may not react.

Figure A1: Six chamber computer controlled differential scanning calorimeter for direct determination of the absorption and release of heat

DCA analysis has been performed to calculate the enthalpy of solution of P3AT polymers. The measurements were carried out using a six chamber computer controlled calorimetry (Figure A1). 2mg of P3AT polymer has taken in a glass tube. A syringe which contains 5 ml of $CHCl_3$ has been placed on top of the glass tube and then wrapped with paraffin film. The glass tube was then placed inside the calorimeter chamber and waited for an hour for the linearization of the sample and the chamber temperature. After starting the measurement, 5 ml of $CHCl_3$ has been dropped by screwing the plunger. The measurement was set at 24 hours and the obtained profiles are shown in Figure A2.

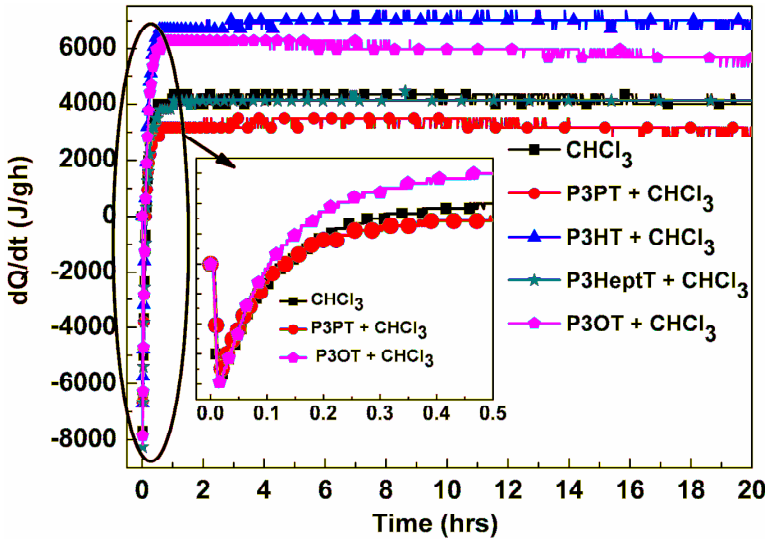


Figure A2. DCA graph of pure $CHCl_3$ and the mixtures of $CHCl_3$ and various P3ATs

An endothermic peak was observed directly after dropping the $CHCl_3$ (inset Figure A2). The same endothermic peak was observed in all the samples, even for the pure $CHCl_3$ which has been dropped in an empty glass tube (inset of Figure A2). It might be due to the evaporation of $CHCl_3$. Rather than that, no other endothermic peak was observed which corresponds to the solvation of polymers. The P3PT polymer did not dissolve completely even though I have left it for a day but P3OT has dissolved completely. So, I could not extract the enthalpy of solution due to the limitation of the calorimetry which I have used and the reduction in solubility of P3ATs as the side chain length decreases.

**Acknowledgements**

I would like to thank many people who have helped me to finish my doctorate degree successfully.

First of all, I would like to express my gratitude to the supervisor Prof. Dr. Ullrich Pietsch who has given me an opportunity to work under him and his support for receiving the DAAD scholarship. Rather than that, I would like to thank for his constant support and unflinching encouragement during my whole dissertation period with his expertise in synchrotron X-ray experiments.

I would like to acknowledge Dr. Souren Grigorian for the valuable discussions on the problem and his support throughout my doctoral work.

I am grateful to Prof. Dr. Ullrich Scherf (University of Wuppertal, Germany) and his students, especially Dr. Nils Koenen who has synthesized highly regioregular and pure poly(3-alkylthiophene) polymers whenever I was requesting him.

Special thanks to Prof. Martin Brinkmann (CNRS-Strasbourg, France) who has given me an opportunity to use his laboratory and for the fruitful discussions. At the same time I would like to thank Mr. Navaphun Kayunkid for his support while performing the experiment at CNRS.

I am thankful to the following professors who have given me an opportunity to use their laboratories and their students who have helped me during the various analyses

i. Photoluminescence and UV-Vis absorption spectroscopy analyses: Prof. Dr. Heiko Ihmels and his student Ms. Anna Bergen (University of Siegen, Germany)
ii. AFM analysis: Prof. Dr. rer. nat. habil. Xin Jiang and his student Mr. Aditya Kumar (University of Siegen, Germany)
iii. Mobility analysis: Prof. Dr. rer. nat. Thomas Riedl and his student Mr. Morteza Fakhri (University of Wuppertal, Germany). I am also thankful to Mr. Mikayelyan Eduard for the mobility analysis of spin coated films.

I am thankful to the beamline scientists from various German synchrotron sources such as BL9, DELTA, Dortmund (Dr. Christian Sternemann and Dr. Michael Paulus) and P08, PETRAIII, Hamburg (Dr. Oliver H. Seeck) for their valuable support during the

experiments. In addition, I would like to express my sincere thanks to the former and present colleagues who has helped me by losing their sleep during the exhausting beamtimes.

I would like to thank all the former and present members of Solid State Physics group at University of Siegen for the valuable discussions and providing a friendly environment in the group.

I acknowledge DAAD for offering the scholarship in order to pursue my doctorate degree in Germany.

I would like to thank Dr. Suresh Sundaram, Mr. Dheeraj Sudhakar, and Mr. Akash Shankar for proofing the thesis.

Finally, I would like to express my sincere thanks to my beloved parents and my brothers and sisters for their support and encouragement throughout my carrier. At the same time I would like to express my gratitude to my friends, former members of CGC, and well wishers.

## Bibliography


1. Wong, W.S. and A. Salleo, *Flexible electronics: materials and applications*. 2009: Springer Verlag.
2. So, F., *Organic electronics: materials, processing, devices and applications*. 2009: CRC.
3. Frommer, J.E., *Conducting polymer solutions.* Accounts of Chemical Research, 1986. **19**(1): p. 2-9.
4. Elsenbaumer, R., K. Jen, and R. Oboodi, *Processible and environmentally stable conducting polymers.* Synthetic Metals, 1986. **15**(2-3): p. 169-174.
5. Jen, K.Y., G. Miller, and R.L. Elsenbaumer, *Highly conducting, soluble, and environmentally-stable poly (3-alkylthiophenes).* J. Chem. Soc., Chem. Commun., 1986(17): p. 1346-1347.
6. Sato, M., S. Tanaka, and K. Kaeriyama, *Soluble conducting polythiophenes.* J. Chem. Soc., Chem. Commun., 1986(11): p. 873-874.
7. Salleo, A., et al., *Microstructural Characterization and Charge Transport in Thin Films of Conjugated Polymers.* Advanced Materials, 2010.
8. Kline, R.J., M.D. McGehee, and M.F. Toney, *Highly oriented crystals at the buried interface in polythiophene thin-film transistors.* Nat. Mater., 2006. **5**(3): p. 222-228.
9. Sirringhaus, H., et al., *Two-dimensional charge transport in self-organized, high-mobility conjugated polymers.* Nature, 1999. **401**(6754): p. 685-688.
10. Krebs, F.C., *Fabrication and processing of polymer solar cells: a review of printing and coating techniques.* Solar energy materials and solar cells, 2009. **93**(4): p. 394-412.
11. Chabinyc, M.L., *X-ray scattering from films of semiconducting polymers.* Polymer Reviews, 2008. **48**(3): p. 463-492.
12. Chang, J.F., et al., *Enhanced mobility of poly (3-hexylthiophene) transistors by spin-coating from high-boiling-point solvents.* Chem. Mater., 2004. **16**(23): p. 4772-4776.
13. Joshi, S., et al., *Bimodal temperature behavior of structure and mobility in high molecular weight P3HT thin films.* Macromolecules, 2009. **42**(13): p. 4651-4660.
14. Crossland, E.J.W., et al., *Systematic Control of Nucleation Density in Poly (3 Hexylthiophene) Thin Films.* Advanced Functional Materials, 2011.

15. Brinkmann, M., et al., *Highly Oriented and Nanotextured Films of Regioregular Poly (3-hexylthiophene) Grown by Epitaxy on the Nanostructured Surface of an Aromatic Substrate.* Macromolecules, 2010.
16. Yang, H., et al., *Solubility-driven thin film structures of regioregular poly (3-hexyl thiophene) using volatile solvents.* Appl. Phys. Lett., 2007. **90**: p. 172116.
17. DeLongchamp, D.M., et al., *Variations in semiconducting polymer microstructure and hole mobility with spin-coating speed.* Chemistry of materials, 2005. **17**(23): p. 5610-5612.
18. Li, G., et al., *High-efficiency solution processable polymer photovoltaic cells by self-organization of polymer blends.* Nature Materials, 2005. **4**(11): p. 864-868.
19. Shirakawa, H., et al., *Synthesis of electrically conducting organic polymers: halogen derivatives of polyacetylene,(CH) x.* J. Chem. Soc., Chem. Commun., 1977(16): p. 578-580.
20. Chiang, C., et al., *Electrical conductivity in doped polyacetylene.* Physical Review Letters, 1977. **39**(17): p. 1098-1101.
21. Shirakawa, H., *Nobel lecture: the discovery of polyacetylene film—the dawning of an era of conducting polymers.* Reviews of Modern Physics, 2001. **73**(3): p. 713.
22. G. Natta, G. Mazzanti, and P. Corradini, Rend. Aecad. Naz. Lincei., 1958. **25**: p. 3.
23. Mastragostino, M. and L. Soddu, *Electrochemical characterization of.* Electrochimica acta, 1990. **35**(2): p. 463-466.
24. Malik, S., T. Jana, and A.K. Nandi, *Thermoreversible gelation of regioregular poly (3-hexylthiophene) in xylene.* Macromolecules, 2001. **34**(2): p. 275-282.
25. Satoh, M., et al., *Electrical conductivity of drawn polythiophene films.* Synthetic Metals, 1989. **30**(1): p. 33-38.
26. McCullough, R.D., et al., *Self-orienting head-to-tail poly (3-alkylthiophenes): new insights on structure-property relationships in conducting polymers.* Journal of the American Chemical Society, 1993. **115**(11): p. 4910-4911.
27. http://nobelprize.org/nobel_prizes/chemistry/laureates/2000/public.html
28. Li, Y. and R. Qian, *Stability of conducting polymers from the electrochemical point of view.* Synthetic Metals, 1993. **53**(2): p. 149-154.
29. Lungenschmied, C., et al., *Flexible, long-lived, large-area, organic solar cells.* Solar energy materials and solar cells, 2007. **91**(5): p. 379-384.
30. McCulloch, I., et al., *Liquid-crystalline semiconducting polymers with high charge-carrier mobility.* Nature Materials, 2006. **5**(4): p. 328.

31. Thompson, B.C. and J.M.J. Fréchet, *Polymer–fullerene composite solar cells.* Angewandte Chemie International Edition, 2008. **47**(1): p. 58-77.
32. Lin, J.W., *Synthesis and properties of poly (2, 5 thienylene).* Journal of Polymer Science: Polymer Chemistry Edition, 1980. **18**(9): p. 2869-2873.
33. Yamamoto, T., K. Sanechika, and A. Yamamoto, *Preparation of thermostable and electric conducting poly (2, 5 thienylene).* Journal of Polymer Science: Polymer Letters Edition, 1980. **18**(1): p. 9-12.
34. Kaneto, K., et al., *Electrochemical preparation of a metallic polythiophene film.* J. Chem. Soc., Chem. Commun., 1983(7): p. 382-383.
35. Brinkmann, M. and J.C. Wittmann, *Orientation of Regioregular Poly (3 hexylthiophene) by Directional Solidification: A Simple Method to Reveal the Semicrystalline Structure of a Conjugated Polymer.* Advanced Materials, 2006. **18**(7): p. 860-863.
36. Hotta, S., *Electrochemical synthesis and spectroscopic study of poly (3-alkylthienylenes).* Synthetic Metals, 1987. **22**(2): p. 103-113.
37. Pingel, P., et al., *Unexpectedly high field-effect mobility of a soluble, low molecular weight oligoquaterthiophene fraction with low polydispersity.* Applied Physics A: Materials Science & Processing, 2009. **95**(1): p. 67-72.
38. Liu, J., et al., *Insight into How Molecular Structures of Thiophene-based Conjugated Polymers Affect Crystallization Behaviors.* Polymer, 2011.
39. Jimison, L.H., et al., *Correlating the microstructure of thin films of poly [5, 5-bis (3-dodecyl-2-thienyl)-2, 2-bithiophene] with charge transport: Effect of dielectric surface energy and thermal annealing.* Phys. Rev. B, 2008. **78**(12): p. 125319.
40. Moule , A.J., et al., *Effect of Polymer Nanoparticle Formation on the Efficiency of Polythiophene Based "Bulk-Heterojunction" Solar Cells.* The Journal of Physical Chemistry C, 2008. **112**(33): p. 12583-12589.
41. Friedel, B., C.R. McNeill, and N.C. Greenham, *Influence of Alkyl Side-Chain Length on the Performance of Poly (3-alkylthiophene)/Polyfluorene All-Polymer Solar Cells.* Chem. Mater., 2010. **22**(11): p. 3389-3398.
42. Roncali, J., *Conjugated poly (thiophenes): synthesis, functionalization, and applications.* Chemical Reviews, 1992. **92**(4): p. 711-738.
43. Prosa, T., et al., *X-ray structural studies of poly (3-alkylthiophenes): an example of an inverse comb.* Macromolecules, 1992. **25**(17): p. 4364-4372.

44. Xie, H., et al., *The thermochromism of poly (3-alkylthiophene) s: the role of the side chains.* Synthetic Metals, 2001. **122**(2): p. 287-296.
45. Corish, J., et al., *Interaction of side-chains in poly (3-alkylthiophene) lattices.* J. Chem. Soc., Faraday Trans., 1996. **92**(4): p. 671-677.
46. Kawai, T., et al., *Crystal Structure of Poly (3-aIkyIthiophene) and Its Doping Effect.* Journal of the Physical Society of Japan, 1992. **61**(9): p. 3400-3406.
47. http://en.wikipedia.org/wiki/Polythiophene#cite_note-30
48. Barbarella, G., A. Bongini, and M. Zambianchi, *Regiochemistry and conformation of poly (3-hexylthiophene) via the synthesis and the spectroscopic characterization of the model configurational triads.* Macromolecules, 1994. **27**(11): p. 3039-3045.
49. Kymissis, I., *Organic Field Effect Transistors: Theory, Fabrication and Characterization*. 2009: Springer Verlag.
50. Semenikhin, O.A., *Mesoscopic inhomogeneity of conducting and semiconducting polymers.* Annu. Rep. Prog. Chem., Sect. C: Phys. Chem., 2010. **106**: p. 163-191.
51. Loewe, R.S., S.M. Khersonsky, and R.D. McCullough, *A Simple Method to Prepare Head to Tail Coupled, Regioregular Poly (3 alkylthiophenes) Using Grignard Metathesis.* Advanced Materials, 1999. **11**(3): p. 250-253.
52. Loewe, R.S., et al., *Regioregular, head-to-tail coupled poly (3-alkylthiophenes) made easy by the GRIM method: Investigation of the reaction and the origin of regioselectivity.* Macromolecules, 2001. **34**(13): p. 4324-4333.
53. Kim, Y., et al., *A strong regioregularity effect in self-organizing conjugated polymer films and high-efficiency polythiophene: fullerene solar cells.* Nature Materials, 2006. **5**(3): p. 197-203.
54. Brinkmann, M., *Structure and morphology control in thin films of regioregular poly (3 hexylthiophene).* Journal of Polymer Science Part B: Polymer Physics.
55. Lu, G., L. Li, and X. Yang, *Achieving Perpendicular Alignment of Rigid Polythiophene Backbones to the Substrate by Using Solvent Vapor Treatment.* Advanced Materials, 2007. **19**(21): p. 3594-3598.
56. Brinkmann, M. and P. Rannou, *Effect of Molecular Weight on the Structure and Morphology of Oriented Thin Films of Regioregular Poly (3 hexylthiophene) Grown by Directional Epitaxial Solidification.* Advanced Functional Materials, 2007. **17**(1): p. 101-108.
57. Zen, A., et al., *Effect of molecular weight on the structure and crystallinity of poly (3-hexylthiophene).* Macromolecules, 2006. **39**(6): p. 2162-2171.

58. Tashiro, K., et al., *Structure and thermochromic solid state phase transition of poly (3 alkylthiophene).* Journal of Polymer Science Part B: Polymer Physics, 1991. **29**(10): p. 1223-1233.

59. Kayunkid, N., S. Uttiya, and M. Brinkmann, *Structural model of regioregular poly (3-hexylthiophene) obtained by electron diffraction analysis.* Macromolecules, 2010. **43**(11): p. 4961-4967.

60. Jimison, L.H., et al., *Correlating the microstructure of thin films of poly [5, 5-bis (3-dodecyl-2-thienyl)-2, 2-bithiophene] with charge transport: Effect of dielectric surface energy and thermal annealing.* Physical Review B, 2008. **78**(12): p. 125319.

61. Jimison, L.H., et al., *Charge Transport Anisotropy Due to Grain Boundaries in Directionally Crystallized Thin Films of Regioregular Poly (3 hexylthiophene).* Advanced Materials, 2009. **21**(16): p. 1568-1572.

62. Kline, R.J., et al., *Controlling the Field Effect Mobility of Regioregular Polythiophene by Changing the Molecular Weight.* Advanced Materials, 2003. **15**(18): p. 1519-1522.

63. Kline, R.J., et al., *Dependence of regioregular poly (3-hexylthiophene) film morphology and field-effect mobility on molecular weight.* Macromolecules, 2005. **38**(8): p. 3312-3319.

64. Brinkmann, M. and P. Rannou, *Molecular weight dependence of chain packing and semicrystalline structure in oriented films of regioregular poly (3-hexylthiophene) revealed by high-resolution transmission electron microscopy.* Macromolecules, 2009. **42**(4): p. 1125-1130.

65. Chang, J.F., et al., *Molecular-weight dependence of interchain polaron delocalization and exciton bandwidth in high-mobility conjugated polymers.* Physical Review B, 2006. **74**(11): p. 115318.

66. Brinkmann, M., *Structure and morphology control in thin films of regioregular poly (3-hexylthiophene).* Journal of Polymer Science Part B: Polymer Physics, 2011.

67. Brinkmann, M., et al., *Epitaxial Growth of Highly Oriented Fibers of Semiconducting Polymers with a Shish Kebab Like Superstructure.* Advanced Functional Materials, 2009. **19**(17): p. 2759-2766.

68. Crossland, E.J.W., et al., *Systematic Control of Nucleation Density in Poly (3 Hexylthiophene) Thin Films.* Advanced Functional Materials, 2011. **21**: p. 518-524.

69. Norrman, K., A. Ghanbari-Siahkali, and N. Larsen, *6 Studies of spin-coated polymer films.* Annu. Rep. Prog. Chem., Sect. C: Phys. Chem., 2005. **101**: p. 174-201.

70. Emslie, A.G., F.T. Bonner, and L.G. Peck, *Flow of a viscous liquid on a rotating disk.* Journal of Applied Physics, 1958. **29**(5): p. 858-862.
71. Baek, W.H., et al., *Effect of P3HT: PCBM concentration in solvent on performances of organic solar cells.* Solar energy materials and solar cells, 2009. **93**(8): p. 1263-1267.
72. Hugger, S., et al., *Semicrystalline morphology in thin films of poly (3-hexylthiophene).* Colloid & Polymer Science, 2004. **282**(8): p. 932-938.
73. Kim, D., et al., *Enhancement of Field Effect Mobility Due to Surface Mediated Molecular Ordering in Regioregular Polythiophene Thin Film Transistors.* Advanced Functional Materials, 2005. **15**(1): p. 77-82.
74. Chabinyc, M.L., et al., *X-ray scattering study of thin films of poly (2, 5-bis (3-alkylthiophen-2-yl) thieno [3, 2-b] thiophene).* J. Am. Chem. Soc., 2007. **129**(11): p. 3226-3237.
75. Meredig, B., A. Salleo, and R. Gee, *Ordering of Poly (3-hexylthiophene) Nanocrystallites on the Basis of Substrate Surface Energy.* ACS nano, 2009. **3**(10): p. 2881-2886.
76. Yang, H., et al., *Effect of Mesoscale Crystalline Structure on the Field Effect Mobility of Regioregular Poly (3 hexyl thiophene) in Thin Film Transistors.* Advanced Functional Materials, 2005. **15**(4): p. 671-676.
77. Yan, H., et al., *Self-Assembling Branched and Hyperbranched Nanostructures of Poly (3-hexylthiophene) by a Solution Process.* The Journal of Physical Chemistry C, 2011.
78. Wong, L.Y., et al., *Interplay of Processing, Morphological Order, and Charge-Carrier Mobility in Polythiophene Thin Films Deposited by Different Methods: Comparison of Spin-Cast, Drop-Cast, and Inkjet-Printed Films.* Langmuir, 2010. **26**(19): p. 15494–15507.
79. Kawase, T., et al., *Inkjet printing of polymer thin film transistors.* Thin Solid Films, 2003. **438**: p. 279-287.
80. Amundson, K.R., et al., *An in-plane anisotropic organic semiconductor based upon poly (3-hexyl thiophene).* Thin Solid Films, 2002. **414**(1): p. 143-149.
81. Wang, T., et al., *The development of nanoscale morphology in polymer: fullerene photovoltaic blends during solvent casting.* Soft Matter, 2010. **6**(17): p. 4128-4134.
82. Leubner, I.H., *Precision crystallization: theory and practice of controlling crystal size*. 2009: CRC.
83. Pamplin, B.R., *Crystal growth*. Vol. 16. 1980: Pergamon.

84. Giulietti, M., et al., *Industrial crystallization and precipitation from solutions: state of the technique.* Brazilian Journal of Chemical Engineering, 2001. **18**(4): p. 423-440.
85. In, C.D.B., *W. Bardsley, DTJ Hurle and JB Mullin, Editors.* Crystal Growth: A Tutorial Approach: p. 189.
86. Katz, J.L., *Homogeneous nucleation theory and experiment: A survey.* Pure and applied chemistry, 1992. **64**: p. 1661-1661.
87. http://en.wikipedia.org/wiki/Nucleation
88. Melia, T. and W. Moffitt, *Secondary nucleation from aqueous solution.* Industrial & Engineering Chemistry Fundamentals, 1964. **3**(4): p. 313-317.
89. Zhai, L., et al., *A simple method to generate side-chain derivatives of regioregular polythiophene via the GRIM metathesis and post-polymerization functionalization.* Macromolecules, 2003. **36**(1): p. 61-64.
90. Clark, J., et al., *Determining exciton bandwidth and film microstructure in polythiophene films using linear absorption spectroscopy.* Applied physics letters, 2009. **94**: p. 163306.
91. Hartmann, L., et al., *2D Versus 3D Crystalline Order in Thin Films of Regioregular Poly (3-hexylthiophene) Oriented by Mechanical Rubbing and Epitaxy.* Advanced Functional Materials, 2011.
92. Als-Nielsen, J. and D. McMorrow, *Elements of modern x-ray physics.* 2001.
93. Guinier, A., *X-ray diffraction in crystals, imperfect crystals, and amorphous bodies*. 1994: Dover Publications.
94. Parratt, L.G., *Surface studies of solids by total reflection of x-rays.* Physical Review, 1954. **95**(2): p. 359.
95. Windover, D., et al., *Thin film density determination by multiple radiation energy dispersive X-ray reflectivity.* 2000.
96. Birkholz, M., P.F. Fewster, and C. Genzel, *Thin film analysis by X-ray scattering*. 2006: Vch Verlagsgesellschaft Mbh.
97. Schmidbauer, M., *X-ray diffuse scattering from self-organized mesoscopic semiconductor structures*. 2004: Springer Verlag.
98. Barshilia, H.C., et al., *Investigation of interface properties of sputter deposited TiN/CrN superlattices by low angle x-ray reflectivity.* Journal of Physics D: Applied Physics, 2008. **41**: p. 205409.
99. Cullity, B.D. and S. Stock, *Elements of X-ray Diffraction*. 2002: Prentice Hall.

100. Pietsch, U., V. Holý, and T. Baumbach, *High-resolution X-ray scattering from thin films to lateral nanostructures*. 2004: Springer Verlag.
101. Bragg, W.L. *The diffraction of short electromagnetic waves by a crystal*. 1913.
102. clav, H.V., U. Pietsch, and T. Baumbach, *High-resolution x-ray scattering from thin films and multilayers*. 1999: Springer Berlin.
103. Dutta, P., *Grazing incidence x-ray diffraction.* Current Science, 2000. **78**(12): p. 1478-1483.
104. Baker, J.L., et al., *Quantification of thin film crystallographic orientation using X-ray diffraction with an area detector.* Langmuir, 2010. **26**(11): p. 9146-9151.
105. Hermann, M., et al., *Impact of silicon incorporation on the formation of structural defects in AlN.* Journal of applied physics, 2006. **100**: p. 113531.
106. Malik, S. and A.K. Nandi, *Crystallization mechanism of regioregular poly (3 alkyl thiophene) s.* Journal of Polymer Science Part B: Polymer Physics, 2002. **40**(18): p. 2073-2085.
107. REIMER, L., *Transmission electron microscopy: physics of image formation and microanalysis.* Springer series in optical sciences, 1984. **36**: p. 1-510.
108. Williams, D. and C. Carter, *Transmission electron microscopy: a textbook for materials science (4 Volume-set).* 2009.
109. Yao, N. and Z.L. Wang, *Handbook of microscopy for nanotechnology*. 2005: Kluwer Academic Pub.
110. Karl, N., *Organic crystals I: characterization*. Vol. 1. 1991: Springer Verlag.
111. HE, S.H., *High-resolution transmission electron microscopy.* Characterization of high Tc materials and devices by electron microscopy, 2000: p. 1.
112. Motaung, D.E., et al., *The influence of thermal annealing on the morphology and structural properties of a conjugated polymer in blends with an organic acceptor material.* Journal of materials science, 2009. **44**(12): p. 3192-3197.
113. Mena Osteritz, E., et al., *Two Dimensional Crystals of Poly (3 Alkyl thiophene) s: Direct Visualization of Polymer Folds in Submolecular Resolution.* Angewandte Chemie, 2000. **112**(15): p. 2791-2796.
114. Tanase, C., et al., *Local charge carrier mobility in disordered organic field-effect transistors.* Organic electronics, 2003. **4**(1): p. 33-37.
115. Gburek, B. and V. Wagner, *Influence of the semiconductor thickness on the charge carrier mobility in P3HT organic field-effect transistors in top-gate architecture on flexible substrates.* Organic electronics, 2010. **11**(5): p. 814-819.

116. Spano, F.C., *Absorption in regio-regular poly (3-hexyl) thiophene thin films: Fermi resonances, interband coupling and disorder.* Chemical physics, 2006. **325**(1): p. 22-35.

117. Spano, F.C., et al., *Determining exciton coherence from the photoluminescence spectral line shape in poly (3-hexylthiophene) thin films.* The Journal of chemical physics, 2009. **130**: p. 074904.

118. Spano, F.C. and H. Yamagata, *Vibronic Coupling in J-Aggregates and Beyond: A Direct Means of Determining the Exciton Coherence Length from the Photoluminescence Spectrum†.* The Journal of Physical Chemistry B, 2011.

119. Clark, J., et al., *Role of intermolecular coupling in the photophysics of disordered organic semiconductors: aggregate emission in regioregular polythiophene.* Physical review letters, 2007. **98**(20): p. 206406.

120. Brown, P.J., et al., *Effect of interchain interactions on the absorption and emission of poly (3-hexylthiophene).* Physical Review B, 2003. **67**(6): p. 064203.

121. Marchant, S., et al., *Ellipsometric analysis of poly (3-hexylthiophene) surfaces.* Journal of materials science letters, 1993. **12**(15): p. 1154-1155.

122. Strawhecker, K. and E. Manias, *AFM of Poly (vinyl alcohol) Crystals Next to an Inorganic Surface.* Macromolecules, 2001. **34**(24): p. 8475-8482.

123. Hosemann, R. and A. Hindeleh, *Structure of crystalline and paracrystalline condensed matter.* Journal of Macromolecular Science, Part B: Physics, 1995. **34**(4): p. 327-356.

124. Wu, T.M., J. Blackwell, and S.N. Chvalun, *Determination of the axial correlation lengths and paracrystalline distortion for aromatic copolyimides of random monomer sequence.* Macromolecules, 1995. **28**(22): p. 7349-7354.

125. Warren, B.E., *X-ray Diffraction*. 1990: Dover Pubns.

126. Rivnay, J., et al., *Drastic Control of Texture in a High Performance n-Type Polymeric Semiconductor and Implications for Charge Transport.* Macromolecules, 2011.

127. Ruland, W., *X-ray determination of crystallinity and diffuse disorder scattering.* Acta Crystallographica, 1961. **14**(11): p. 1180-1185.

128. Rabiej, S. and A. Włochowicz, *Investigations of the crystallinity of polyamide-6 fibers by two x-ray diffraction methods.* Journal of Applied Polymer Science, 1992. **46**(7): p. 1205-1214.

129. Zhokhavets, U., et al., *Relation between absorption and crystallinity of poly (3-hexylthiophene)/fullerene films for plastic solar cells.* Chemical physics letters, 2006. **418**(4-6): p. 347-350.

130. Joshi, S., et al., *Thickness dependence of the crystalline structure and hole mobility in thin films of low molecular weight poly (3-hexylthiophene).* Macromolecules, 2008. **41**(18): p. 6800-6808.

131. Liu, J., et al., *Controlling Poly (3-hexylthiophene) Crystal Dimension: Nanowhiskers and Nanoribbons.* Macromolecules, 2009. **42**(24): p. 9390-9393.

132. Sauvé, G., et al., *Well-defined, high molecular weight poly (3-alkylthiophene) s in thin-film transistors: side chain invariance in field-effect mobility.* J. Mater. Chem., 2010. **20**(16): p. 3195-3201.

133. Roe, R.J. and R. Roe, *Methods of X-ray and neutron scattering in polymer science*. 2000: Oxford University Press New York.

134. Glatter, O. and O. Kratky, *Small angle X-ray scattering*. Vol. 102. 1982: Academic press London.

135. Ogawa, T., et al., *Fractal properties of polymer crystals.* The Journal of Chemical Physics, 1989. **90**: p. 2063.

136. Payerne, R., et al., *STM studies of poly (3-alkylthiophene) s: model systems for plastic electronics.* Synthetic metals, 2004. **146**(3): p. 311-315.

137. Brédas, J.L. and R.J. Silbey, *Conjugated polymers: the novel science and technology of highly conducting and nonlinear optically active materials*. 1991: Springer.

138. Wu, P.T., et al., *Regioregular Poly (3-pentylthiophene): Synthesis, Self-Assembly of Nanowires, High-Mobility Field-Effect Transistors, and Efficient Photovoltaic Cells.* Macromolecules, 2009. **42**(22): p. 8817-8826.

139. Drummy, L., et al., *Direct imaging of defect structures in pentacene nanocrystals.* Advanced Materials, 2002. **14**(1): p. 54-57.

140. Brinkmann, M., *Directional epitaxial crystallization and tentative crystal structure of poly (9, 9'-di-n-octyl-2, 7-fluorene).* Macromolecules, 2007. **40**(21): p. 7532-7541.

141. Brinkmann, M., et al., *Structure and Morphology in Highly Oriented Films of Poly (9, 9-bis (n-octyl) fluorene-2, 7-diyl) and Poly (9, 9-bis (2-ethylhexyl) fluorene-2, 7-diyl) Grown on Friction Transferred Poly (tetrafluoroethylene).* Macromolecules, 2009. **42**(21): p. 8298-8306.

142. Park, Y.D., et al., *Effect of side chain length on molecular ordering and field-effect mobility in poly (3-alkylthiophene) transistors.* Organic electronics, 2006. **7**(6): p. 514-520.
143. Babel, A. and S.A. Jenekhe, *Alkyl chain length dependence of the field-effect carrier mobility in regioregular poly (3-alkylthiophene) s.* Synthetic metals, 2005. **148**(2): p. 169-173.
144. Cho, S., et al., *Thermal annealing-induced enhancement of the field-effect mobility of regioregular poly (3-hexylthiophene) films.* Journal of applied physics, 2006. **100**: p. 114503.
145. Zen, A., et al., *Effect of molecular weight and annealing of poly (3-hexylthiophene) s on the performance of organic field-effect transistors.* Advanced Functional Materials, 2004. **14**(8): p. 757-764.
146. Causin, V., et al., *Crystallization and Melting Behavior of Poly (3-butylthiophene), Poly (3-octylthiophene), and Poly (3-dodecylthiophene).* Macromolecules, 2005. **38**(2): p. 409-415.
147. http://www.chm.davidson.edu/vce/calorimetry/heatofsolutionofammoniumnitrate.html
148. http://en.wikipedia.org/wiki/Enthalpy_change_of_solution

**Eidesstattliche Erklärung**

Ich versichere hiermit an Eides statt, dass ich die vorliegende Arbeit ohne fremde Hilfe und ohne Benutzung anderer als der angegebenen Hilfsmittel angefertigt habe. Alle Ausführungen, die wortlich order singemäß aus fremden Quellen übernommen wurden sind als solche gekennzeichnet. Die Arbeit wurde bisher in gleicher order ähnlicher Form noch keiner anderen Jury vorgelegt und wird noch nicht komerziell genutzt.

Ich bin bewusst dass eine falsche Erklärung den Ausschluss aus dem verfahren zur Folge haben wird.

Siegen, 03.07.2012

Ort , Datum Unterschrift